Pals1 functions as a tumor suppressor regulating cell polarity, Hippo signaling and cancer progression

DISSERTATION ZUR ERLANGUNG DES DOKTORGRADES DER NATURWISSENSCHAFTEN (DR. RER. NAT.) DER FAKULTÄT FÜR BIOLOGIE UND VORKLINISCHE MEDIZIN DER UNIVERSITÄT REGENSBURG

vorgelegt von

Panichkina Olga

aus

Kiew, Ukraine

im Jahr

2017

Das Promotionsgesuch wurde eingereicht am:

Die Arbeit wurde angeleitet von:

Prof. Dr. Dr. Michael Krahn

Unterschrift:

Table of contents

Acknowledgments

First and foremost, I would like to thank Prof. Dr. Dr. Michael Krahn for giving me the opportunity to do my Ph.D. within his research group. Thank you for continuous support and for being my first referee.

I owe my deepest gratitude to PD Dr. Anja K. Wege, who provided me an opportunity to join their team and who was supporting me during all animal studies. Without this collaboration, it would not be possible to conduct this research.

I would like to thank Prof. Dr. Klein and Prof. Dr. Sprenger for being my Ph.D. mentors, for your support, patience and the intense discussions which gave me exciting insights into the project. Thank you for your encouragement and the extra time spent. Besides my advisors and mentors, I would like to thank the rest of my thesis committee: Prof. Dr. Witzgall and Prof. Dr. Längst.

A heartfelt thank you to all my colleagues from the Institute of Molecular and Cellular Anatomy at the University of Regensburg, for your great support, especially V.Menath, C. Maassen, L.Osten and O.Maier. Sincere thanks to all the members of Pathology Department at Uniklinik Regensburg, especially to Rudolf Jung, for helping with IHC studies. Many thanks to all the Ph.D. students within the research group not only for providing direct back-up and advice but also for a very friendly atmosphere. In particular, I would like to acknowledge S. Feicht, R. Sun, B. Schwertner, L.Kullman for their friendship, excellent insights into the work and for sharing their comprehensive knowledge. I would also like to thank you to all undergraduate students I was supervising during my Ph.D., for your hard work and for fun activities we've done together.

I wish to express my sincere thanks to Dr. O. Stelmashenko and to R.Sun for comments and criticisms from reading various drafts and parts of my thesis.

Dear Alex, mom, dad and all my family members, thank you for the opportunity to complete my Ph.D., your unceasing encouragement and support. Thank you to all my friends I got to know during my Ph.D., for helping me focus on the research while having a great time! Thank you to every mentioned person as well as anyone I might have forgotten.

Abstract

Epithelial cell polarity is of vital importance for the organization and function of epithelial tissues and is primarily maintained by three protein complexes, the Crumbs complex, the Par complex and the Scribble complex. Most of the polarity proteins within these complexes are highly conserved and play pivotal roles in embryonic development, cell-cell adhesion and cell migration. Recent studies have demonstrated that deregulation of epithelial polarity is a hallmark of tumor progression, in particular during the metastatic process. This study was conducted to examine the role of the tight junction protein Pals1 in the maintenance of cell polarity, and cancer. RNA interference and CRISPR/Cas9 gene deletion approaches were used to downregulate or deplete Pals1 in MDCKII, HCT116 and DLD1 cell lines. Reduction in Pals1 resulted in atypical expression levels of polarity proteins and defects in Hippo pathway regulation. Moreover, Pals1 loss caused E-cadherin reduction and enhanced cell migration. Pals1 deficient cells exhibited typical markers, inferring epithelial-to-mesenchymal transition. Further *in vivo* xenograft experiments revealed a function of Pals1 in cancer progression, as tumors derived from Pals1-deficient cells showed increased growth and more extensive liver and lung metastases. Taken together, these findings support a close link between epithelial cell polarity and tumorigenesis, and suggest the existence of a novel Pals1-mediated mechanism of tumor suppression. Thus, the pathophysiological consequences of Pals1 alteration must be investigated further, and used to develop new therapeutic strategies against this devastating disease.

I. Abbreviations

Abbreviation	Name
AJ	Adherens junctions
AJC	Apical junctional complex
AMOT	Angiomotin
ANOVA	Analysis of variances
AP	Alkaline phosphatase
APC	Adenomatous polyposis coli
aPKC	Atypical protein kinase C
APS	Ammonium persulfate
ATP	Adenosine triphosphate
Birc2	Baculoviral inhibitors of apoptosis repeat-containing 2
BSA	Bovine serum albumin
C.elegans	*Caenorhabditis elegans*
Cas9	CRISPR-associated protein 9
Cdc42	Cell division control protein 42
Crb	Crumbs
CRIB	Cdc42/Rac interactive binding
CRISPR	Clustered regularly interspaced short palindromic repeats
CTGF	Connective tissue growth factor
Cyr61	Cysteine-rich angiogenic inducer 61
DAPI	4',6-diamidino-2-phenylindole
$_{dd}H_2O$	Double distilled water

DLD1	Colorectal adenocarcinoma cell line, isolated by D.L.Dexter
DLG	Disks large
DMEM	Dulbecco's Modified of Eagle's Medium
DMSO	Dimethyl sulfoxide
DNA	Deoxyribonucleic acid
dNTP	Deoxyribonucleotide triphosphate
DTT	Dithiothreitol
E.coli	*Escherichia coli*
ECM	Extracellular matrix
EDTA	Ethylenediaminetetraacetic acid
EMT	Epithelial-to-mesenchymal transition
EtBr	Ethidium bromide
FCS	Fetal calf serum
FERM	4.1, Ezrin, Radixin, Moesin
gRNA	Guide RNA
GSK	Glycogen synthase kinase
GTP	Guanosine-5'-triphosphate
Guk	Guanylate kinase
HCT116	Human colon carcinoma tissue 116
HEK	Human embryonic kidney cell line
HRP	Horseradish peroxidase
IF	Immunofluorescence
IHC	Immunohistochemistry
IKK	Inhibitors of κB kinase

kb	Kilobases
KD	Knockdown
kDa	Kilodalton, 1000 unified atomic mass units
KO	Knockout
LATS	Large tumor suppressor
LB	Lysogeny broth
LD	Loading dye
Lgl	Lethal giant larvae
LSM	Laser scanning microscope
MAPK	Mitogen-activated protein kinase
MDCK	Madin-Darby Canine Kidney Epithelial Cells
MET	Mesenchymal-to-epithelial transition
MTT	3-(4,5-dimethylthiazol-2-yl)-2,5-diphenyltetrazolium bromide
NF-κB	Nuclear factor kappa-light-chain-enhancer of activated B cells
NSG	Nod Scid gamma
OD	Optical density
PAGE	Polyacrylamide gel electrophoresis
Pai1	Plasminogen activator inhibitor 1
Pals1	Protein associated with Lin seven 1
par	Partitioning defective
Patj	Pals1-associated tight junction protein
PBS	Phosphate buffered saline
PBTw	Phosphate buffered saline with tween
PDZ	Postsynaptic density protein 95, Dlg, ZO-1

PEI	Polyethyleneimine
PFA	Paraformaldehyde
PMSF	Phenylmethylsulfonylfluoride
PNK	Polynucleotide kinase
PTEN	Phosphatase and tensin homolog deleted on chromosome 10
puro	Puromycine
RNA	Ribonucleic acid
rpm	Revolutions per minute
RPMI	Roswell Park Memorial Institute medium
SAV1	Salvador family WW domain-containing protein 1
Scrbld	Scrambled
SD	Standard deviation
SDS	Sodium dodecyl sulfate
SEM	Standard error of the mean
SH3	Src Homolgy3
shRNA	Short hairpin RNA
SMA	Smooth muscle actin
Smad	Sma and Mad related proteins
TAO	Thousand-and-one amino acid protein kinases
TAZ	Transcriptional coactivator with PDZ-binding motif
TBS	Tris-buffered saline
TEAD	TEA domain
TEMED	Tetramethylethylenediamine
TGF	Transforming growth factor

TIAM1	T-cell lymphoma invasion and metastasis 1
TJ	Tight junctions
TNF	Tumor necrosis factor
TRAF	TNF receptor-associated factor
V	Volt
WB	Western Blot
wt	Wild type
YAP	Yes-associated protein
YTA	Yeast extract tryptone agar
ZEB1	Zinc finger E-box-binding homeobox 1
ZO	Zonula occludens

II. Introduction

2.1 Epithelial tissue and cell polarity

Mammalian anatomy and physiology are one of the most sophisticated areas of biology and medicine. Remarkably, in humans, there are only four tissue types identified: epithelial, connective, muscular, and nervous tissues. Cell similarity and their related function give tissue identity, although different types of tissues can be found in distinct organs (Mescher, Junqueira 2010). Additionally, each basic tissue has a unique extracellular matrix (ECM) - a highly dynamic structure, consisting of components as water, proteins and polysaccharides. ECM continuously undergoes structural remodeling, provides a crucial scaffold for all the cellular constituents and participates in cell-cell interactions, tissue homeostasis, morphogenesis and biochemical signaling (Frantz et al. 2010).

Whereas nervous tissue is composed of "finger-like" long cells as axons and dendrites, epithelial tissue is mostly made up of polyhedral cells. They form different layers with strong cell-cell contacts, and line most internal body cavities. Depending on the number of layers and cell shape in the upper layers, epithelial tissues are divided into several types. Simple epithelium is presented by one layer of cells, while stratified epithelia are considered to have more than two cell lining layers. Pseudostratified epithelium belongs to the simple epithelia, as the cell nuclei are lying at different levels and only giving an appearance of stratification. Further separation of epithelia into subcategories is based on differences in cell shape: flat, cubic or elongated morphology, which dictates the wide variety of epithelia functions. As the epithelial tissue forms boundaries between environments, its main function is a physical and semipermeable barrier, regulating absorption and secretion of substances such as water, nutrients and ions (Betts 2013; Mescher, Junqueira 2010).

All cells in epithelial tissues exhibit some differences in shape and structure due to differences in their function, with two types of cell polarization: apicobasal polarity and planar cell polarity. This refers to morphological and functional asymmetry within an epithelial cell or in the plane of tissue and is relevant in a wide range of cellular functions and processes. Planar cell polarity

coordinates cell distribution and behavior across the tissue plane, correlates to collective cell movements during body axes elongation, embryonic development, hair and bristle growth in *Drosophila* and mammals. A continuously changing environment and polarity information from neighboring cells requires stringent coordination and dynamic changes including cell rearrangement, cell division and cell-shape changes (Devenport 2014; Zallen 2007). Apico-basal cell polarity is established by two different cell-cell junctions - tight junctions (TJ) and adherens junctions (AJ), dividing the cell into two biochemically and structurally distinct domains. Whereas an apical membrane faces the outside surface of the body or the lumen of internal cavities, the basolateral membrane is oriented towards the basal lamina and adjacent cells (Khursheed, Bashyam 2014).

Despite differences in the distribution of cell-cell junctions, many studies in *Drosophila*, *C.elegans* and mammals illustrate evolutionary conservation of core mechanisms determining cell polarity (Gibson, Perrimon 2003). Three major polarity complexes have been identified to date and they serve as the core proteins maintaining apicobasal identity in epithelial cells. First, the Crumbs (Crb) complex, consisting of the transmembrane protein Crb, the adaptor protein associated with Lin seven 1 (Pals1) and Pals1-associated tight junction protein (Patj). Together with the partitioning defective (Par) - atypical protein kinase C (aPKC) complex, with the adaptor proteins Par3 and Par6 they activate the kinase aPKC. Crb and Par-aPKC complexes are required to establish the apical plasma membrane. In contrast, the Scribble homolog (Scrib)–Lethal giant larvae homolog (Lgl)–Discs-large homolog (Dlg) complex defines the basolateral plasma domain (Martin-Belmonte, Perez-Moreno 2012).

Par-aPKC complex serves as a core complex maintaining cell polarity and together with Crb complex it is implicated in TJ formation. TJ help to keep epithelial cell polarity by forming a paracellular diffusion barrier between the apical and basolateral cell domains and hence prevent the movement of solutes and lipids across the cell layer (Zihni et al. 2014; Hurd et al. 2003). To date, TJ represent the greatest number of known transmembrane (occludin and claudin families) and adaptor zonula occludens (ZO) proteins (ZO-1, ZO-2 and ZO-3) as well as signaling proteins, including protein kinases, phosphatases, guanosine-5'-triphosphate (GTP)-binding proteins, transcriptional and post-transcriptional

regulators. Together with more basally formed adherens junctions and desmosomes, they establish the apical junctional complex (AJC) and maintain polarity and cell-cell adhesion. Figure 2.1 is a simplified representation of the organization of epithelial tissue.

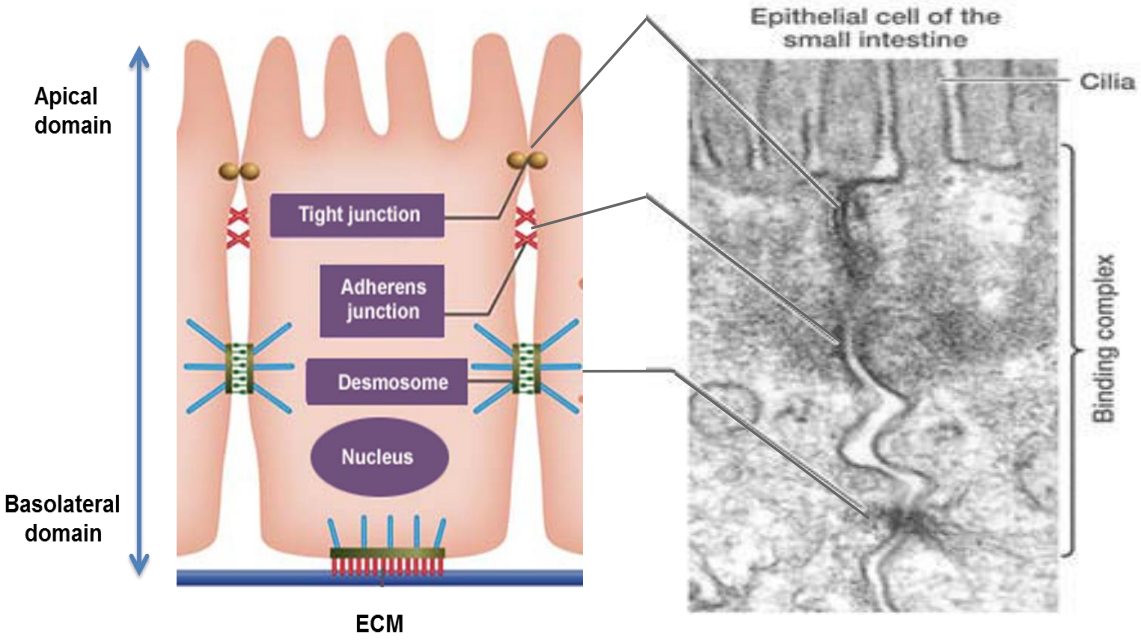

Figure 2.1: Epithelial cell-cell contacts and adhesion

Organization and maintenance of cell-cell adhesion in epithelial tissues. (Retrieved and adapted from comprehensive system for life science education, University of Tokyo, http://csls-text3.c.u-tokyo.ac.jp).

The AJ regulate epithelial paracellular permeability and are linked to the actin and microtubule cytoskeletons. The main transmembrane protein of AJ in epithelial cells is E-cadherin. It belongs to the family of Ca^{2+}-dependent glycoproteins and promotes tight cell-cell contacts by homophilic interaction with the cadherin molecules of the neighboring cells. E-cadherin consists of five extracellular cadherin repeat domains, one transmembrane domain and a highly conserved intracellular tail. Several phosphorylation sites in the intracellular domain promote binding affinity to p120-catenin (Reynolds, Roczniak-Ferguson 2004) and β-catenin (Mehta et al. 2015), further interaction with α-catenin and thus actin cytoskeleton.

2.1.1 The Par complex

The *par*-titioning-defective or Par proteins were first described in *Caenorhabditis elegans* and afterwards were found in almost all living organisms, all the way up to mammals. Interestingly, not only the components of Par complex are conserved - they also show a remarkable conservation of their localization in epithelial cells from worms to flies and humans. Par proteins comprise a complex cell polarity network and are involved in development, asymmetric cell division, spatial restriction of the cytoskeleton, formation of cells' polarity axes as well as asymmetric cell division (Aranda et al. 2008). Two proteins of the Par family, Par3 and Par6, together with aPKC and small GTPase cell division control protein 42 (Cdc42) assemble in the so-called Par complex. Par6 serves as a cornerstone protein and is likely to promote an interplay and coordination of all polarity complexes (Pieczynski, Margolis 2011a). There are three different Par6 isoforms, identified to date in mammals: Par6α, Par6β and Par6γ. They are all around 40 kDa in size and share structural organization; however, they have different patterns of tissue and subcellular localization. Par6 is a scaffolding protein and contains a single postsynaptic-density protein 95-Dlg-ZO-1 (PDZ) domain, responsible for protein-protein interactions usually with other PDZ domains or with specific carboxy-terminal motifs, and contributes to direct interaction with Par3. Adjacent to PDZ, the CRIB (Cdc42/Rac interactive binding) domain binds the Rho GTPase Cdc42 in a GTP-dependent manner, causing conformational changes in Par6 and increasing the affinity of the Par6 PDZ for its carboxy-terminal ligand by ~13-fold (Peterson et al. 2004).

Two Par3 genes have been identified so far in mammals – Par3A and Par3B. Par3A encodes three protein isoforms (180 kDa, 150 kDa, 100 kDa), whereas Par3B encodes only one around 140 kDa. Par3A and Par3B are both shown to localize apically to TJ at cell-cell contact regions in mammalian cells. All three Par3A proteins are characterized by three PDZ domains and a C-terminal region that interacts with the kinase domain of aPKC. Par3B is not fully described to date, however, in contrast to Par3A, it does not seem to bind to aPKC. Par3A is broadly expressed in various tissues and can dimerize through its N-terminal tail. In the early stages of polarization and junction development, Par3A is recruited to the junctional adhesion molecule, thus further serving as an

anchor. It also initiates Par6 and aPKC transition to TJ at later developmental stages (Assemat et al. 2008). The functionality of Par3 is highly dependent on its phosphorylation state, regulated by aPKC.

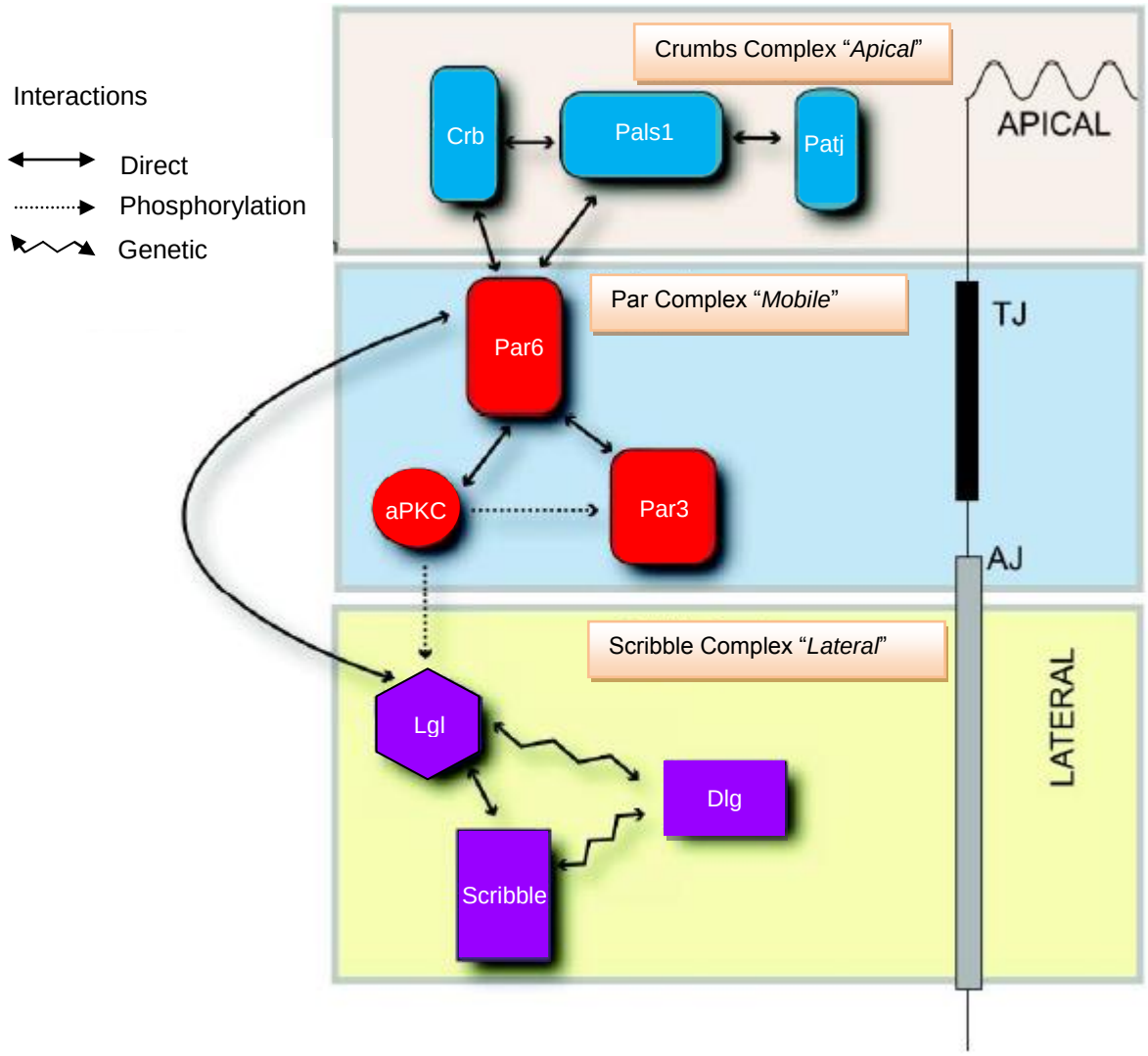

Figure 2.2: Protein complexes maintaining cell polarity

Although many proteins participate in apicobasal polarity, three major polarity complexes serve as the core proteins maintaining apicobasal cell polarity. These complexes are the apical Crb (includes Crb, Pals1 and Patj proteins), Par (includes Par6, Par3 and aPKC proteins) and the basolateral Scribble (includes Scribble, Dlg and Lgl proteins) complexes. All of these proteins are in a tight interrelation with each other and are highly conserved through evolution (Pieczynski, Margolis 2011b).

Par3 also shows Par6/aPKC-independent activity, as Par3 can interact with some of the adhesion molecules through its PDZ domain, including p75 and nectin. Furthermore, Par3 together with lipid phosphatase and tensin homolog

deleted on chromosome 10 (PTEN) might participate in phosphatidylinositide 3 kinase (PI3K)-Akt-mTOR signaling (Chen, Zhang 2013).

Two different aPKC isoforms (aPKC*λ*/ι and aPKC*ζ)* both play a pivotal role in Par complex function. They share a similarity in their unique protein structure*,* having a PB1 domain in the N-terminal, which is required for aPKC-Par6 interaction. The C-terminal catalytic domain is known to promote phosphorylation of Par3 by aPKC (Plant et al. 2003; Chen, Zhang 2013). aPKC-depended phosphorylation of other polarity regulators outside the Par complex, like Crb3 or Lgl proteins, provides the cross talk among all polarity determinants and is crucial in apical domain establishment (Aranda et al. 2008). Figure 2.2 represents the interaction and signaling redundancy of all polarity complexes.

Apart from controlling different aspects of cell polarity, Par proteins are also implicated in migratory processes (Crespo et al. 2014), asymmetric cell division (Betschinger et al. 2003) and microtubule organization, particularly in the positioning and orientation of centrosomes and spindle formation. In neurons, Par6-aPKC was shown to co-localize together with dynein to the centrosome and thus might play a role in dynein-based transport and glial-guided migration (Solecki et al. 2004). In addition, Par complex coordinates actomyosin fiber activity, thus is involved in polarized cell migration (Aranda et al. 2008).

Despite recent progress in the field, the biochemical relationship and crosstalk between Par6, Par3, aPKC and Cdc42 is still not fully understood and the functional redundancy of different isoforms makes this network even more complicated.

2.1.2 The Crb complex

The Crb complex is highly conserved in both invertebrates and vertebrates, consisting of four scaffolding proteins (Crb, Pals1, Patj and Lin-7) with numerous protein-protein interaction domains. Decades of research have showed Crb to be the key regulator of epithelial integrity. Fly embryos lacking Crb were characterized by disruption of apicobasal polarity and zonula adherence defects (Tepass, Knust 1993), whereas the overexpression of Crb leads to an enormous expansion of the apical domain with simultaneous contraction of the basolateral plasma domain (Wodarz et al. 1995). Crb is a

transmembrane protein with a highly conserved intracellular part, containing PDZ- and 4.1/ezrin/radixin/moesin (FERM) binding domains (Figure 2.3). In flies, through its PDZ-binding motif, the Crb protein can recruit other members of the Crb complex, like Stardust (Pals1 homolog in *Drosophila*), Par6 and aPKC to the plasma membrane. The FERM domain is required to recruit Expanded protein to the apical membrane, linking Crb complex to Hippo pathway (Pocha, Knust 2013). In mammals, Crb is encoded by three *Crb* genes (*Crb1, Crb2 and Crb3*). Crb1 and Crb2 are found to be highly expressed in human retina and brain. Crb3 is the primary form of Crb and is highly expressed in mammalian epithelial tissues (Slavotinek 2016). Crb3 maintains cell polarity and is crucial for correct positioning of the Crb complex at the apical membrane (Makarova et al. 2003).

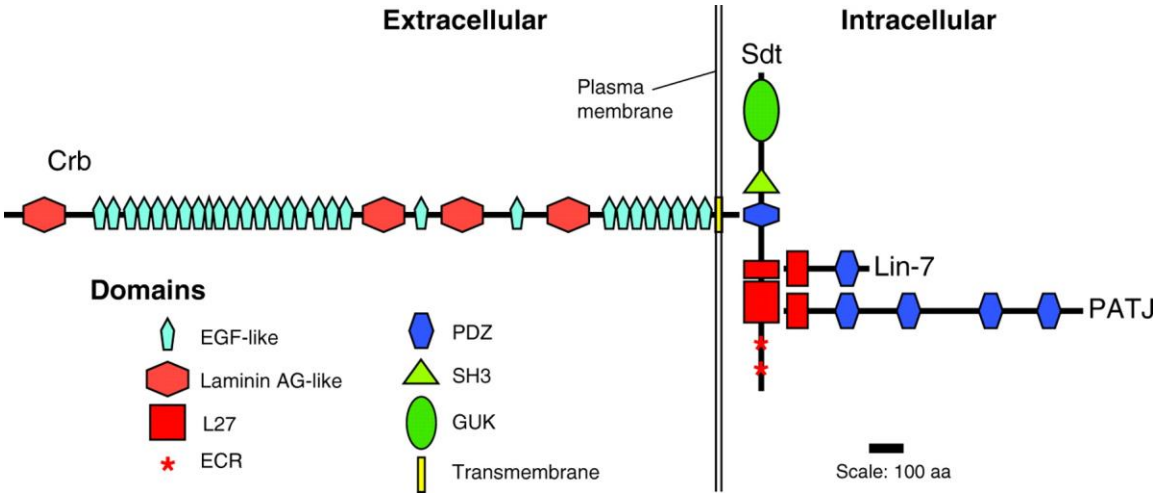

Figure 2.3: Structure of the Crb complex in *Drosophila (Bulgakova, Knust 2009)*
Proposed model, depicting the structure and organization of *Drosophila* Crb complex, comprising of Crb, Sdt (Pals1 homolog in flies), PATJ and Lin-7 proteins.

Pals1 (also known as membrane-associated palmitoylated protein 5 (MPP5) is a member of a guanylate kinase family protein consisting of two Lin-2 and Lin-7 (L27) domains (L27N and L27C), a PDZ domain, an SH3 (Src Homolgy3) domain, and a Guk (Guanylate kinase) domain. The PDZ domain of Pals1 binds Crb3, meanwhile Pals1 via its L27 domain interacts with Pals1-associated tight junction protein Patj - another member of Crb complex. Hence, Pals1 serves as a membrane-associated protein scaffold, linking and mediating the indirect interaction of Crb3 and Patj. For instance, Perrimon *et al.* identified a

mechanism in vertebrates by which Crb might act through Pals1 to recruit the Par3-Baz complex to the apical cell domain (Hurd et al. 2003). Furthermore, mammalian Pals1 is shown to maintain the delivery of E-cadherin to the cell surface and is not only sufficient for tight junction development but also is shown to be necessary for adherens junction maintenance (Wang et al. 2007). Interestingly, Pals1 was also shown to be expressed in T lymphocytes and plays a role in nuclear factor kappa-light-chain-enhancer of activated B cells (NFκB) signaling (Carvalho et al. 2011a).

In contrast to *Drosophila* (Figure 2.3), mammalian Patj contains ten PDZ domains and localizes to TJ. According to Shin *et al.,* MDCK cells lacking Patj had delayed tight junction formation and cell polarization defects, suggesting that Patj plays and important role in Crb complex assembly (Shin et al. 2005). Moreover, Patj has been demonstrated to regulate Pals1 accumulation at TJ, and Crb3 localization and trafficking (Michel et al. 2005). Furthermore, Patj regulates the positioning of aPKC and Par3 to the leading edge during directional cell migration (Shin et al. 2007). In flies, Patj regulates AJ stability, by direct binding to the myosin-binding subunit, subsequent dephosphorylation and inactivation of myosin (Sen et al. 2012). In addition, Patj has a wide range of interaction partners, including claudin-1, ZO-1 (Knust, Bossinger 2002), ZO-3 (Roh et al. 2002a), junctional adhesion molecule 1, nectins (Adachi et al. 2009) and angiomotin (AMOT) proteins (Whiteman et al. 2014). Thus, Patj is functionally significant for epithelial polarization and plays a key role in establishing the apical plasma domain.

2.1.3 The Scribble complex

The Scribble protein was first identified in flies as a crucial regulator of morphogenesis and septate junction formation. In combination with the lethal giant larvae Lgl and disc large Dlg proteins, it forms the Scribble complex and creates the basolateral determinant of a polarized cell. These three proteins are known to be tumor suppressors and show multiple interactions via their PDZ-domain with polarity determinants in Par and Crb complexes. Scribble is shown to regulate epithelial cell adhesion and migration, whereas Lgl is likely more involved in cell-cell cross-talk and promotes antagonistic interactions with the

aPKC-Par3-Par6 complex. Phosphorylation of Lgl by aPKC depends on its binding to Par6 and aPKC and leads to a release of Lgl from the plasma membrane, and thus helps to control cell shape formation during development. Interestingly, besides Dlg function in junctional development which is necessary for its targeting to the cytoskeleton, Dlg takes part in proliferation control. Taken together, the antagonistic crosstalk between the basal Scribble and apical Par and Crb polarity complexes is critical for the establishment of correct apicobasal polarity (Su et al. 2012; Woods et al. 1996; Humbert et al. 2008)

2.2 Disruption of cell polarity, epithelial-to-mesenchymal transition and cancer

Epithelial cell polarity is fundamental for tissue organization and allows cells to respond appropriately to signals from the surrounding microenvironment. Hence, a loss of cell polarity might delay or even abort cell responses to inhibitory signals and consequently the cell may evade differentiation, senescence or apoptosis. Decades of research have demonstrated that a wide number of polarity proteins are either tumor suppressors or proto-oncoproteins. For instance, Crb3 may act as a tumor suppressor, as downregulation of Crb3 promotes disruption of cell-cell junctions and increased metastatic potential. Loss of Par3, as well as overexpression of Par6α and Par6β proteins, was shown to cause hyperproliferation and enhanced invasiveness in breast cancer cell lines and primary tumor tissues (McCaffrey et al. 2012). In addition, Par6γ acts as a tumor-suppressor by repressing Akt pathway (Marques et al. 2016). Another member of Par complex, aPKCζ, is crucial in pancreatic and hepatocellular tissues, as its overexpression correlates with invasiveness and enhanced cell proliferation. In addition, all three members of the Scribble complex are known to be tumor suppressors, maintaining cell polarity and inhibiting uncontrolled cell proliferation (Martin-Belmonte, Perez-Moreno 2012).

Polarity proteins might play a crucial role in the metastatic progression of cancer, as they are known to mediate front-rear polarization in epithelial cell migration during development and tissue repair. Cdc42 is an important regulator of directed cell migration. Cdc42 activation of the Par-aPKC complex is shown to be important for actin and microtubule network repolarization along the migration

axis during spatial migration process (Etienne-Manneville et al. 2005). In addition, Par6 and aPKC promote E3 ubiquitin ligase-mediated degradation of RhoA and thus control disorganization of the actin cytoskeleton (Wang et al. 2003). Meanwhile, Par3 is known to control the leading edge of migration by activating Rac exchange factor, TIAM1 (T-cell lymphoma invasion and metastasis 1) (Pegtel et al. 2007). In intestinal epithelial cells, TIAM1 suppresses tumor growth and invasion by regulating Wnt and Hippo signaling (Diamantopoulou et al. 2017). Furthermore, numerous studies have underlined the physiological importance of proper E-cadherin regulation not only in cell-cell adhesion but predominantly in metastatic progression. E-cadherin deregulation and depletion cause cellular dedifferentiation and promotes invasiveness in human cancers (Rodriguez et al. 2012; Onder et al. 2008; Schneider et al. 2014; Singhai et al. 2011).

During metastasis, cancer spreads from its original place through the lymph or blood stream to other organs, where it gives rise to secondary tumors at the distant site. Epithelial-to-mesenchymal transition (EMT) – transdifferentiation of epithelial cells into motile fibroblast-like mesenchymal cells has been shown to be decisive for tumor cell dissemination in epithelium-derived carcinogenesis. EMT is first and foremost essential in embryonic development, as during EMT cell loses junctional and apicobasal polarity, undergoes a change in the cytoskeleton and signaling programs which enables plasticity and distinct cell development during embryogenesis (Lamouille et al. 2014). Moreover, in adults, EMT also plays a crucial role, promoting wound healing and tissue regeneration and is constituted to the second type of EMT. EMT type III is involved in malignant cancer progression (Kalluri 2009). Once the migratory cancer cell in type III EMT anchors at the distant epithelial tissue, it undergoes a mesenchymal-to-epithelial transition (MET), the reverse process to EMT, and is able to form secondary tumors, characterized by an epithelial phenotype (Figure 2.4).

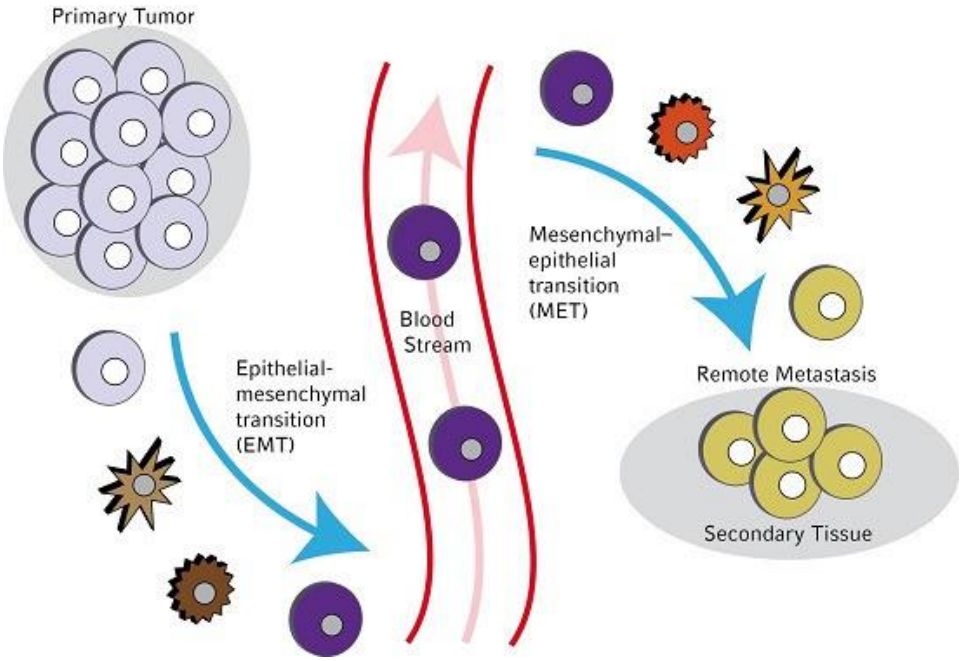

Figure 2.4: Epithelial-to-mesenchymal transition and reverse process of mesenchymal-to-epithelial transition (Kolbl et al. 2016)

EMT is a process by which the cell loses its epithelial phenotype, adopts migratory mesenchymal characteristics, enters the blood stream and might migrate to distinct body parts, where through reverse metamorphosis MET is able to give rise to remote metastases.

EMT and epithelial polarity are closely connected, as during EMT initiation epithelial cell-cell junctions are reorganized and the expression pattern of polarity proteins is drastically changed. Upon EMT, RhoA degradation by ubiquitin ligase Smurf1 leads to disassembly of tight junctions in epithelial cells, and is characterized by subsequently reduced claudin-1 and claudin-7 expression (Tabaries, Siegel 2016; Moustakas, Heldin 2007), ZO-1 downregulation and further internalization. Furthermore, disruption of adherens junctions, desmosomes and cadherin switch comprise an integral part of the EMT (Knights et al. 2012). E-cadherin is cleaved at the plasma membrane by metalloproteases (i.e. MMP7 and ADAM10) and replaced by N-cadherin. The shredded C-terminal of E-cadherin translocates into the nucleus resulting in dissociation of E-cadherin – β-catenin – p120 catenin complex and AJ disruption (Grabowska, Day 2012). Rho GTPases also counterpart to EMT, as RhoA promotes increased cell

contractility and actin stress fiber formation, whereas Cdc42 plays a role in lamellipodia and filopodia organization (Lamouille et al. 2014).

Recent evidence suggests that the transforming growth factor (TGF)-β pathway can trigger an EMT initiation (Katsuno et al. 2013). Indeed, TGF-β was shown to initiate loss of cell polarity due to Par complex disassembly during EMT (Ozdamar et al. 2005). Although TGF-β is mostly known as a proinflammatory cytokine, its excrescent secretion leads to EMT activation via two interrelated pathways: canonical and non-canonical TGF-β pathways (Figure 2.5).

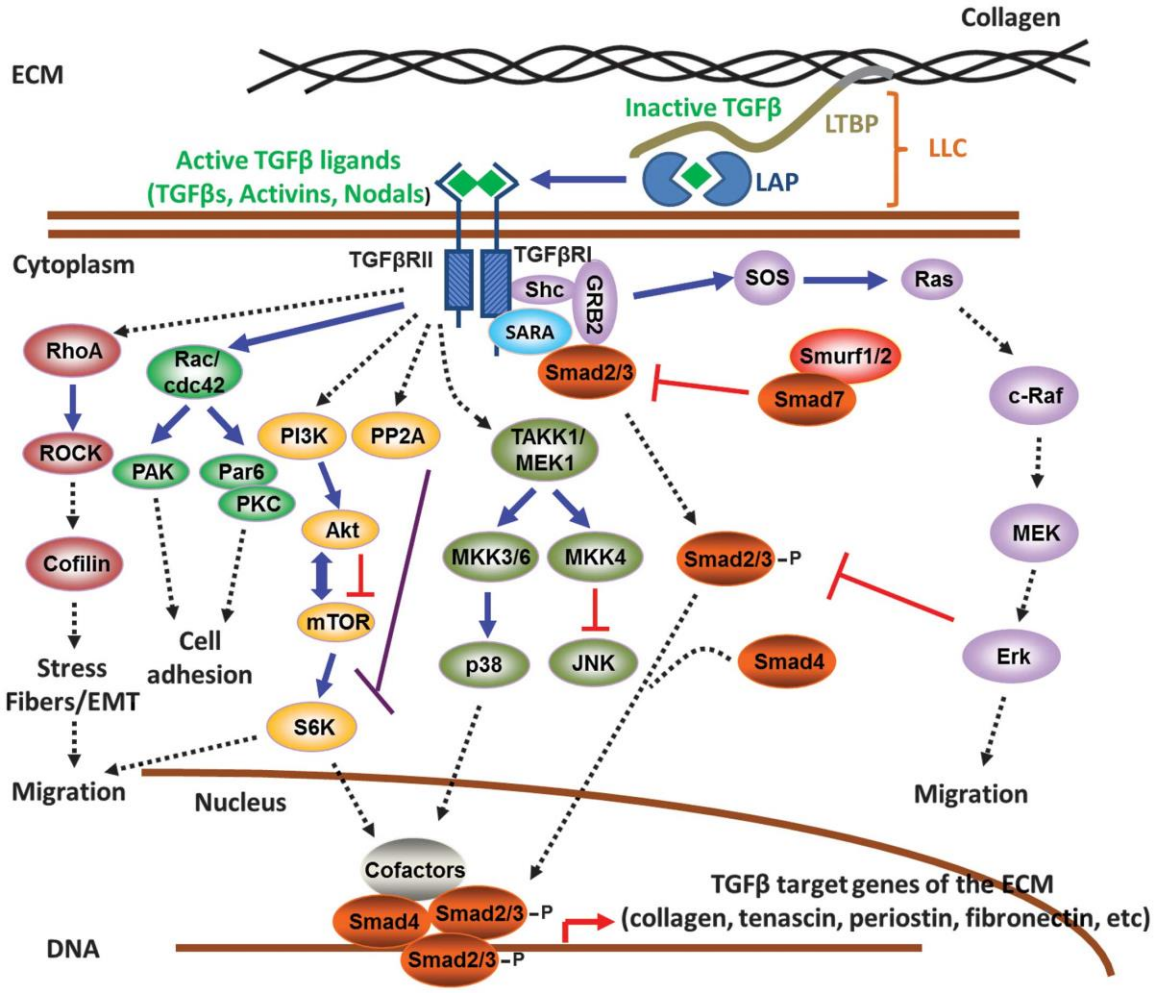

Figure 2.5: Smad-dependent (canonical) and -independent (non-canonical) TGF-β pathways (Papageorgis, Stylianopoulos 2015)

TGF-β acts through the downstream mediators to exert a vast range of biological activities during inflammation, EMT and cancer progression.

TGF-β binding to its receptors leads to phosphorylation of Smad2/3, activating the canonical Smad-dependent pathway. It causes gene reprogramming by directly activating the key EMT transcription factors including Snail, Twist and zinc-finger E-box-binding (ZEB) proteins.

Snail1, the mostly studied member of Snail family, is characterized by the SNAG box in its N-terminus, required for transcriptional repression of *CDH1* cadherin gene by recruitment of histone deacetylases or C-terminal binding proteins during cancer progression. At the C-terminus Snail1 contains four zinc finger domains and a nuclear localization signal motif, required for deoxyribonucleic acid (DNA) binding and nuclear translocation, respectively. ZEB1 shares structural similarity with Snail1, however preliminary Snail induction is required to trigger ZEB1 expression, as Snail1 also contributes to NFκB nuclear import. Twist belongs to the basic helix-loop-helix (bHLH) family of transcription factors and is also able to repress the *CDH1* gene, although indirectly via chromatin remodeling complex recruitment (Diaz et al. 2014). Dynamic co-interaction of Snail, Zeb and Twist proteins promote the downregulation of genes responsible for tight junction and adherens junction polarity protein processing and simultaneously enhance fibronectin, vimentin, N-cadherin and matrix metalloproteinases expression, considered to be the hallmarks of a mesenchymal phenotype (Peinado et al. 2007).

Additionally, TGF-β induces non-Smad signaling pathways, leading to activation of Rho GTPases, MAP kinase (MAPK) pathways and the PI3-Akt-mTOR pathway (Saitoh 2015; Yilmaz, Christofori 2009; Nistico et al. 2012; Lamouille et al. 2014; Derynck et al. 2014).

In the non-canonical TGF-β signaling pathway, TGF-β has been demonstrated to activate tumor necrosis factor (TNF)-receptor-associated factor 6 (TRAF6). In turn, TRAF6 activates mitogen-activated protein kinases, including extracellular signal-related kinase (ERK) 1/2, p38 mitogen-activated kinase (p38) and c-Jun N-terminal kinase pathways. TRAF6 also activates the inhibitors of the κB (IκB) kinase (IKK) complex. IκBs phosphorylation results in their polyubiquitination and subsequent degradation, allowing NF-κB to translocate into the nucleus and activate the transcription of many κB-dependent genes

implicated in the regulation of apoptosis and EMT (Mu et al. 2012; Wu, Zhou 2010).

Changes and deregulation in protein translation process are also considered to participate in cancer progression. The PI3K-Akt-mTOR pathway is known to regulate protein biosynthesis and cell size in mammals. TGF-β induced PI3K and mTOR signaling activity are demonstrated to be highly enhanced in a broad number of cancers, including breast and colorectal cancer. Activated Akt can phosphorylate many target proteins, most notably glycogen synthase kinase 3β (GSK-3β). In turn, GSK-3β stimulates the transcription of Snail and thus acts indirectly as a repressor of E-cadherin expression and EMT induction (Yu, Cui 2016; Bachelder et al. 2005). Taken together, cell polarity is essential for the proper functioning of eukaryotic cells, relies on a strong interplay between polarity proteins and a wide variety of signaling pathways and is crucial to regulate tumor progression and metastatic processes.

2.3 Hippo signaling pathway and its link to cell polarity

The Hippo pathway (Figure 2.6) was first described in studies of *Drosophila* that examined genes involved in tissue growth (Justice et al. 1995; Xu et al. 1995; Tapon et al. 2002). For some time, the Hippo pathway was thought to be evolutionarily conserved from flies to mammals, however, in mammals the Hippo signaling network seems to be more extensive and complicated. To date, this signaling pathway is known to control organ size by inhibiting cell proliferation and promoting apoptosis, and to play an important role in tissue repair and regeneration. Deregulation of the Hippo pathway is closely connected with cancer progression and metastasis, as mutations in its core proteins have been shown to result in overgrowth phenotype (Yu et al. 2015).

The core of the Hippo pathway includes several kinase cascades that work redundantly to regulate the activity and localization of the downstream effectors Yes-associated protein (YAP) and transcriptional coactivator with a PDZ-binding motif (TAZ) (Figure 2.6). Initially, the cascade begins with MST protein activation via its phosphorylation by thousand-and-one amino acid (TAO) protein kinases.

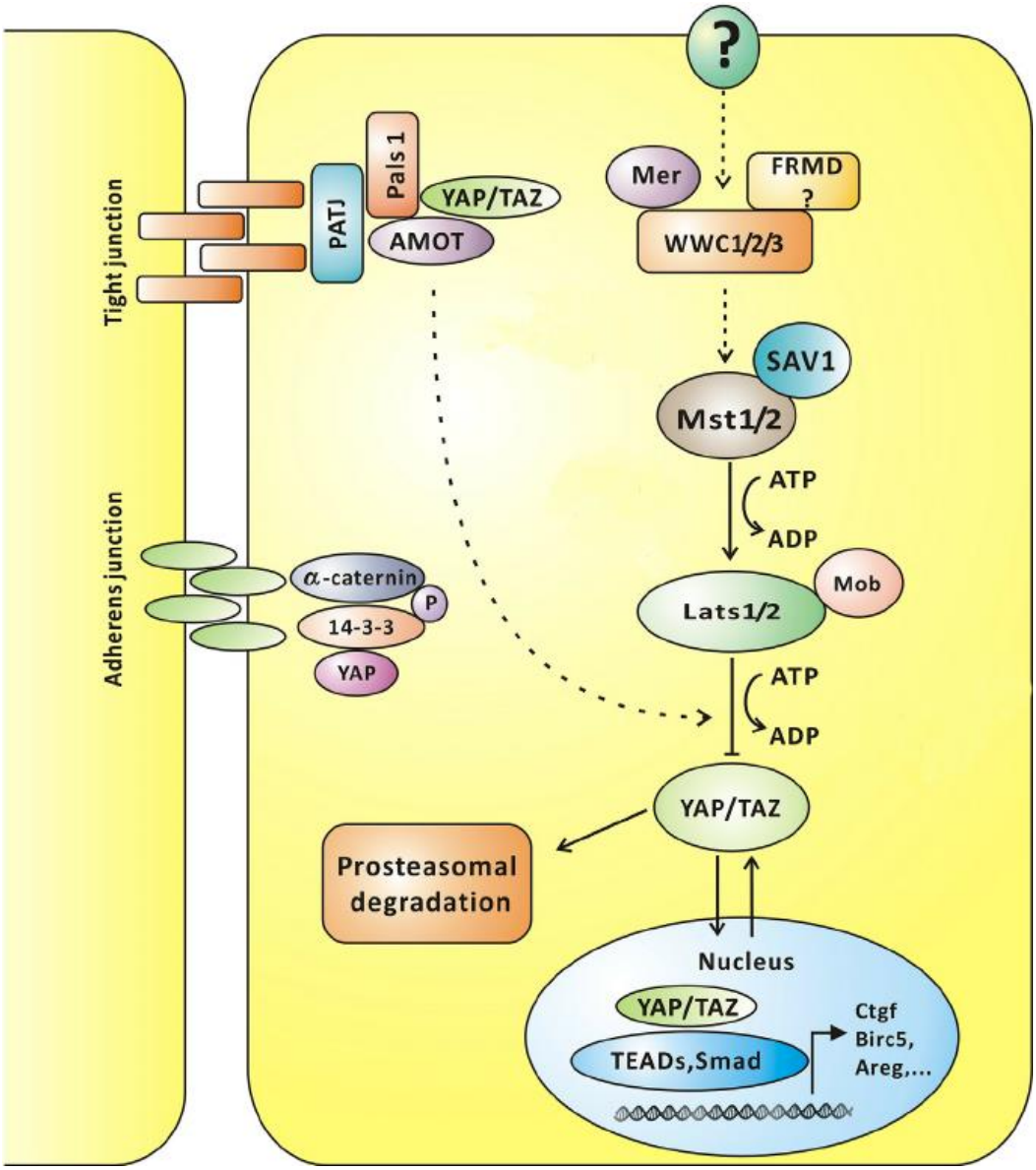

Figure 2.6: Hippo pathway signaling in mammals (adapted from Hao et al. 2014)

The Hippo pathway is known to regulate cell size and tissue growth via several kinase cascades, the common goal of which is the regulation of YAP/TAZ localization via physical interaction with AMOT and other proteins. These kinases promote YAP/TAZ phosphorylation and nuclear sequestration, thus controlling and regulating gene transcription.

Phosphorylated MSTs together with the adaptor protein Salvador family WW domain-containing protein (SAV)1/WW45 are able to phosphorylate and activate large tumor suppressor (LATS) proteins, especially LATS1 and LATS2, promoting their autophosphorylation (Meng et al. 2016; Ehmer, Sage 2016). Afterwards, the LATS protein subset is believed to phosphorylate and inactivate YAP and TAZ. Phosphorylation of YAP and TAZ leads to their binding with 14-3-3 protein binding site and causes cytoplasmic sequestration and accumulation or

ubiquitin-depended degradation. When the Hippo pathway is off, non-phosphorylated YAP and TAZ translocate into the nucleus, bind the TEA domain (TEAD) transcription factor family and prompt expression of a wide range of genes that are involved in cell proliferation and migration (Yu et al. 2015; Meng et al. 2016). Connective tissue growth factor (CTGF), Cysteine-rich angiogenic inducer 61 (Cyr61) and baculoviral inhibitors of apoptosis repeat-containing 2 (Birc2) have been shown to be direct targets induced by YAP-dependent TEAD activation, and to play a role in proliferation and anchorage-independent growth (Liu et al. 2015; Zhao et al. 2010b). Moreover, YAP and TAZ are known to interact with Smad2 and Smad3, connecting another transcriptional target of YAP plasminogen activator inhibitor 1 (Pai1) with activation of TGF-β signaling during tissue fibrosis and cancer (Zhao et al. 2010a).

Additionally, Hippo pathway activity is regulated by upstream signals. In *Drosophila*, the Mer/Ex/Kibra complex acts as an apical tumor suppressor complex, recruits Hpo (MST1/2 flies homolog) to the plasma membrane and enhances its phosphorylation, which could also influence YAP localization (Mo et al. 2014). In mammals, Kibra was shown to interact with aPKC and angiomotin family proteins (Zhang et al. 2014). AMOT was first described as a protein promoting endothelial cell migration and angiogenesis. However, two different isoforms of AMOT exhibit different functions, as only p80 was shown to promote cell migration and is not able to bind to YAP (Yi et al. 2013). Binding p130 AMOT to YAP family proteins is crucial for YAP and TAZ phosphorylation and their right localization to the tight junction. Furthermore, AMOT inhibits YAP-induced transformation and loss of cell contact inhibition in the epithelial cells.

Remarkably, AMOT is shown to interact through its C-terminal PDZ binding motif with Pals1 and Patj, maintain their proper localization and thus is important for the long-term TJ integrity in epithelial cells (Wells et al. 2006). The phosphorylation state of AMOT is also highly important and drives the association with Pals1/Patj at the plasma membrane, whereas the non-phosphorylated form concomitantly induces YAP and TEAD association, enhances its transcriptional activation and promotes uncontrolled cell proliferation (Moleirinho et al. 2017). Interestingly, in MCF10A human breast epithelial cell line Pals1 and Patj were determined to co-precipitate with YAP.

This might involve AMOT proteins as well, as they were also present in pull-downs, verified by Western Blot (Zhao et al. 2011; Varelas et al. 2010). In addition, AMOT is able to form a complex with Patj and by controlling GTPase activity regulates migration capacity of endothelial cells (Ernkvist et al. 2009). Recent data also identified AMOT as a novel binding partner of cadherin -11, a marker of EMT in prostate cancer cells. Together with cadherin-11, AMOT could influence mediated migration of these cells (Ortiz et al. 2014)

In addition, Crb3 is considered to interact with AMOT and Merlin to regulate YAP- and TAZ-dependent transcription and MAP kinase signaling, hence Crb3 is linked to cell-density-dependent regulation of proliferation and cancer (Varelas et al. 2010; Zihni et al. 2014).

Taken together, precise control of cell-cell adhesion in combination with decisive physiological function and molecular interplay of polarity determinants with Hippo and other signaling pathways is crucial in development as well as in cancer progression.

III. Aim of the study

Every year the number of cancer suffering patients increases drastically, reflecting the biggest medical worldwide problem to date. By 2020, there will be approximately 15 million new cancer patients diagnosed (Bray, Moller 2006). For this reason, the mechanisms triggering cancer, and the basic differences between a 'normal' cell and cancer cells must be intensely investigated.

Proper regulation and maintenance of cell polarity are required for development and homeostasis. There is strong evidence that the disruption of cell polarity and loss of cell-cell adhesion are implicated in cancer growth. Two fundamental roles of epithelial cells contribute to tumor development: the regulation of asymmetric cell division and the maintenance of the apical junction complex (Royer, Lu 2011).

Several cell polarity genes have been identified as tumor suppressors in flies and mammals, simultaneously playing a fundamental role in cell fate decisions and epithelial cell polarity. Mutations of Dlg, Lgl, Scribble, deregulation of Par3 and Crb3 cause excessive non-controlled epithelial growth, loss of apical-basal polarity, enhance EMT and metastatic progression (Wodarz 2000; McCaffrey et al. 2012; Karp et al. 2008; Elsum et al. 2013).

However, little is known about the direct Crb3 interaction partner protein Pals1, its implication in establishment and maintenance of cell polarity as well as cell proliferation and migration. Hence, the present study was designed to assess the variety of Pals1 functions in epithelial cell polarity, with the goal of describing its possible implication in tumor progression. The role of Pals1 in both apicobasal polarity maintenance and junction formation was investigated. Moreover, the function of Pals1 in the Hippo pathway and TGF-β signaling remains perplexing. Since Pals1 is involved in E-cadherin trafficking, the next objective of the study was to explore the possible influence of Pals1 on cell migration and EMT. In addition, it was of interest to analyze the potential role of Pals1 in tumor growth and metastasis development *in vivo*.

IV. Materials and Methods

4.1 Equipment

Table 1 Equipment

Equipment	Label	Manufacturer
Autoclave	5050 ELV	Tuttnauer
Cell culture incubator	CB 160	Binder
Centrifuge	Multifuge 3	Heraeus
Centrifuge	Microstar 12	VWR
Chemical balance	BL 1500 S	Sartorius
Chemiluminescence-system	Fusion FX 7	Vilber
Drying chamber	Heraeus T 6200	Thermo Scientific
Drying chamber	Heraeus UT 6120	Thermo Scientific
Electric pipetting aid	Pipetboy	Integra
Electrophoresis Module	Eco-Mini	Biometra
Floor centrifuge	Varifuge 3.0 RS	Heraeus
Freezer -20 °C	GNP 3376	Liebherr
Freezer -80 °C	GFL Chest Freezer 6485	Novolab
Heating block	Thermomixer comfort	Labnet
Heating/shaking block	Thermomixer R	Eppendorf
Imager	GelDoc XR+	Biorad
Incubator shaker	Unitron	Infors HT
Laminar Airflow Bench	LaminAir HBB2472S	Heraeus
Laminar Flow Hood	Herasafe HS18	Heraeus
Light microscope	Eclipse TS100	Nikon
Laser scanning microscope	LSM 510 Meta	Zeiss
Light/fluorescence microscop	Axiovert 200	Zeiss
LightCycler	480 System	Roche

Magnet stirring bar retriever	MR3001	Heidolph
Microwave	8018 E	Privileg
pH Meter	CG842	Schott
Platform shaker	Duomex 1030	Heidolph
Refrigerator	Medline	Liebherr
Sonicator	Sonopuls HD2070	Bandelin
Spectrometer	Nanodrop 2000	Thermo Scientific
Table centrifuge	CT 15 RE	Hitachi
Thermocycler	Mastercycler nexus	Eppendorf
transilluminator	UV slider	Intas
Vortex mixer	Vortex Genie 2	Intas
Waterbath	3042	Koetterman

4.2 Materials

4.2.1 Consumables

Table 2 Consumables

Disposables	**Manufacturer**
96 Biosphere® Filter Tips, 0.1 – 10 µl	Sarstedt
96 Biosphere® Filter Tips, 2 – 20 µl	Sarstedt
Autoclave tape, 50 m	Brand
Cell Scraper 25 cm	Sarstedt
Cuvettes, 10 x 4 x 45 mm	Sarstedt
Delicate Task Wipes – White	Kimberly-Clark
Folded Filters (Qual.), Ø 240 mm	Sartorius
Micro tube, 1.5 ml	Sarstedt
Microscope Cover Glasses, Ø 22 mm	Thermo Scientific
Microscope Slides, 25 x 75 x 1.0 mm	Thermo Scientific
Multiply -Pro cup, 0.2 ml	Sarstedt

Nitril Extra-Sensitive Gloves	Nitrisense
Parafilm “M”	Bemis
Pipette tip, 1000 µl	Sarstedt
Pipette tip, 200 µl	Sarstedt
Pipette tip, 20 µl	Sarstedt
Pipette tip, 10 µl	Sarstedt
SafeSeal micro tube, 2 ml	Sarstedt
Serological pipette, 10 ml	Sarstedt
Serological pipette, 5 ml	Sarstedt
Serological pipette, 2 ml	Sarstedt
TC-Dish 150, Standard	Sarstedt
TC-Flask T25, Stand., Vent. Cap	Sarstedt
TC-Flask T75, Stand., Vent. Cap	Sarstedt
TC-Plate 6 Well, Standard, F	Sarstedt
TC-Plate 12 Well, Standard, F	Sarstedt
TC-Plate 24 Well, Standard, F	Sarstedt
Transfer pipette, 3.5 ml	Sarstedt
Tube, 15 ml	Sarstedt
Tube, 50 ml	Sarstedt
Gel blotting paper	Roth
Nitrocellulose membrane	GE Healthcare
96 wells light cycler plates	Sarstedt
96 wells light cycler plates sealing foils	Sarstedt
Culture-Inserts 2 Well for self-insertion	Ibidi
Cell culture insert 24 well 8.0 µm pore size	Falcon

4.2.2 Chemicals

Table 3 Chemicals

Name	Source
6x Loading Dye (LD)	Thermo Scientific
Acrylamide	Roth
Agarose	Bioenzym scientific
Ammonium per sulfate (APS)	Thermo scientific
Ampicillin	Roth
Bovine serum albumin (BSA)	Roth
Bromphenol blue	Pharmacia Biotech
Chloroform	Merck
Crystal violet	Roth
Diamidino-2-phenylindol Dihydrochlorid (DAPI)	Roth
Dimethyl sulfoxide (DMSO)	Sigma
Dithiothreitol (DTT)	Roth
Dntps (datp, dgtp, dctp, dttp)	Thermo scientific
Ethanol	Roth
Ethidium bromide (EtBr)	Sigma
Ethylenediaminetetraacetic acid (EDTA)	Roth
Fugene	Promega
GeneRule 1 kilo bases (kb) DNA ladder	Thermo Scientific
Glycerol	Merck
Glycine	Merck
Hydrochloric acid	Fluka
Isopropanol	Merck
Kanamycin	Roth
Lysogeny broth (LB)-agar	Roth
LB-medium	Roth
Mercaptoethanol	Merck
Methanol	Merck
Methylene blue	Sigma
Monopotassium phosphate KH_3PO_4	Merck

Mowiol	Calbiochem
N,n,n',n'-tetramethylethylenediamine (TEMED)	Sigma
PageRuler Prestained protein ladder	Thermo Scientific
Paraformaldehyde (PFA)	Polysciences
Polybrene	Sigma
Polyethylenimine (PEI)	Polysciences
Penicillin/streptomycin	Sigma
Ponceau S solution	Sigma
Potassium acetate	Merck
Potassium chloride	Roth
RNase	Roth
SB431542	Sigma
Skimmed milk powder	Sucofin
Sodium chloride	Thermo scientific
Sodium dodecyl sulfate (SDS)	Merck
Sodium hydroxide	Merck
Sodium phosphate dibasic Na_2HPO_4	Merck
Triethylamine	Sigma
Trizma (TRIS base)	Sigma
Trypsin	Sigma
Trypton	Becton-Dickinson
Tween 20	Roth
Verteporfin	Sigma
Yeast extract	Becton-Dickinson
Zeocine	Invitrogen
Thiazolyl Blue Tetrazolium Bromide (MTT) reagent	Sigma
Bradford Roti-Quant solution	Roth

4.2.3 Antibodies

Table 4 Antibodies used for Western Blot (WB) and Immunofluorescence (IF)

Antigen	Organism	Utilization (Dilution)	Source
Actin	Mouse	WB (1:1000)	Santa Cruz sc-47778
aPKC (PKCζ)	Rabbit	WB (1:500)	Santa Cruz, sc-216
Cdc42	Rabbit	WB (1:200)	Santa Cruz, sc-87
dogE-cadherin	Mouse	WB/IF (1:10)	DSHB #rr1
dogZO-1	Rat	IF (1:10)	DSHB #R26.4C
E-Cadherin	Mouse	IF (1:200)	Santa Cruz, sc-21791
E-Cadherin	Mouse	WB (1:1000)	BD #610181
Pals1	Rabbit	WB/IF (1:1000)	Thermo Scientific PA5-30966
Pals1	Mouse	WB (1:100) /IF (1:200)	Santa Cruz sc-365411
Par3	Rabbit	WB (1:1000)	Millipore 07-330
Par6α	Rabbit	WB (1:100)	Santa Cruz, sc-25525
Par6β	Rabbit	WB (1:500)	Santa Cruz, sc-67392
Par6γ	Rabbit	WB (1:500)	Santa Cruz, sc-85097
Patj	Rabbit	WB (1:1000)	Millipore 07-330
Patj	Rabbit	WB (1:1000)	Abcam ab151257
pYAP	Rabbit	WB (1:1000)	Cell signaling 4911
Smooth Muscle Actin (SMA)	Mouse	WB (1:100)	Abcam ab7817
Vimentin	Mouse	WB (1:200)	Santa Cruz sc-32322
YAP	Rabbit	WB (1:1000)/ IF (1:400)	Cell signaling 4074

Table 5 Secondary antibodies for Western Blot

Sec. Antigen	Organism	Dilution	Source
Anti-rabbit horseradish peroxidase (HRP)	Donkey	1:10000	Invitrogen
Anti-mouse HRP	Donkey	1:10000	Invitrogen

Table 6 Secondary antibodies for Immunofluorescence

Sec. Antigen	Organism	Dilution	Source
Alexa Fluor 488-anti Rat	Goat	1:200	Life Technologies
Alexa Fluor 488-anti Rabbit	Donkey	1:200	Life Technologies
Alexa Fluor 488-anti Mouse	Donkey	1:200	Life Technologies
Alexa Fluor 488-anti Goat	Donkey	1:200	Life Technologies
Alex Fluor a 568-anti Rabbit	Donkey	1:200	Life Technologies
Alexa Fluor 568-anti Mouse	Donkey	1:200	Life Technologies
Alexa Fluor 647-anti Rabbit	Donkey	1:200	Life Technologies
Alexa Fluor 647-anti Rat	Goat	1:200	Life Technologies
Alexa Fluor 647-anti Goat	Donkey	1:200	Life Technologies

4.2.4 Enzymes

Table 7 Restriction enzymes

Name	Restriction site	Buffer	Source
AscI	GG/CGCGCC	yellow buffer	Fermentas/Thermoscientific
BamHI	G/GATCC	unique buffer	Fermentas/Thermoscientific
BbsI	GAAGAC/GAAGAC	green buffer	Fermentas/Thermoscientific
BglI	GCCNNNN/NGGC	orange buffer	Fermentas/Thermoscientific
BglII	A/GATCT	orange buffer	Fermentas/Thermoscientific
EcoRI	G/AATTC	unique buffer	Fermentas/Thermoscientific
EcoRV	GAT/ATC	red buffer	Fermentas/Thermoscientific
HindIII	A/GCTT	red buffer	Fermentas/Thermoscientific
NotI	GC/GGCCGC	orange buffer	Fermentas/Thermoscientific
PstI	CTGCA/G	orange buffer	Fermentas/Thermoscientific
SacII	CCGC/GG	blue buffer	Fermentas/Thermoscientific
StuI	AAG/CCT	blue buffer	Fermentas/Thermoscientific
XhoI	C/TCGAG	red buffer	Fermentas/Thermoscientific

Table 8 Enzymes

Name	Source
Accuzyme Polymerase	New England BioLabs
FAST- alkaline phosphatase (AP)	Thermo Scientific
Polynucleotide kinase (PNK)	Thermo Scientific
T4 DNA Ligase	Fermentas
Taq Polymerase	homemade

4.2.5 Oligonucleotides

Table 9 Short hairpin RNA (shRNA) oligonucleotides

Name	Sequence	Source
dogPals1-shRNA-1-F	GATCCCGCATGGTACGCTGACATT TGTTTCAAGAGAACAAATGTCAGC GTACCATGC TTTTTA	Invitrogen designer shRNA, Microsytnth
dogPals1-shRNA-1-R	AGCTTAAAAAGCATGGTACGCTGA CATTTGTTCTCTTGAAACAAATGTC AGCGTACCATGC GG	Invitrogen designer shRNA, Microsytnth
dogPals1-shRNA-2-F	GATCCCAGAGGATAGTAGACAAG TTCTTTCAAGAGAAGAACTTGTCT ACTATCCTCT TTTTTA	designed by DSIR shRNA tool, Microsynth
dogPals1-shRNA-2-R	AGCTTAAAAAAGAGGATAGTAGAC AAGTTCTTCTCTTGAAAGAACTTG TCTACTATCCTCT GG	designed by DSIR shRNA tool, Microsynth
hPals1-shRNA-1-F	GATCCCGCCAGTTCATCATAAGGA AGGTTCAAGAGACCTTCCTTATGA TGAACTGGCTTTTTA	designed by DSIR shRNA tool, Microsynth

hPals1-shRNA-1-R	AGCTTAAAAAGCCAGTTCATCATA AGGAAGGTCTCTTGAACCTTCCTT ATGATGAACTGGCGG	designed by DSIR shRNA tool, Microsynth
hPals1-shRNA-2-F	GATCCCGCTACAGTTCGTAATGAA ATGTTCAAGAGACATTTCATTACG AACTGTAGCTTTTTA	designed by DSIR shRNA tool, Microsynth
hPals1-shRNA-2-R	AGCTTAAAAAGCTACAGTTCGTAA TGAAATGTCTCTTGAACATTTCATT ACGAACTGTAGCGG	designed by DSIR shRNA tool, Microsynth

Table 10 Guide RNA (gRNA) sequences for CRISPR/Cas9 gene deletion

Name	**Sequence**	**Source**
dogPals1-CRISPR1-F	CACC GGCGTAGGCGAGAGGAAG AA	CRISPR design tool, Microsynth
dogPals1-CRISPR1-R	AAAC TTCTTCCTCTCGCCTACGCC	CRISPR design tool, Microsynth
hPals1-CRISPR1-F	CACC GCCCTGGAGATTTGGGCACC	CRISPR design tool, Microsynth
hPals1-CRISPR1-R	AAAC GGTGCCCAAATCTCCAGGGC	CRISPR design tool, Microsynth

4.2.6 Primers for quantitative RT–PCR

Table 11 Primers for quantitative RT–PCR

Gene name	Primer name	Sequence	Source
dogSnail1 (231 bp)	dogSnail1-F	AAGATGCACATCCGAAGCCA	Primer-BLAST NCBI, Microsynth
	dogSnail1-R	GGAGAAGGTTCGGGAACAGG	
dogZEB1 (295 bp)	dogZEB1-F	CAGTCCGGGGGTAATCGTAA	
	dogZEB1-R	TTTGCCGTATCTGTGGTCGT	
dogCyr61 (116 bp)	dCyr61-F	CAATGACAACCTTGAATGCC	
	dCyr61-R	TCTTGGTCTTGCTGCATTTC	
dogCTGF (126 bp)	dCtgf-F	ATGTGCCTCCTCTTTGGAGT	
	dCtgf-R	AGAACTTGACCCAGCCTCAT	
dogBirc2 (124 bp)	dBirc2-F	CTATTACGTGGGTCGCAATG	
	dBirc2-R	CAAGAACTCACACCTGGGAA	
dogPai-1 (134 bp)	dPai1-F	GTGGAGAGAGCCAGGTTCAT	
	dPai1-R	CCGTTGAAGTAGAGGGCATT	
dogGAPDH (125 bp)	dGapdh-F	AGTGGATATTGTCGCCATCA	
	dGapdh-R	TGACAAGTTTCCCGTTCTCA	

hSnail1 (237 bp)	hSnail1-F	AAGATGCACATCCGAAGCCA
	hSnail1-R	CATTCGGGAGAAGGTCCGAG
hZEB1 (242 bp)	hZEB1-F	AGATCAAAGACATGTGACGCAG
	hZEB1-R	TGAGTCCTGTTCTTGGTCGC
hCyr61 (265 bp)	hCyr61-F	GAAGCGGCTCCCTGTTTTTG
	hCyr61-R	TGGTTCGGGGGATTTCTTGG
hCTGF (285 bp)	hCtgf-F	GTGTGCACCGCCAAAGATG
	hCtgf-R	AAACGTGTCTTCCAGTCGGT
hBirc2 (297 bp)	hBirc2-F	CTGGCCATCTAGTGTTCCAGT
	hBirc2-R	TGAATAATTGGTGGGTCAGCAT
hPai-1 (257 bp)	hPai1-F	GACCTCAGGAAGCCCCTAGA
	hPai1-R	ACTGTTCCTGTGGGGTTGTG
hTwist1 (244 bp)	hTwist-F	TCTCGGTCTGGAGGATGGAG
	hTwist-R	TTTTAAAAGTGCGCCCCACG
hLamine A/C (507 bp)	hLam A/C-F	CTCGTCGTCCTCAACCACAGT
	hLam A/C-R	TGCGTACGGCTCTCATCAACT

4.2.7 Sequencing primers and cloning vectors

Table 12 Sequencing primers for cloning vectors

Vector name	Primer	Sequence	Source
pSuperior.puro	pSuperior-copy-seq-F	CTCCCCTACCCGGTAGAA	Microsynth
pX330-U6-Chimeric_BB-CBh-hSpCas9	px-seq-R	CGTCAATGGAAAGTCCCTATTGGCGT	Microsynth
pSpCas9(BB)-2A-Puro (PX459) V2.0	px-seq-R	CGTCAATGGAAAGTCCCTATTGGCGT	Microsynth
CWG	CMV-seq-F	GGCGTGTACGGTGGGAGG	Microsynth
pLX302	CMV-seq-F	GGCGTGTACGGTGGGAGG	Microsynth
pENTR	M13-seq-F	CGTTGTAAAACGACGGCCAG	Microsynth
pENTR	M13-seq-R	CAGGAAACAGCTATGAC	Microsynth

Table 13 Cloning vectors

Vector name	Backbone size (bp)	Vector type	Bacterial resistance in *E.coli*	Selectable markers	Source
pSuperior.puro	4354	Mammalian Expression, RNAi	Ampicillin	Puromycin	Oligoengine
pX330-U6-Chimeric_BB-CBh-hSpCas9	8854	Mammalian Expression, CRISPR	Ampicillin	Zeocine	Addgene, Feng Zhang lab
pSpCas9(BB)-2A-Puro (PX459) V2.0	9200	Mammalian Expression, CRISPR	Ampicillin	Puromycin	Addgene, Feng Zhang lab
CWG	6194	Mammalian Expression	Ampicillin	Neomycin (G418)	Homemade

pLX302	9573	Mammalian Expression, Lentiviral; Gateway Destination vector	Ampicillin	Puromycin	Addgene
pENTR	2351	Gateway entry vector	Kanamycin	-	Thermo Fisher Scientific

4.2.8 Kits

The kits shown in the following table were always performed according to their instructions.

Table 14 Commercially available kits

Kit	**Utilization**	**Source**
Nucleo Bond® PC 20/100	Midi-preparation	Magery-Nagel
Nucleo Spin®Gel and PCR Clean-Up	PCR purification	Magery-Nagel
qScript™ cDNA Synthesis Kit	cDNA Synthesis	QuantaScience™
TRIzol®Reagent	RNA-preparation	lifetechnologies™
RNeasy Mini Kit	RNA-preparation	Qiagen
Western Blot Detection Kit	Developing Western Blot	Advansta
SensiFAST SYBR® No-ROX Kit	RT-PCR	Bioline

4.2.9 Cell culture media and additives

Table 15 Cell culture media and additives

Name	Source
Dulbecco's Modified of Eagle's Culture Medium (DMEM) with 4.5 g/l glucose	Sigma
Roswell Park Memorial Institute Culture medium (RPMI) 1640	Sigma
Fetal calf serum	Life technologies
L-glutamine, 200 mM	Lonza
Penicillin/Streptomycin, 10.000 U/ml + 10.0000 µg/ml	Sigma
Puromycine	Sigma
Neomycin (G418)	Sigma
Zeocin	Invitrogen

4.2.10 Solutions and reagents

Solutions, buffer and media are produced with sterile H_2O and, if necessary, consecutively autoclaved or sterile filtered. The following list contains the composition of all homemade buffers and solutions, which were used. Unless otherwise stated, the following solutions and buffers were stored at room temperature (RT).

Table 16 List of all homemade buffers and solutions

Name	Composition	
10 % Tween 20	41 mM	tween
2 - Yeast extract trypton agar (YTA)	16 %	tryptone
	10 %	yeast extract
	5 %	NaCl
	ad	H_2O
		stored at 4°C

5x SDS loading dye	250 mM	tris base-HCl (pH 6.8)
	30 %	glycerol
	10 %	SDS
	0.02 %	bromophenol blue
	5 %	β-mercaptoethanol
		stored at -20°C
6-DNA loading dye	10 mM	tris base-HCl
	0.03 %	bromophenol blue
Ammonium persulfate	10 %	APS
	ad	H_2O
Ampicillin	1 g	ampicillin
	10 ml	H_2O
		stored at 4°C
Blocking buffer for immunofluorescence		PBTw (pH 7.4)
	5%	BSA
Blocking buffer for Western Blot		Tris-buffered saline (TBS)
	0.1 %	Tween 20
	2.5 %	BSA
	5 %	milk powder
	ad	H_2O (pH 7.5)
		stored 4°C
Buffer TE 1x pH 8.0	5 ml	Tris base-HCl
	1 ml	EDTA
	494 ml	H_2O
Crystal Violet	0.1 %	crystal violet
	10 %	EtOH
	ad	H_2O
Freezing medium	60 %	fresh medium
	30 %	Fetal calf serum (FCS)
	10 %	DMSO
Kanamycin	500 mg	kanamycin
	10 ml	H_2O
		stored 4°C

Laemli buffer 5x	0.01 %	bromophenol blue
	60 mM	tris base-HCl
	5 %	β-mercaptoethanol
	2 %	SDS
	10 %	glycerine
		stored 4°C
LB- medium	1 %	trypton
	0.5 %	yeast extract
	1 %	NaCl
	ad	H_2O
		stored 4°C
LB_0 Plates	10%	tryptone
	5%	yeast extract
	5%	sodium chloride
	15%	agar agar
		pH 7.0
LB_{amp} Plates		LB_0 Plates 100 mg/ml
	100 mg/ml	ampicillin
LB_{kana} Plates		LB_0 Plates 50 mg/ml
	50 mg/ml	kanamycin
Lysis buffer		TNT buffer (pH 7.5)
	0.2 %	Pepstatin A
	0.2 %	Aprotinin
	0.2 %	Phyenylmethylsulfonylfluorid (PMSF)
	0.2 %	Leupeptin
Mild stripping buffer	200 mM	glycine
	1 %	Tween 20
	1%	SDS
	ad	H_2O
		pH 2.2
Mowiol	0.4 g/ml	Mowiol

	1 g/ml	Glycerol
	2%	Tris-HCl (0.2 M)
P1 mini buffer	50 mM	tris base-HCl (pH 8.0)
	10 mM	EDTA
	100 µg	RNase A
	ad	H_2O
		stored at 4 °C
P2 mini buffer	200 mM	NaOH
	1 %	SDS
	ad	H_2O
P3 mini buffer	3 M	potassium acetate
	ad	H_2O
		stored at 4°C
Paraformaldehyde	3.7 %	paraformaldehyde
	in	Phosphate buffered saline PBS (pH 7.4)
		stored at -20°C
PBS 10x pH 7.4	1.37 M	NaCl
	27 mM	KCl
	100 mM	Na_2HPO_4 x 2 H_2O
	18 mM	KH_2HPO_4
	5 mM	glucose
	ad	H_2O
PBTw		PBS (1x)
	0.1 %	Tween 20
PNK buffer 10x	500 mM	Tris-HCl (pH 7.6)
	100 mM	$MgCl_2$
	50 mM	DTT
	1mM	ADP
	1 mM	spermidine
Ponceau-solution	0.1 %	ponceau S

	5 %	glacial acetic acid
SDS loading dye 2x	2.5% (w/v)	SDS
	25 %	Glycerol
	125 mM	tris-HCl
	0.01 %	bromophenol blue
	100 mM	dithiothreitol
SDS-running buffer pH 8.3	380 mM	glycine
	50 mM	tris base
	0.2 %	SDS
	ad	H_2O
		stored at 4°C
T4 ligase buffer 10x	400 mM	Tris-HCl
	100 mM	$MgCl_2$
	100 mM	DTT
	5 mM	Adenosine triphosphate (ATP)
TAE buffer	40 mM	tris base-acetate
	1 mM	EDTA
	0.1%	glacial acetic acid
	ad	H_2O
TBS (pH 7.6)	150 mM	NaCl
	3 mM	KCl
	25 mM	tris base
	ad	H_2O
TBS-T		TBS
	0.1 %	tween 20
TNT buffer	100 mM	tris base-HCl
	150 mM	NaCl
	0.1 %	tween 20
		stored at 4°C
Transfer buffer	200 mM	glycine
	25 mM	Tris base-HCl (pH 6.8)

	20 %	methanol
	ad	H_2O
		stored 4°C

4.2.11 Data bases and software

Table 17 Data bases and software

Data bases and software	**Utilization**
Citavi	Citation program
DnaDynamo	Theoretical cloning
IMAGEJ	Editing pictures, WB Quantifications
LSM Image Browser	Imaging editor for LSM pictures
NCBI	Database for human genes
Microsoft Word 2013	Writing program
Microsoft Power Point 2013	Editing pictures
Thermo Insight	Measurement of protein concentration
Fusion	Chemiluminescence imaging
GelDoc Biorad	Image Analysis of agarose gels
LightCycler 480 software	Software for analyzing Real-Time PCR data
NanoDrop 2000	DNA/RNA measurement
DSIR	shRNA target design
E-CRISPR	CRISPRs: designing gRNA

IV.III Methods

4.3 Cloning

4.3.1 Oligonucleotide hybridization for shRNA (gRNA)

To obtain stable cell line showing the downregulation or knockout of the gene of interest, the shRNA vectors/ gRNA CRISPR vectors have to be constructed. First, the most promising shRNA's/ gRNA are chosen using the shRNA/gRNA designing tools, as it is an essential step for identification of active shRNA/gRNA sequences. Than short pieces of synthetic single-stranded DNA with defined chemical structure, complementary to the target mRNA/gDNA, have to be synthetized and fused to double-stranded subsequent shRNA/gRNA. This short RNA molecule can afterwards bind target mRNA/gDNA and inactivate it, which in turn causes sequence-specific gene silencing or knockout.

Oligonucleotide hybridization implicates oligonucleotide phosphorylation, denaturation of all secondary structures and final annealing of complementary strands.

Reagents

- T4 PNK
- 10x T4 Polynucleotide Kinase reaction buffer
- ATP 10 mM

Procedure

1. For each shRNA/ gRNA it was mixed together in PCR-tubes

   20 µl total volume:

   8 µl oligo F (100µM)

   8 µl oligo R (100µM)

   2 µl 10 x PNK buffer

   1 µl 10 mM ATP

   1 µl PNK

2. Further ligation was performed according to the program below

   1 h - 37 °C

   5 min - 95 °C

   10 min - cool down from 95 to 20 (-1°C, 70 cycles)

   20 min - 65 °C

4.3.2 Polymerase chain reaction (PCR)

PCR is a method used to amplify a selected piece of DNA. Utilizing the enzyme, called polymerase, the DNA fragment can be multiplied from the template - dsDNA containing the sequence of the gene of interest. To start the reaction, the dsDNA has to be uncoiled to get ssDNA, applying a drastic increase of temperature. This step called denaturation. Afterwards the temperature is reduced, allowing the 5'-3' forward and 3'-5' reverse primers to bind to ssDNA and then the polymerase can elongate the defined fragment. These three steps are repeated 20-40 times giving subsequently specific DNA fragment. In this thesis conventional PCR technic was used to obtain DNA sequence, encoding the gene of interest, to rescue the knockdown (KD) or knockout (KO) mutants.

Reagents

- 10x Taq polymerase buffer
- dNTPs (dATP, dCTP, dGTP and dTTP) 10 mM
- Taq polymerase
- Forward primer 50 µM
- Reverse primer 50 µM
- DNA template 50-500 ng

Procedure

1. For each PCR reaction it was mixed in PCR-tubes

   25 µl total volume:

   16 µl H_2O
   2.5 µl 10x Taq polymerase buffer
   1 µl Primer forward
   1 µl Primer reverse
   1 µl dNTPs
   1 µl Taq polymerase
   0.5 µg Template

2. Further PCR was performed according to the program below

   5 min - 95 °C Initial denaturation

30 s - 95 °C Denaturation
30 s - 55 °C Annealing
1 – 2 min/kb - 72 °C Elongation
} x 30 cycles

15 min - 72 °C Final elongation
Infinite - 10 °C storage

4.3.3 Vector preparation

To allow subsequent ligation of the insert into the certain vector, it has to be accordingly "prepared". Cloning by restriction digest is one of the most common methods in molecular biology. To be able to clone the desired insert into a cloning or expression vector, both have to be digested or formerly designed (i.e. shRNA) to create compatible ends. It is highly recommended to cut the vector with two enzymes; otherwise, the risk of re-ligation is pretty high. To minimize it, the ends of the vector have to be dephosphorylated using alkaline phosphatase. To remove the nicked, supercoiled and undigested rests, the vector after digestion and dephosphorylation has to be purified by agarose gel electrophoresis.

4.3.4 Plasmid digestion

Reagents

- Restriction enzymes (BglII+HindIII for pSuperior.puro, BbsI and EcoRI for px330 and px459, KpnI for plx302 and CWG-TO)
- Compatible restriction buffer 10x
- Plasmid

Procedure

In order to cut off the vector 1 µg plasmid, 4 µl buffer and 2 µl enzyme were mixed well and the samples were then incubated over night at 37°C. On the next day, the digested vector was purified by methylene-blue stained agarose gel.

4.3.5 Agarose gel electrophoresis

Gel electrophoresis is used after the PCR to isolate PCR-products, after the plasmid digestion to purify the digested vector and for control digestion of the

plasmid DNA. The agarose gels for PCR-products and vector purification are stained with methylene blue, whereas the gels showing the result of plasmid DNA control digestion are stained with ethidium bromide (EtBr). These chemical agents incorporate into dsDNA and may then be visible in the gel (methylene blue) or visualized under ultraviolet light (EtBr). To determine the molecular size of the DNA product molecular weight markers are used. These markers contain a mixture of proteins of known sizes and are stained as well.

Reagents

- Agarose
- 1 x TAE buffer
- Ethidium bromide (10 mg/ml)
- 6 x DNA Loading Dye Solution
- Gene Ruler 1kb DNA ladder

Procedure

1. 0.7 g agarose was boiled with 70 ml 1 x TAE-Buffer
2. 20 µl of ethidium bromide were added to the melted agarose
3. Gel was then poured in the gel holder and the gel comb was inserted
4. The gel had to polymerize for 1 h at room temperature
5. The gel was placed in the gel box (electrophoresis unit) and fully covered with 1x TAE-Buffer; the gel comb was removed
6. 4 µl of the loading dye were added to 20 µl of each sample
7. 10 µl of the DNA ladder standard solution and the samples were then placed in the wells
8. The electrophoresis was performed for approximately 30 min at 130 V
9. The bands were visualized with methylene blue or under UV light, when EtBr was added

4.3.6 Purification of vector/PCR product

After the methylene-blue staining, the required bands were cut out as accurate as possible and transferred into a 1.5 ml Eppendorf tubes. Afterwards the desired DNA fragments were purified with Nucleo Spin®Gel and PCR Clean-Up Kit according to the manufacturer instructions.

4.3.7 Vector dephosphorylation/PCR product digestion

In order to avoid the re-ligation of the digested and purified vector, the 5' end has to be dephosphorylated. To allow the insertion of the PCR product into the purified vector the insert was digested to obtain the sticky ends.

Reagents

- Purified vector/ PCR product
- FAST-AP/ restriction enzymes
- 10x FAST-AP buffer/ 10x appropriate restriction enzyme buffer

Procedure

1. 26 µl of the purified vector/ PCR product were mixed with 3 µl of the appropriate buffer and 1 µl FAST-AP/ 2 µl of each restriction enzyme
2. The mixture was incubated for 30 minutes to 2 hours at 37°C before the enzymes were inactivated for 20 minutes at 75 °C

4.3.8 Ligation

In the last step of the cloning procedure, the ligation of insert and vector followed.

Reagents

- T4 Ligase
- T4 Ligase buffer
- Vector
- Insert

Procedure

Three ligations were set up according to the table 18. The ligations were incubated 3 hours at RT or overnight at 16 °C and then transformed into cells as explained in 4.3.10.

1. The ligation mixture was set up according to the Table 18.

Table 18 Setup for insert - vector ligation

	control	**ligation 1:1**	**ligation 1:4**
H_2O_{dd}	17.3 µl	16.8 µl	15.3 µl
T4 ligase buffer	2 µl	2 µl	2 µl

Insert	0.5 µl	0.5 µl	0.5 µl
Vector	-	0.5 µl	2 µl
T4 ligase	0.2 µl	0.2 µl	0.2 µl

4.3.9 CRISPR/Cas9 cloning

In contrary to the normal cloning method, the Clustered regularly interspaced short palindromic repeats (CRISPR)/CRISPR associated protein 9 (Cas9) cloning underlines the combination of cutting of vector technique and simultaneous ligation process.

Reagents

- Px330/459 plasmid
- Annealed phospho-oligos F+R
- T4 ligation buffer
- BbsI
- T4 ligase

Procedure

1. For each gRNA, the reaction mix was prepared in an Eppendorf tube

50 ng	px330/px459 plasmid
0.5 µl	annealed phospho-oligo F+R
1 µl	10x T4 ligation buffer
0.5 µl	BbsI
0.5 µl	T4 ligase
up to 10 µl	H_2O

2. Further ligation/digestion was performed according to the program below

5 min - 37 °C
5 min - 23 °C
5 min - 37 °C
5 min - 23 °C } x 30 cycles
Infinite - 10°C

4.3.10 Transformation of chemically competent *E. coli* cells – DH5 alpha

The goal of this method is to transfer a desired ligated plasmid into bacterial cells in order to cultivate them and thereby amplify the amount of the plasmid. In this study, only *E.coli* DH5alpha cells were used for transformation. By $CaCl_2$ or $MgCl_2$ incubation, the cells became competent and thus the cell membrane was permeable for plasmid DNA.

Regents

- Competent *E. coli* cells – DH5 alpha
- Vector (ligation mix)
- LB-plates

Procedure

1. DH5 alpha competent *E. coli* cells were thawed on ice
2. 20 µl of plasmid DNA were added to the cell mixture and flicked
3. The mixture was placed on ice for 30 min
4. Heat shock was performed exactly at 42 °C for exactly 1 min
5. The mixture was placed on ice for 5 min
6. 200 µl of prewarmed LB-medium were pipetted into the mixture
7. The mixture was shacked for 30 min at 37°C to allow to double and to recover
8. The mixture was spread onto a selection plate and incubated overnight at 37°C

4.3.11 DNA-preparation

The main goal of molecular cloning is to assemble recombinant DNA and introduce it into the host organisms. The transformation process is used to amplify vector DNA and to select the cells containing the vector of interest. Thus, the first part of DNA preparation is picking the cells form plate. Afterwards picked colonies were inoculated and amplified by adding 2 ml LB-medium. After growing overnight, the Mini-preparation and following Midi-preparation were used to isolate desired plasmid DNA.

4.3.12 Mini-preparation

The Mini-preparation of the plasmid DNA is a small-scale isolation of plasmid DNA from bacteria to test the construct for its propriety.

Reagents

- P1 mini-buffer
- P2 mini-buffer
- P3 mini-buffer
- 100 % EtOH
- 70 % EtOH

Procedure

1. 1.5 ml of overnight culture were poured into the tubes and centrifuged for 1 min at 6000 rpm
2. The pellet was resuspended in 100 µl buffer P1
3. 200 µl of P2 buffer were added
4. Following addition of 150 µl P3 buffer, the tubes were inverted 3-4 times
5. The samples were centrifuged for 6 min at 14000 rpm at 4°C
6. New tubes with 900 µl of 100 % EtOH were prepared
7. The supernatant was transferred into the new tubes with EtOH and mixed
8. The samples were centrifuged for 12 min at 15000 rpm at 4 °C
9. The pellets were washed with 1 ml 70% EtOH and centrifuged for 3 min at 14000 rpm
10. The pellets were dried at 65°C in incubator and dissolved in 25 µl H_2O_{dd}

4.3.13 Restriction digestion

The restriction digestion is used after mini-preparation, in order to verify the accuracy of molecular cloning. Restriction enzymes are cutting the purified in 4.3.12 plasmid DNA in a site-specific manner. After the separation by agarose gel, different band pattern should occur depending on the assembly of the insert. On the one hand, it should be proved whether the insert was assembled into the vector and on the other hand whether the direction of the insert is correct. Thus,

the specific restriction enzymes have to be chosen. For this reason, it is important to find unique restriction sites, which occur in the insert and in the cloned vector as well. After determination of appropriate restriction enzymes, the following master mix has to be prepared per each Mini-purified plasmid DNA (Table 19).

Table 19 Master mix composition for restriction digest

	Amount
Appropriate buffer	2 µl
Each restriction enzyme	0.3 µl
ad H_2O	20 µl

For CRISPR/ Cas9 (px330/459) and pSuperior.puro vectors, upon successful cloning of gRNA or shRNA, BbsI and BglII cutting sites respectively are destroyed, so those purified plasmids cut by these enzymes will not contain the insert fragment, thus making the restriction digestion for these vectors and further positive clone selection much easier.

The control digestion of the purified Mini-samples is followed by EtBr-containing agarose gel electrophoresis and consecutive band pattern could be verified in transilluminator under UV light.

Restriction digestion enzymes for each plasmid and band patterns are shown in Table 20.

Table 20 Restriction digestion enzymes and band patterns for each plasmid

Plasmid	Restriction enzymes	Expected positive band sizes
pSuperior.puro for all shRNAs‘s	PstI, BglII	ca. 4600 bp
pX330-U6-Chimeric_BB-CBh-hSpCas9 for gRNA’s	BbsI, EcoRI	ca. 9000 bp
pSpCas9(BB)-2A-Puro (PX459) V2.0 for gRNA’s	BbsI, EcoRI	ca. 8500 bp+700 bp
pLX302 for over-expression	XhoI	ca. 7000 bp+2000 bp+ 650 bp

pENTR gateway	StyI, NotI	ca. 1800 bp+2800 bp

Afterwards, the positive clones could be inoculated for further Midi-preparation. For this purpose, 55 ml LB-medium and 55 µl of antibiotics (ampicillin/kanamycin) were filled in a volumetric flask and after that 10 µl of the positive clones of the Mini-preparation were added. The culture was incubated overnight at 37 °C with continuous agitation.

4.3.14 Midi-preparation and sequencing

After overnight incubation, the Midi-cultures were spun down and purified with Nucleo Bond® PC 20/100 kit according to the manufacturer instructions and sent to Microsynth AG for further sequencing.

4.4 Cell culture

4.4.1 Cell line propagation

The cell lines and media used are listed in Table 21. Cells were maintained in standard medium supplemented with 100 units/ml penicillin, 100 µg/ml streptomycin and 10 % fetal calf serum (FCS), which is inactivated by centrifuging at 3000 g 10 min prior to addition to the medium. All cell lines were grown at 37 °C in a cell incubator in a 5 % carbon dioxide/100 % humidity atmosphere. When confluence was reached, cells were sub-cultured upon trypsinisation. After detachment, the cells were resuspended in standard medium and seeded at the desired dilution in the new culture flasks. For storage in liquid nitrogen, the cells were frozen in a solution composed of 60 % nutrition medium, 30 % FCS and 10 % DMSO.

Table 21 Cell lines and corresponding culture media with supplements

Cell line	**Origin**	**Characteristics**	**Medium**
HCT116 ATCC: CCL-247	Human, Colorectal carcinoma Dukes D stage	Epithelial, adherent	DMEM 4.5 g/l Glucose + 10 % FCS
HCT116 Scrbld	Human, Colorectal carcinoma, with a nonsense / scrambled sequence as negative control	Epithelial, adherent	DMEM 4.5 g/l Glucose + 10 % FCS + 0.5 µg/ml puromycine
HCT116 hPals1 sh1	Human, colorectal carcinoma stable cell line showing the downregulation of Pals1 expression by hPals1 shRNA1	Epithelial, adherent	DMEM 4.5 g/l Glucose + 10 % FCS + 0.5 µg/ml puromycine
HCT116 hPals1 sh2	Human, colorectal carcinoma stable cell line showing the downregulation of Pals1 expression by hPals1 shRNA2	Epithelial, adherent	DMEM 4.5 g/l Glucose + 10 % FCS +0.5 µg/ml puromycine

HCT116 ΔhPals1	Human, colorectal carcinoma, showing the knockout of Pals1	Epithelial, adherent	DMEM 4.5 g/l Glucose + 10 % FCS +100 µg/ml zeocine
HCT116 ΔhPals1+ hPals1	Human, colorectal carcinoma, showing the rescue of Pals1 expression in a HCT116 ΔhPals1 cell line	Epithelial, adherent	DMEM 4.5 g/l Glucose + 10 % FCS + 0.5 µg/ml puromycine
MDCK ATCC: CCL-34	Canine kidney, normal, non-cancer	Epithelial, adherent	DMEM 4.5 g/l Glucose + 10 % FCS
MDCK Scrbld	Canine kidney cell line, with a nonsense / scrambled sequence as negative control	Epithelial, adherent	DMEM 4.5 g/l Glucose + 10 % FCS + 1 µg/ml puromycine
MDCK dogPals1 sh1	Canine kidney cell line, showing the downregulation of Pals1 expression by dogPals1 shRNA1	Epithelial, adherent	DMEM 4.5 g/l Glucose + 10 % FCS + 1 µg/ml puromycine
MDCK dogPals1 sh2	Canine kidney cell line, showing the	Epithelial, adherent	DMEM 4.5 g/l Glucose + 10 %

	downregulation of Pals1 expression by dogPals1 shRNA2		FCS + 1 µg/ml puromycine
MDCK ΔdogPals1	Canine kidney cell line, showing the knockout of Pals1	Epithelial, adherent	DMEM 4.5 g/l Glucose + 10 % FCS + 1 µg/ml puromycine
DLD1 ATCC: CCL-221	Human, Colorectal carcinoma, Dukes C stage	Epithelial, adherent	RPMI + 10 % FCS
DLD1 ΔhPals1	Human, colorectal carcinoma, showing the knockout of Pals1	Epithelial, adherent	RPMI + 10 % FCS + 1 µg/ml puromycine
HEK 293T ATCC:CRL-3216	Human, embryonic kidney	Epithelial, adherent	DMEM 4.5 g/l Glucose + 10 % FCS

4.4.2 Transfection

Transfection is a powerful biological tool that enables the study of the particular gene role and its products in the cell. Mammalian cell transfection is a technique commonly used to deliver and express exogenous DNA or RNA in a host cell line and genetically modify it. There are two primary categories of cell transfection: transient and stable. Unlike transient transfection, in which introduced DNA persists in cells only for some days, stable transfection introduces foreign nucleic acid into cells for a long term and usually has a marker gene for selection, to maintain the permanent DNA integration into the host genome. Genetically modified cell lines, used in this thesis, are stable cell lines and were created either by conventional liposome/lipid-mediated transfection or by lentivirus-mediated gene delivery (transduction).

4.4.3 Conventional liposome/lipid-mediated transfection

Liposomes are synthetic analogs, characterized by the hydrophobic and hydrophilic regions. Under aqueous conditions, these molecules can encapsulate free nucleic acid, fuse with a cell membrane and deliver DNA or RNA into the cell. As an alternative to liposomes, some lipids and polymers are able to form micelles with encapsulated foreign nucleic acid and also bring them into cultured cells. All genetically modified cell lines in this thesis, showing the knockdown or knockout of the gene of interest were created as follows.

Reagents

- DMEM w/o FCS and any additives
- Fugene HD Transfection Reagent
- Plasmid

Procedure

1. One day before transfection the cells were counted in the Neubauer chamber, adjusted to 300 000 cells/ml and seeded one ml per well in a 6-well plate
2. 150 µl of DMEM medium w/o FCS were added to a sterile Eppendorf tube together with 1 µg of the plasmid and vortexed
3. 3 µl of Fugene (DNA: Fugene = 1:3) were added, vortexed briefly and the mix was incubated for 15 min at RT
4. The Fugene/DNA mixture was added drop-wise to the cells
5. Next day the cells were transferred to a bigger plate and selection antibiotics were added. The medium was replaced every 3-4 days till the colonies grew
6. The colonies were picked and verified for an expected phenotype via Western blot or immunofluorescence

4.4.4 Lentivirus-mediated gene delivery (transduction)

The use of viruses to deliver the plasmid DNA into the cell is an alternative and more efficient method for mammalian cell transfection, as not every cell line is equally good amendable for conventional transfection. In this study, lentiviral transduction was used to create the rescue of the mutant knockout phenotype by re-expression of the corresponding gene.

Reagents

- HEK 293 T cells
- PEI 1 mg/ml in H_2O
- DMEM Medium w/o FCS and additives
- Lentiviral Plasmid
- Viral envelope expressing plasmid pMD2.G
- Lentiviral packaging plasmid pCMVΔR8.2
- Polybrene 100 mg/ml in PBS

Procedure

I. Virus preparation

1. HEK 293T cells were plated one day before the transfection so that they were approximately 80% confluent a day after

2. Next morning, the medium was replaced with 20 ml of DMEM without FCS and antibiotics

3. DNA was mixed together with DMEM and PEI in a final volume of 1380 µl

DMEM Ø FCS	to 1380 µl
Lentiviral Plasmid	15 µg
pMD2.G	3.75 µg
pCMVΔR8.2	11.25 µg
PEI	120 µl

4. The mixture was vortexed for 10 sec, incubated for 10 min at RT and afterwards the DNA/PEI mixture was added drop-wise to the cells

5. Cells were incubated for 4-6 hours at 37°C

6. Afterwards the medium was replaced with 30 ml of DMEM/10% FCS

II. Virus collection

7. After 48 to 72h the supernatant was collected into 50 ml tube

8. The supernatant was spun down for 15 min at 3000 g

9. The supernatant was transferred into new special centrifuge tube

10. Virus particles were pelleted for 2 h at 75.000 g at 4°C

11. The pellet was marked and the supernatant was discarded

12. The pellet was dissolved in 150 µl DMEM/10% FCS by gentle pipetting

13. The tubes were left on ice at 4°C overnight

14. Next morning the virus was carefully pipetted up and down a few times and frozen in small aliquots (a 30-50 µl) at -80°C

III. Transduction of target cells

15. The day before transduction, target cells were plated to be around 50-60% confluent on the day of transduction

16. Next morning the old media was replaced with 20 ml of DMEM/10% FCS

17. 20 µl Polybrene (8 mg/ml) and 50 µl of the virus were simultaneously drop-wise pipetted to the plate

18. 4-6 h after the medium was replaced with the new ones DMEM/10% FCS still w/o selection antibiotics

19. Next day the medium was replaced again and selection antibiotics were added. The medium was replaced every 3-4 days till the colonies grew

20. The colonies were picked and verified for an expected phenotype via Western Blot or immunofluorescence

4. 5 Cell proliferation and invasion assays

4.5.1 MTT cell proliferation assay

This colorimetric assay is based on the ability of mitochondrial enzyme succinate dehydrogenase to reduce the yellow 3-(4,5-dimethythiazol-2-yl)-2,5-diphenyl tetrazolium bromide (MTT) to colored (dark purple) formazan. When MTT enters the cells and passes into the mitochondria, the above-mentioned reaction proceeds. The cells are then solubilized with an organic solvent and the released formazan is measured spectrophotometrically. Since MTT is reduced only by live cells, the level of activity is a measure of the cell viability and proliferation.

Reagents

- MTT (5 mg/ml in PBS)
- Dimethyl sulfoxide

Procedure

1. The cells were seeded 50000 cell/well in 12 well plate in triplicates for 6 days

2. One well for a blank w/o cells was prepared by putting only medium inside

2. 24 h after the medium was removed from the plate for the first day and 500 µl of the new medium were added to each well (including blank well)

3. 100 µl of MTT were added per well, including blank well and incubated for 30 min at 37°C

4. The supernatant was removed from the plate, 500 µl DMSO were added per well and shacked for 10 min on a shaker

5. The cuvettes for each sample in triplicates and for a blank were prepared

6. 900 µl H_2O were added into each cuvette

7. 100 µl from each well were pipetted to the cuvettes in triplicates and mixed

9. The procedure was repeated on the day 2 to 6. The extinction was measured at 570 nm in a photometer. Cell proliferation was then calculated through on all days in comparison to the control sample

4.5.2 Transwell cell migration assay

The transwell migration assay known also as the Boyden or modified Boyden chamber assay is a widely distributed method to investigate the migratory response of cells investigated. Boyden chamber represents a cylindrical cell insert with a semipermeable polycarbonate membrane with defined pore size. Cells are placed in the top of the insert in serum-free media, while serum-containing media is covering the well below. The cells are then moving through the pores towards the FCS (chemoattractant) below. Afterwards migratory cells are stained and their number is determined.

Reagents

- DMEM w/o FCS
- DMEM + 20 % FCS
- Paraformaldehyde 3.7 % in PBS
- DAPI 1 mg/ml
- Methanol ice cold

Procedure

1. The migration chambers were put into 24-well plate

2. 100 µL serum-free medium were added in the chamber

3. 200 µL of the cell suspension were placed in the chamber ($2.5*10^5$/mL in serum-free medium)

4. 750 µL of the culture medium (with serum) were added in lower chamber
5. Migration chamber was put into the lower well
6. The samples were incubated at 37°C for 12-16 hours
7. Afterwards the medium was removed
8. The migration chamber was washed twice with PBS
9. The cells were fixed by paraformaldehyde for 2 min at RT
10. The migration chamber was washed twice with PBS
11. The cells were permeabilized by 100 % methanol for 10 min at RT
12. Methanol was removed and the chamber was washed twice with PBS
13. The cells were stained with DAPI (1:1000 in PBTw) at RT for 15 min
14. The stain was removed and the chamber was washed twice with PBS
15. Non-migrated cells were scraped off with cotton swabs
16. Migrated cells were counted under microscope

4.5.3 Scratch/wound healing assay

An additional method to describe the cell migration pattern is scratch/wound healing assay. During this test, the cells were grown to a confluence and the "wound" was then created by scratching in the middle of the monolayer with a pipette tip. Immediately after, the picture of the "wound" was taken, determining a zero time point. The "healing" of the gap by cell migration towards the center of the gap was observed and documented at the defined time points. Another opportunity to create the "wound" is the use of special cell inserts (culture-insert 2 well, Ibidi) according to the manufacturer instructions.

4.5.4 Soft Agar Colony Formation Assay

One of the most notable hallmarks of carcinogenesis is the ability of cancer cells to grow without attaching to a solid surface. Soft agar colony formation assay shows whether investigated cells are able to grow in semi-solid matrices and provides an ideal tool to examine cell transformation *in vitro*. Additionally, this assay enables to observe probable changes in a cell behavior comparing the control and genetically modified cell lines.

Reagents

- 1 % agarose and 0.6 % agarose in H_2O_{dd}
- 2xDMEM with 20 % FCS and 2 % Penicillin/Streptomycin

- 0.1 % Crystal Violet in 10 % EtOH

Procedure

I. Preparation of Base Agarose

1. 1 % agarose and 0.6 % agarose were prepare in H_2O_{dd} and autoclaved
2. 1 % agarose was melted in a microwave and cooled down to 40 °C in a water bath
3. 2x DMEM with 20 % FCS and 2 % P/S was prepared and prewarmed to 40 °C in a water bath
4. 6 ml of 2x DMEM were mixed with 6 ml 1 % agarose and added 1.5 ml/well in a 6-well plate
5. The plates were at RT for 10-30 min to solidify

II. Preparation of Top Agarose

1. Cell samples were prepared by trypsinizing cells and counting them. An aliquot of each sample with a concentration of $1x10^4$ cells/ml was made. Each aliquot was kept at 37 °C for 10-20 min
2. 0.6 % agarose was melted in a microwave and cooled down to 40 °C in a water bath
3. 3 ml of cell suspension in 2x DMEM were mixed with 3 ml 0.6 % agarose. 1 ml of the mixture was pipetted into the well and allowed 15 minutes to solidify
4. 1 mL 1x full media was added to each well
5. Plates were incubated at 37 °C in humidified incubator for 28 days
6. Cells were fed once - twice per week

III. Staining

1. The cells were stained with 0.5 mL 0.1% Crystal Violet in 10% EtOH for 10 min
2. Crystal violet was washed off by adding 1-2 mL water to soft agar 4-5 times
3. Colonies were imaged on a dissecting microscope and counted

4.6 Western Blot

4.6.1 Western Blot and SDS-PAGE sample preparation

Polyacrylamide gel electrophoresis (PAGE) is one of the most common analytical techniques used to separate proteins. Proteins can be separated on polyacrylamide gels on the basis of their electrophoretic mobility. To separate the

band(s) of interest, different polyacrylamide gel concentrations are used. To obtain optimal resolution of proteins, two gels are used: a ‘stacking’ gel is cast on the top of the ‘resolving’ gel. The stacking gel has a lower concentration of acrylamide, lower pH and a different ionic content. This allows the proteins in the samples to be concentrated into a tight band before entering the resolving gel.

Sodium dodecyl sulfate (SDS) is an amphipathic detergent and binds non-covalently to proteins, prompting protein denaturation and disassociation from each other while conferring a negative charge. The addition of β-mercaptoethanol-containing sample buffer disrupts disulfide bridges within polypeptides. Furthermore, secondary and tertiary structures are lost after 5 minutes of protein-boiling.

Reagents

- 5x Loading buffer
- Ammonium persulfate (APS) (10 %)
- β-mercaptoethanol or DTT 1 M
- TNT lysis buffer with protease inhibitors
- Bradford solution 1:5 in H_2O_{dd}
- Stacking gel buffer: Tris-HCl (1 M, pH 8.8)
- Resolving gel buffer: Tris-HCl (1 M, pH 6.8)
- Electrophoresis buffer (5x) (0.12 M Tris base, 0.96 M glycine, 0.5% SDS, pH 8.3)
- Acrylamide/Bisacrylamide (30%)
- TEMED
- Prestained protein ladder

Procedure

1. The cells were grown in 10 cm dishes till 80% of confluence
2. If required, the cells were starved overnight and FCS was added for 1 h
3. 1 % β-mercaptoethanol or 200 µM DTT were added to the sample buffer
4. The cells were detached with the help of a cell scraper and gathered into an Eppendorf tube
5. The culture medium was discarded after centrifugation and 60-100 µl of TNT lysis buffer with supplements were added
6. The cells had to lyse 20 min on ice

7. The samples were sonicated for 10 s
8. The samples were spun down for 10 min at 15000 rpm
9. The supernatant was transferred into a new tube
10. 1 µl of the sample was measured with Bradford reagent and all samples were adjusted with TNT buffer to the same protein amount in 16 µl and 4 µl of 5x sample buffer were added
11. The samples were boiled at 95 ˚C for 5 min to denature them
12. The glass gel plates were rinsed with 70 % ethanol and placed in the gel holders
13. The reagents for the four 10 % resolving gels were mixed according to Table 22, pipetted between the glass plates, layered with isopropanol and left for 30 min for polymerization

Table 22 Polyacrylamide gel composition

10% resolving gel		**4% stacking gel**	
Water	9.8 ml	**Water**	7.2 ml
1 M TrisHCl, pH 8.8	14 ml	**1 M TrisHCl, pH 6.8**	1.2 ml
Acrylamide 30%	12.2 ml	**Acrylamide 30%**	1.6 ml
SDS 10%	350 µl	**SDS 10%**	100 µl
APS 10%	185 µl	**APS 10%**	52 µl
TEMED	30 µl	**TEMED**	20 µl

14. The water was removed and 4 % stacking gel was applied (see Table 22) to the top of the polymerized resolving gel
15. The combs were placed in the gel and the gel was allowed to polymerize for 30 min
16. The glass plates containing the polymerized gel were removed and placed into the electrophoresis chamber
17. The chamber was filled with 1x electrophoresis buffer
18. 7 µl of molecular weight marker and 20 µl of the samples were pipetted into the gel slots
15. The electrophoresis was conducted at 180 V for 90-120 min

4.6.2 Western Blot

The first step in the Western blotting procedure is the separation of proteins using gel electrophoresis. Thereafter, the separated molecules are transferred onto a second matrix, a nitrocellulose membrane, utilizing electrical fields. Since the protein-bound SDS is washed out in this step, the proteins regain their original primary, secondary, and tertiary structure to some extent. Next, the membrane is blocked with protein solutions containing bovine serum albumin or fat-free milk powder to prevent any nonspecific binding of antibodies to the surface of the membrane. Thereafter primary and secondary antibodies are added one by one. Primary antibody binds the target protein, whereas the secondary antibody, conjugated to the enzyme horseradish peroxidase, allows the detection. Horseradish peroxidase converts substrate (Advansta solution) into its oxidized form, which then can be detected in chemiluminescence analyzer.

Reagents

- Transfer buffer
- Ponceau S solution
- Tris-buffered saline (TBS) -buffer (20x):
- TBS/T buffer (1x): TBS, 0.1% Tween 20
- Blocking buffer
- Primary antibody in blocking buffer at desired concentration (see Table 4)
- Secondary antibody in blocking buffer (see Table 5)
- Detection solution

Procedure

1. The filter paper and nitrocellulose membrane were adjusted to match the gel size
2. The membrane, gel blotting paper, and sponges were moistened in transfer buffer
3. Gel blotting paper, nitrocellulose membrane, gel and sponges were taken together to form a blotting sandwich
4. The blotting sandwich was placed in the blot module with the gel facing the cathode side, and the membrane facing the anode side

5. The module was filled up with transfer buffer
6. The blotting process was performed for 80 min at 100 V
7. The membrane was placed in a Ponceau S solution to check the proper blotting and to visualize the blotted proteins
8. The membrane was washed with distilled water
9. The rests of the Ponceau S solution were washed away from the membrane in TBS/T buffer and then rinsed with distilled water
10. The membrane was incubated in 10 ml blocking buffer for 1 h at room temperature
11. The membrane was incubated with the primary antibody at 4 °C overnight
12. The membrane was washed 3x 5 min each with TBS/T buffer
13. The membrane was incubated with the secondary antibody for 1 h at room temperature
14. The membrane was washed 3x 5 min each with TBS/T buffer
15. The membrane was covered with the detection solution for 1 min and the chemiluminescence was detected by Fusion FX7 imager

4.7 Immunofluorescence

Immunofluorescence is a widely applicable method and allows researchers to visualize the localization, structure or intracellular behavior of antigen directly in a cell or in a tissue section. In this assay, target molecules are captured by the specific primary antibody, which in its turn is able to bind the secondary antibody conjugated to a fluorophore. This fluorophore generates photons and emits light, thus allowing microscope detection of the protein of interest. Use of several fluorophores enables simultaneous detection of multiple proteins and is helpful to gain the knowledge about proteins interaction and their co-localization.

Reagents

- 1x PBS pH 7.4
- 1x PBTw (0.1 % Tween in PBS)
- 1x PBTw + 5 % BSA
- Mowiol
- Methanol 100 %
- PFA 4 % in 1x PBS

- DAPI 1 mg/ml

Procedure

1. The cells were grown on glass coverslips in a 6-well plate
2. The medium was discarded and coverslips were washed with PBS
3. The coverslips were covered either with 4 % PFA in PBS for 20 min at RT or with ice-cold methanol and for 20 min at -20 °C
4. The coverslips were washed three times with PBTw, 10 min each
5. The coverslips were blocked for 30 min - 1 hour in PBTw 5 % BSA
6. The first antibody was incubated in an appropriate dilution overnight in PBTw 5% BSA, covered against light, at 4°
7. The coverslips were shortly washed three times with PBTw
8. The secondary antibodies were incubated in PBTw 5 % BSA 1-2 hours, covered against light, at RT
9. The coverslips were shortly washed three times with PBTw
10. The coverslips were stained with DAPI (1:1000 in PBTw) at RT for 15 minutes
11. The coverslips were shortly washed three times with PBTw
12. Glass slides with a drop Mowiol on it were prepare
13. The coverslips were placed on the glass slides upside down
14. The glass slides were dried at 37° for at least 1h
15. The IFs were visualized using fluorescence microscope

4.8 Real-time PCR

4.8.1 RNA-isolation

To analyze the genes transcribed, RNA isolation and purification was carried out with the help of Trizol (TRI Reagent Solution) reagent. This method can be used not only for RNA isolation but for protein and DNA-isolation as well, as these three compounds are separated in three different phases. After centrifugation, the mixture separates into a lower red phenol-chloroform phase, a white interphase and a colorless upper aqueous phase. RNA is found entirely in the aqueous phase. To prevent the degradation of RNA by RNases, the Trizol reagent contains phenol and guanidine-thiocyanate.

Reagents

- Trizol (TRI Reagent Solution)
- Chloroform
- Isopropanol 100%
- 75% EtOH in diethylpyrocarbonate water
- RNAse free water

Procedure

1. The cells were seeded in 6-well plates, starved overnight, fed in the morning with 20 % FCS for 2 hours and lysed by adding 1 ml Trizol to each sample
2. 200 µl chloroform were added to each sample
3. The samples were mixed for 15 sec and kept at room temperature for 2-3 min
4. The samples were spun down at 4 ºC for 15 min at 12 000 g
5. The top aqueous phase was transferred to a new Eppendorf tube and 500 µl of isopropyl alcohol were added to each sample
6. The samples were mixed briefly and left for 10 min at room temperature
7. The samples were spun down at 4 ºC for 10 min at 12 000 g
8. The supernatant was discarded and 1 ml of 75 % ethanol was added to the pellet
9. The samples were vortexed and centrifuged at 4 ºC for 5 min at 7 500 g
10. The supernatant was removed and the pellet was air-dried for 10 min
11. The pellet was resuspended in 15 µl RNAse free water
12. The samples were frozen for 15 min or overnight at -80 ºC
13. The RNA concentration was measured at Nanodrop

4.8.2 Reverse transcription

For reverse transcription of isolated RNA into cDNA (complementary DNA) the qScript cDNA Synthesis Kit (Quanta Biosciences) was used. This kit provides oligo-dT primer (complementary to the poly-A-tail at the 3'end of the mRNA) and random hexamer primers. Primer annealing to mRNA results in double-stranded DNA/RNA molecules serving as a starting point for DNA synthesis by reverse transcriptase enzymes.

Reagents

- RNase-Free Distilled Water
- 5x qScript Reaction Mix (qScript cDNA Synthesis Kit)
- Reverse Transcriptase (qScript cDNA Synthesis Kit)

Procedure

1. RNase-Free distilled water, the 5x mix and reverse transcriptase were mixed in an Eppendorf tube
2. The calculated amounts of the RNA-sample (1 µg) and RNase-Free distilled water were added to 15 µl of the mixture. The total volume constituted 20 µl
3. The samples were incubated for 5 min at 25 ºC
4. The samples were incubated for 45 min at 42 ºC
5. The samples were incubated for 5 min at 85 ºC
6. The PCR samples were stored at -20 ºC

4.8.3 Real-time PCR

Real-time quantitative PCR provides sensitive, specific and reproducible quantitation of nucleic acids. Real-time PCR enables reliable detection and measurement of products obtained during each cycle of the PCR process. The DNA amount is measured after each cycle by the use of fluorescent markers that are incorporated into the PCR product. In the exponential phase of the reaction, the increase in fluorescent signal is directly proportional to the number of PCR product molecules generated. One of the commonly used fluorescent DNA-binding dyes is SYBR Green. It binds all double–stranded DNA and the increase in fluorescence is detected. SYBR Green has excitation and emission maxima of 494 nm and 521 nm, respectively.

To observe the ’purity’ of the obtained product, check the primer-dimer artifacts and contamination, post-amplification melting curve analysis is performed. To get the melting curves the PCR product is exposed to a temperature gradient. While heating, the dsDNA dissociates and SYBRGreen is released, resulting in a decrease in fluorescence. Thereafter the change of fluorescence with time is plotted against temperature. Contaminating DNA or

primer dimers would appear as an additional peak separated from the desired peak.

For quantification, the detected fluorescence is plotted against the number of PCR cycles, which shows the amplification of the PCR-product in time. As the equivalent of the amount of DNA in each sample, the Ct (threshold cycle) value is determined. The Ct defines the number of cycles required for the fluorescent signal to cross the specified threshold for being detectable. The lower the Ct level the greater the amount of target nucleic acid in the sample, thus Ct levels are inversely proportional to the amount of target nucleic acid in the sample. The Ct of each sample is chosen to be in the exponential phase of the amplification curve.

To determine the concentration of DNA relative to the housekeeping gene GAPDH or Lamin A/C, whose expression remains constant under a wide variety of physiological conditions, the ΔΔCt method is used. ΔΔCt is obtained by deducting the ΔCt value of the reference sample (i.e. control sample) from the ΔCt value of the target sample. ΔCt value is determined by subtracting the Ct value of the sample and Ct value of the housekeeping gene. The relative expression difference between sample and control or reference sample normalized to a housekeeping gene is calculated by using the formula:

$$\text{Relative expression difference} = 2^{-\Delta\Delta Ct}$$

In this thesis, real-time PCR was applied for mRNA expression analysis.

Reagents

- SensiFAST SYBR® No-ROX Kit - SYBR Green QPCR Master Mix
- Primers dissolved in H_2O_{dd}
- cDNA 25 ng/µl

Procedure

1. Separate master mixes were prepared for each sample (the gene of interest and the housekeeping gene) in sterile 1.5 ml reaction tubes on ice as summarized in the Table 23.

Table 23 Reagents per each cDNA/DNA sample for real-time PCR

Reagent	Volume (µl)
H_2O_{dd}	4.4
SYBR Green QPCR Master Mix	10
Primers sense + antisense (10 µM)	1.6
Template	4

2. 4 µl of cDNA were added to 16 µl master mix and pipetted into a 96-well PCR plate in triplicates
3. For each primer pair a real-time PCR standard curve slope showing primer efficacy was pipetted in triplicates as well (100 ng/µl, 50 ng/µl, 25 ng/µl template)
4. Amplification was performed as shown in the Table 24.

Table 24 PCR program

Temperature	Duration	Cycles
95 ºC	7 min	1x
95 ºC	20 sec	40x
60 ºC	10 sec	
72 ºC	10 sec	
20 ºC	∞	
Melting curve		
Temperature	**Duration**	**Cycles**
95 ºC	5 sec	1x
40 ºC	1 min	1x
97 ºC	∞	

4.9 Animal treatment and xenotransplantation

Male and female newborn NOD Scid Gamma (NSG) mice were kindly provided by Dr. Anja-Kathrin Wege (Institute for Experimental Immunology, University of Regensburg) and maintained in the pathogen-free animal facilities of the University Hospital Regensburg. An NSG mouse is the best model for engraftment of human cancer cells, as it combines the features of the

NOD/ShiLtJ background, the severe combined immune deficiency mutation (scid) and IL2 receptor gamma chain. As a result of these mutations this mouse is highly immunodeficient, lacking mature T, B and NK cells and showing an absence of functional complement system.

The mice of 2-3 days age were irradiated and injected subcutaneously with 20 000 cells with a syringe under the right front paw. Tumor growth was monitored twice a week and tumor size was measured. After 5 weeks the mice were sacrificed and lungs, liver and brain were taken for further immunohistochemistry (IHC), kindly performed by Rudolf Jung and Florian Weber (Institute of Pathology, University Hospital Regensburg).

4.10 Statistical analysis

The results obtained from a series of experiments (number of experiments is shown as n = x) are expressed as mean values together with the standard deviation (SD) or standard error of the mean (SEM). The statistical significance was calculated using GraphPad Prism (GraphPad software, La Jolla, CA, USA). Statistical significances calculated by Student's or ANOVA/Dunnett's post hoc test are represented as follows: *p< 0.05, **p< 0.01 and ***p< 0.001. Multiple comparisons involved ANOVA calculation with Tukey's post-hoc-tests. The values lying below the detection range or such that they were not detected, were not taken into consideration in the statistical analysis.

V. Results

5.1 Pals1 knockdown affects TJ formation

The Madin-Darby Canine Kidney (MDCK) cell line is one of the most widely used models to study cell polarity, as these cells are characterized by well-defined apicobasal polarity and well-formed tight junctions. This cell line also grows fast (Cho et al. 1989) and forms an obvious monolayer, making it well suited for molecular studies, as well as for immunofluorescence staining (Dukes et al. 2011). Since its establishment from canine kidney in 1966 (Gaush et al. 1966), this cell line remains the most applicable model for epithelial cell polarity studies. There are several sub-types of a parental MDCK cell line, however, all experiments performed in this thesis utilized MDCK II sub-type.

To explore the role of Pals1 protein *in vitro*, several oligonucleotides (shRNA's) were chosen to target Pals1 canine mRNA to promote long-term Pals1 knockdown. The chosen shRNA's were cloned into a pSuperior.puro destination vector and subsequently transfected into MDCK II cells. Around two weeks after transfection and puromycine selection, distinct clones were picked and screened via Western Blot to determine the level of Pals1 suppression. Two stable cell lines showing Pals1 knockdown via two different shRNA's were obtained.

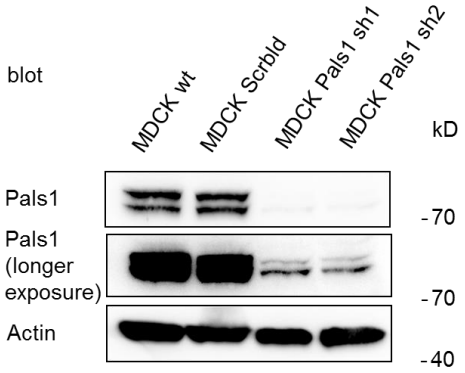

Figure 5.1.1: Stable Pals1 knockdown cell lines, showing a reduction of Pals1 protein levels in MDCK cells

Cell lysates of determined cell lines were prepared and subjected to Western Blot using anti-Pals1 antibody. Representative Western Blot is shown together with actin blot to verify equal loading. Relative molecular mass is presented to the right in kilodaltons (kD).

To exclude possible off-target effects, a scrambled (Scrbld) nonsense shRNA was cloned into a pSuperior.puro vector and introduced into MDCK wildtype cells (wt) to act as a negative control in all further experiments. Figure 5.1.1 represents the reduction of Pals1 expression by 70-80 % in MDCK with Pals1 sh1 and MDCK Pals1 sh2, whereas Pals1 expression in MDCK Scrbld remains unaffected. By using a Western Blot, Pals1 is determined by two specific bands near to each other, probably defining two *MPP5* splicing variants.

It is worth noting that the first visible observation of MDCK Pals1-KD cell lines under a microscope revealed a clear morphological transition. Cells lacking Pals1 switched their polygonal epithelial phenotype to a spindle-like mesenchymal cell morphology (Figure 5.1.2), whereas MDCK Scrbld cells remained relatively unchanged.

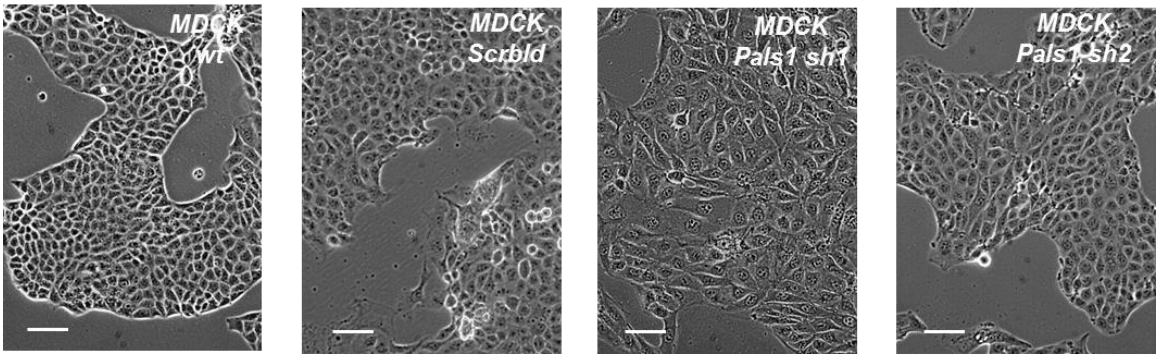

Figure 5.1.2: Light field microscopy of MDCK Pals1 knockdown cell lines

Cells were grown in Petri dishes to nicely formed islets. For imaging, the growth medium was removed, cells were washed once with PBS and covered with 5 ml new PBS. Brightfield pictures were obtained on an inverted microscope. The scale bars = 100 µm.

Interestingly, not only cell shape changes were observed. It is clearly seen that Pals1 knockdown is associated with an increase in cell size, especially comparing MDCK Pals1 sh1 and MDCK wt. MDCK Pals1 sh2 in contrast to MDCK wt also seems to cause an excess cell growth, although to a lesser extent. However, MDCK Scrbld cells are slightly enlarged as well, indicating probable side-effects of the transfection procedure and unpredicted genome integrations.

To find out, whether Pals1 knockdown influences tight junction formation and the integrity of cell-cell contacts, the cells were stained for the tight junction marker ZO-1, and AJ protein E-cadherin, as it plays a key role at adherens junctions between epithelial cells. Co-staining with Pals1 confirmed the Pals1 reduction obtained in Pals1 knockdown cell lines.

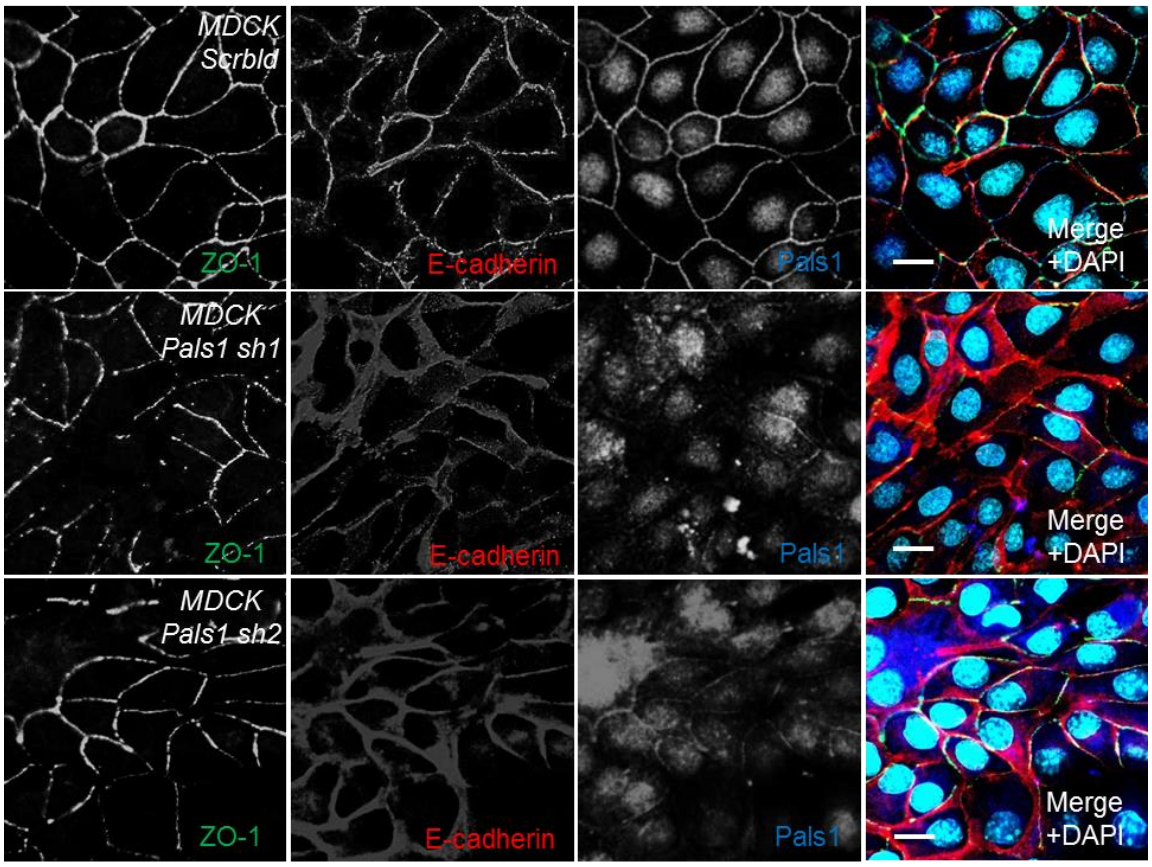

Figure 5.1.3: Immunostaining of stable MDCK Pals1 knockdown cell lines

Cells were grown on coverslips to confluence, fixed in methanol and stained for Pals1, ZO-1 and E-cadherin. Secondary antibodies coupled to fluorochromes enabled visualization. Merged images between the individual channels with DAPI nuclear counterstains are shown on the right. All images were acquired using similar settings on the laser-scanning microscope. The scale bars = 20 µm.

Moreover, MDCK Pals1-KD cell lines showed a slight decrease in ZO-1 expression and partial TJ structure disruption in contrast to MDCK Scrbld (Figure 5.1.3). Interestingly, although E-cadherin shows the expected localization pattern at lateral cell-cell junctions, the expression levels in MDCK Pals1-KD cell lines seem to be partially reduced and internalized.

Next, it was of interest to examine the role of Pals1 in the formation of cell-cell contacts and TJ dynamics. In order to answer this question, a calcium switch assay was performed.

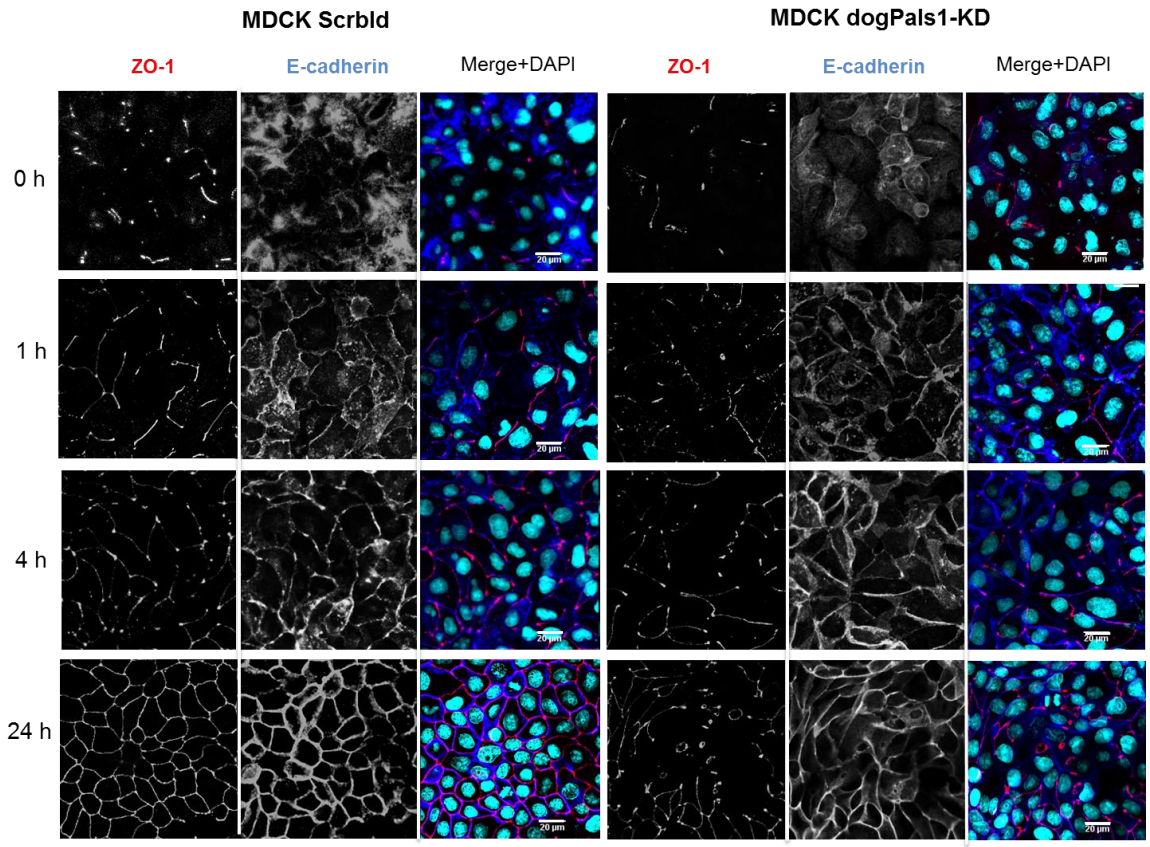

Figure 5.1.4: Calcium switch assay in stable MDCK Pals1 knockdown cell lines

Cells were grown on coverslips to confluence, placed overnight to calcium-low medium, then transferred back to the normal growth medium. At 0h, 1h, 4h and 24h after recovery cells were fixed in methanol and stained for ZO-1 and E-cadherin. Secondary antibodies coupled to fluorochromes enabled visualization. Merged images between the individual channels with DAPI nuclear counterstains are shown. All images were acquired using similar settings on the laser-scanning microscope. The scale bars = 20 µm.

Cells were cultured on coverslips to confluence, placed into medium without Ca^{2+} and only with 5% dialyzed FCS and incubated for 16 h at 37°C to break cell-cell contacts. Next morning the cells were placed back to the normal growth medium and TJ formation *de novo* was observed. For this reason, the cells were fixed at different time points and immunostained for E-cadherin and ZO-1 to observe tight junction and cell-cell contact rehabilitation (Figure 5.1.4).

As it is clearly seen at zero time point after calcium starvation, both MDCK Scrbld and MDCK Pals1-KD cell lines showed similar, almost complete

dissolution of cell-cell contacts. However, after placing to the normal growth medium, MDCK Scrbld reformed TJ faster, recruiting up to 90% of ZO-1 protein to TJ within 4 hours. In comparison, even after 24 hours, the MDCK Pals1-KD cell line was still unable to complete reassembly of cell-cell contacts. Thus, Pals1 knockdown cell line showed a dramatic delay in tight junction formation in comparison to the control cells. Additionally, in MDCK Scrbld cells E-cadherin was fully recruited back and formed adherens junctions within 24 hours, whereas MDCK Pals1-KD showed only slight differences in E-cadherin localization during all time points observed, indicating E-cadherin internalization and cell-cell contact weakening under Pals1 knockdown in MDCK cells.

5.2 Loss of Pals1 results in altered expression of polarity proteins

Regulation of apicobasal polarity relies on a complex interplay between evolutionarily conserved groups of polarity proteins. To characterize the impact of Pals1 knockdown on epithelial cell polarity maintenance and investigate the role of Pals1 in polarity establishment, Western Blot was carried out on MDCK Pals1-KD cell lines to determine the expression levels of other polarity proteins. It was of interest to analyze the members of Par complex, especially the Par6 protein, as Pals1 interacts directly with Par6. However, in mammals, distinct Par6 isoforms (Par6α, Par6β and Par6γ) were shown to exhibit different functions and divergent Pals1 binding capacity. For instance, Par6α and Pals1 interactions are much weaker in a comparison to Par6β and Par6γ, even in the presence of active Cdc42 (Gao, Macara 2004). Thus, the levels of Cdc42 were verified as well. In addition, with the observation that loss of Pals1 in MDCK cells results in mesenchymal-like cell morphology and adherens junction disruption, the level of E-cadherin as well as the expression rates of EMT markers αSMA and Vimentin were determined (Figure 5.2.1). To ensure that the band density was not influenced by different protein amounts, β-actin was used as a loading control.

Immunoblotting showed that cells with Pals1 knockdown displayed a marked increase in aPKC and Cdc42 levels. Moreover, loss of Pals1 had a

distinct impact on Par6 isoforms, demonstrating enhanced Par6α expression, no changes in Par6β and a significant decrease in Par6γ levels.

In contrast to the scrambled control, reduced E-cadherin expression in both MDCK Pals1-KD cell lines with a simultaneous increase in αSMA and Vimentin amounts might be inherent to EMT. So, reduced Pals1 levels result in altered polarity protein expression pattern and might be one of the reasons for epithelial-to-mesenchymal transition.

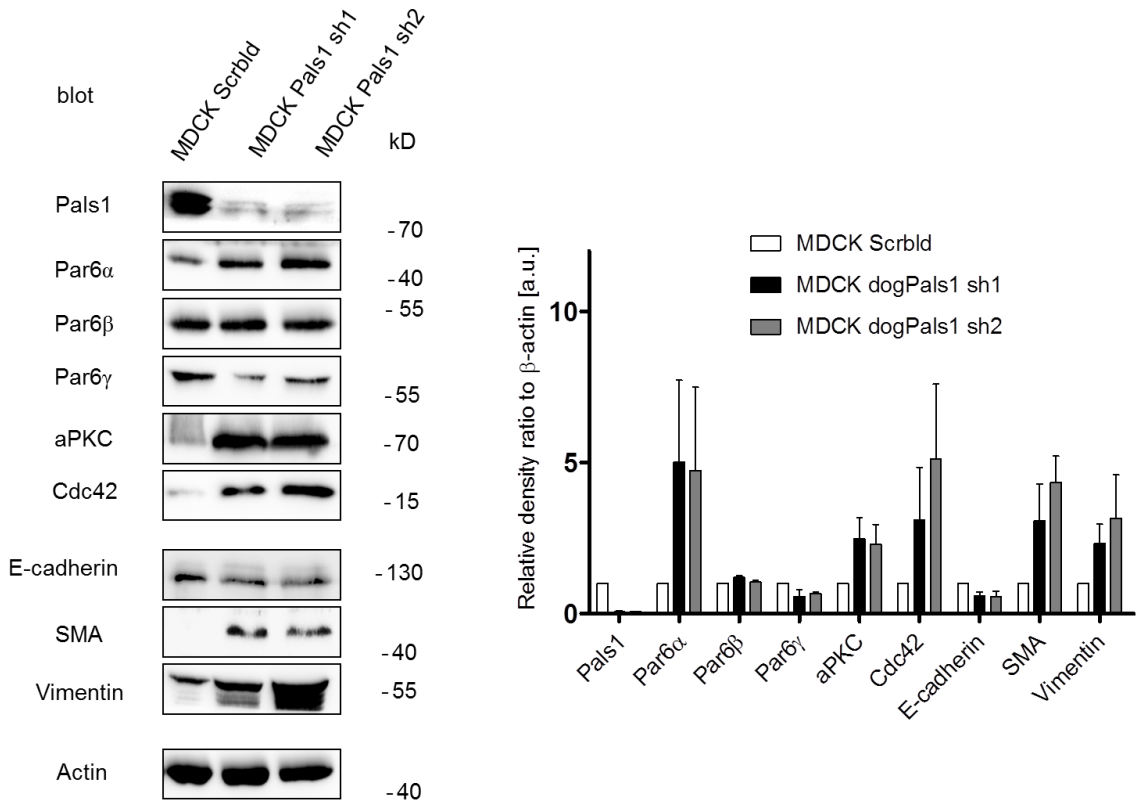

Figure 5.2.1: Western Blot analysis of stable MDCK Pals1 knockdown cell lines

Cells were grown in 10 cm plates to confluence, scraped and lysed in TNT lysis buffer with subsequent sonication. Protein quantification was performed by Bradford method. Afterwards, each sample was adjusted to 30 µg of the whole cell lysate and differential protein expression levels were determined by immunoblotting. β – actin was used as a loading control. Representative Western Blots are shown (**left**) and quantifications (**right**) are then given as means + SEM from n = 3 independent experiments.

5.3 Lack of Pals1 expression leads to enhanced cell motility

Combining the data obtained by Western Blot and immunofluorescence analysis of MDCK Pals1-KD cell lines, it seems plausible that Pals1 might be related to EMT. Hence, it was of interest to evaluate the possible contribution of Pals1 to cell migration. For this reason, scratch/wound healing and transwell migration assays were performed. To quantify cell motility out from the scratch/wound healing assay, cells were seeded in 6-well plates and grown to confluence. Next, the cell monolayer was disrupted mechanically creating a "wound" with a pipette tip. To evaluate cell migration *in vitro,* images representing "wound" closure at different time points, were taken.

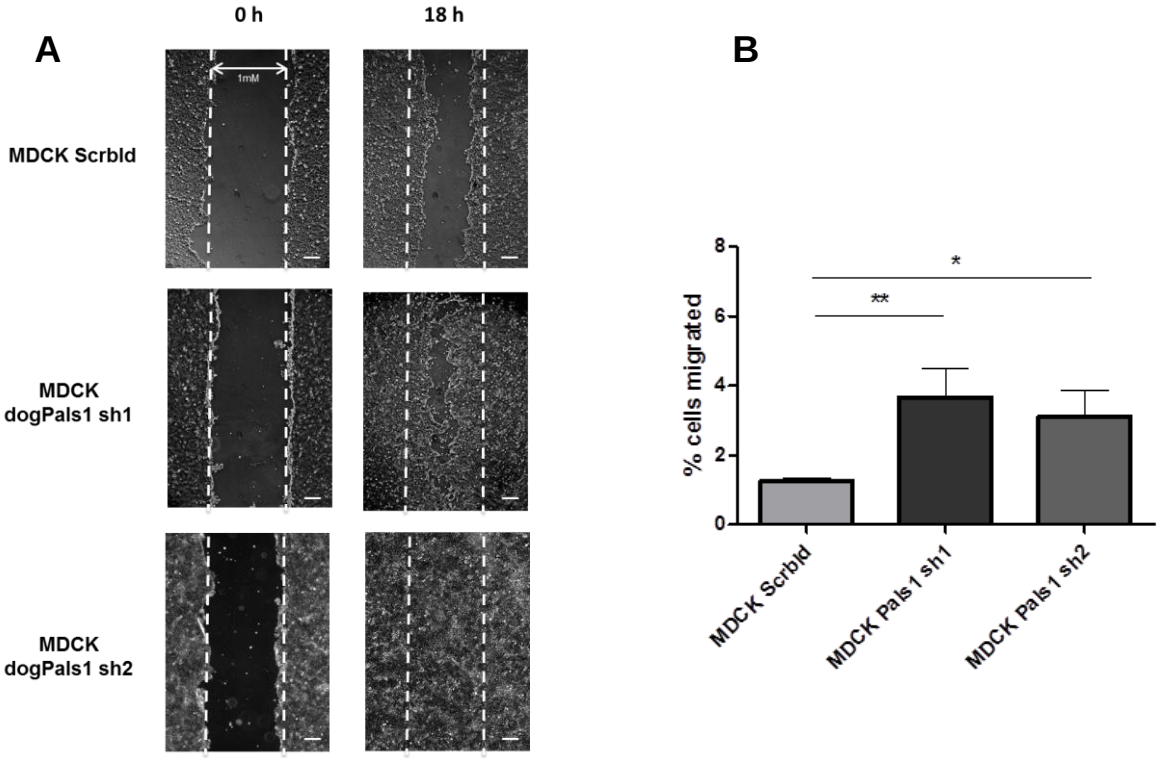

Figure 5.3.1: Scratch/wound healing (A) and transwell migration (B) assays of stable MDCK Pals1 knockdown cell lines

A. Confluent monolayer of cells was scratched with a tip to mimic the wound. Pictures, illustrating the healing, were taken at 0 h (immediately after scratch) and 18 h. One representative assay of n=3 independent experiments is shown. B. Cells were seeded in the FCS-free medium on transwell inserts. Cell migration towards FCS was evaluated by a number of cells, passed through the semipermeable membrane. Data are shown as means + SEM from n = 3 independent experiments. Statistically significant differences between MDCK Scrbld and MDCK Pals1 sh1/MDCK Pals1 sh2 respectively are indicated: *p<0.05, **p<0.01, Student's t-test.

As shown in Figure 5.3.1 A, cells with Pals1 knockdown close the gap and recover the monolayer significantly faster than the control group. Markedly enhanced cell motility was also confirmed performing cell transwell migration assay (Figure 5.3.1 B). Cells lacking Pals1 migrated up to 50% more compared to the control cell line. These results suggest that downregulation of Pals1 drastically enhances the migration capacity of MDCK cells.

5.4 Pals1 downregulation leads to overexpression of EMT markers and affects Hippo signaling pathway

The Hippo pathway controls cell proliferation and tissue growth while sensing cell density and mediating YAP cytoplasmic or nuclear localization. Transcriptionally active YAP promotes gene expression, whereas the phosphorylated form of YAP is not able to translocate into the nucleus and sequesters in the cytoplasm. According to Varelas *et al.,* in immunoprecipitation studies Pals1 was shown to interact directly with YAP thus linking cellular proliferative activity to epithelial polarity (Varelas et al. 2010). Therefore, in the next step, it was of interest to assess the feasible impact of Pals1 loss on the Hippo pathway. Western Blot analysis of MDCK Pals1-KD cell lines revealed a significant drop in YAP phosphorylation with Pals1 knockdown, whereas YAP levels remained unaffected (Figure 5.4.1). The immunofluorescent analysis confirmed deregulation in Hippo signaling under Pals1 knockdown. In contrast to the control MDCK Scrbld cell line, where YAP localizes to the TJ, loss of Pals1 stimulates translocation of YAP into the nucleus (Figure 5.4.2).

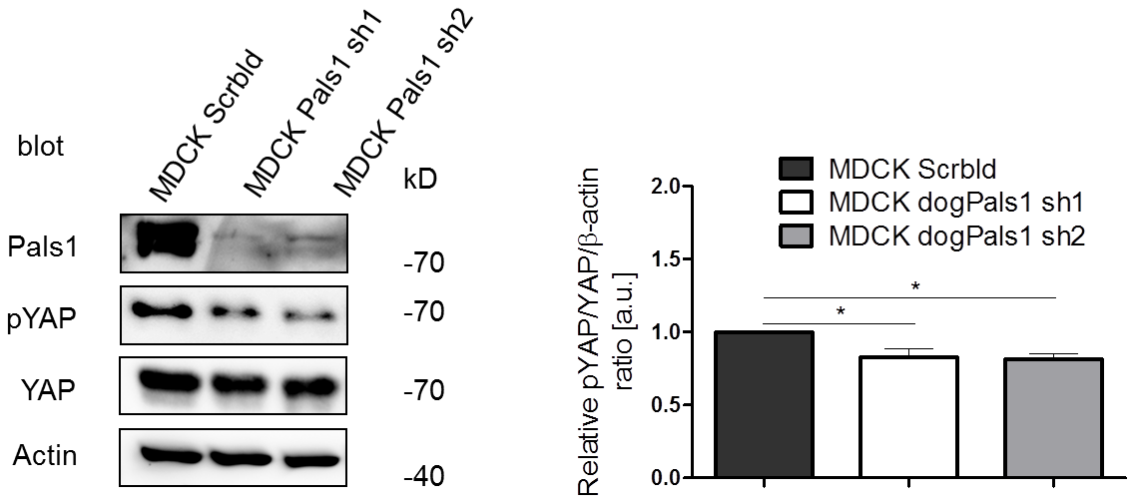

Figure 5.4.1: Western Blot analysis of stable MDCK Pals1 knockdown cell lines against transcriptional regulator YAP

Cells were grown in 10 cm plates, starved overnight in DMEM w/o FCS. After 16 h Hippo pathway was reactivated by FCS addition for 1 h. Afterward, cells were lysed in Laemli buffer and applied to Western Blot against YAP and pYAP. β-actin was used as loading control. Representative Western Blots are shown (**left**) and quantifications (**right**) are then given as means + SEM from n = 3 independent experiments. Band intensities were quantified by densitometry and are indicated as pYAP/YAP expression relative to that of β-actin. Statistically significant differences are indicated (*p < 0.05, ANOVA/Dunnett's post hoc test).

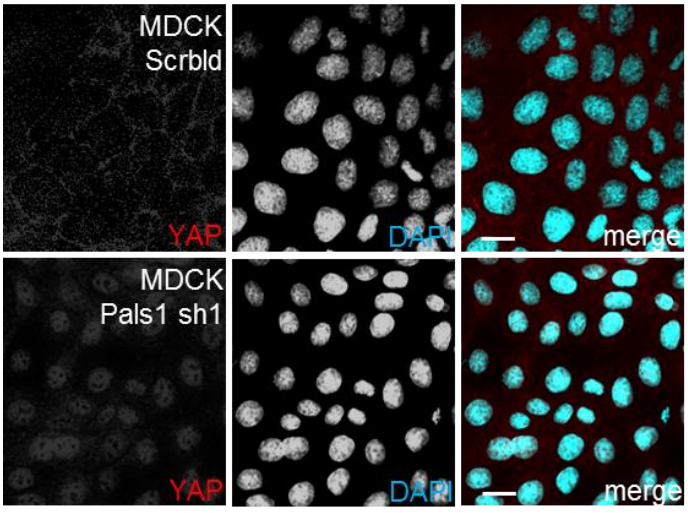

Figure 5.4.2: Immunofluorescent analysis of stable MDCK Pals1 sh1 knockdown cell line against transcriptional regulator YAP

Cells were grown in 6-well plates on coverslips. Upon pre-confluency cells were starved overnight in DMEM w/o FCS. After 16 h the Hippo pathway was reactivated by FCS addition for 1 h. Afterward, cells were fixed in immunostained against YAP and counterstained with DAPI. The scale bars = 20 µm.

To elucidate whether nuclear sequestration of YAP in MDCK Pals1-KD cells promotes further transcriptional activation, RT-PCR for Hippo downstream targets was performed. Figure 5.4.3 represents the analysis of CTGF, Pai-1 and Cyr61 mRNA. In addition, to validate epithelial to mesenchymal transition under Pals1 depletion, expression levels of EMT markers Snail and ZEB1 were investigated.

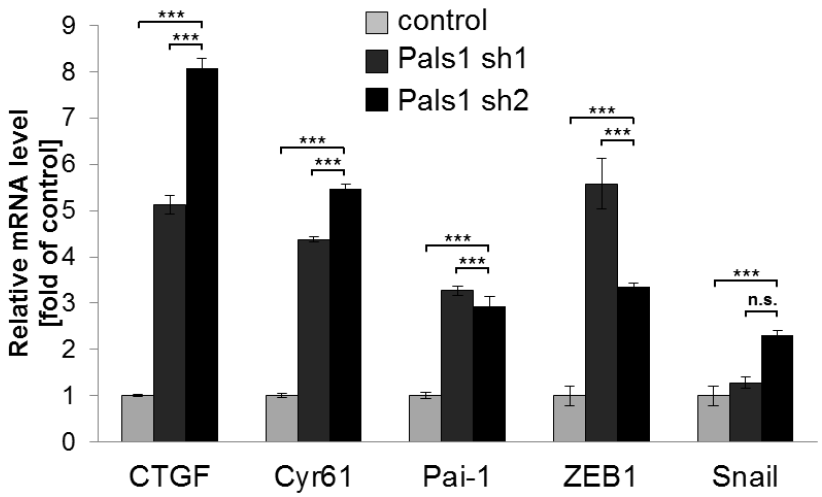

Figure 5.4.3: Relative mRNA expression of CTGF, Cyr61, Pai-1, ZEB1 and Snail in MDCK Pals1-KD cell lines in contrast to the control cell line

MDCK Scrbld, MDCK dogPals1 sh1 and MDCK dogPals1 sh2 cells were seeded in 12-well plates. The whole mRNA of each sample was extracted and after cDNA synthesis, real-time PCR was performed to quantify expression of defined genes. The fold of gene expression is defined as the fold of control of relative signal as compared to control cell line. GAPDH was used as a housekeeping gene control. The bars represent the means + SD from n = 3 independent experiments. Asterisks indicate statistically significant differences between groups (ANOVA/ Dunnett post hoc test, ***p < 0.001).

As can be seen in Figure 5.4.3, expression levels of three investigated YAP-downstream targets CTGF, Cyr 61 and Pai-1 are strongly increased in both Pals1-depleted cell lines in contrast to the MDCK Scrbld. Interestingly, Pai1 is also known to be TGF-β target gene, suggesting a further link between Pals1, the Hippo pathway and TGF-β–mediated signaling. Moreover, there are significant differences determined when comparing expression levels of Snail

and ZEB1. Elevated levels of this both master regulators indicate EMT switch in MDCK Pals1-KD cells.

5.5 Pals1 knockdown affects cell polarity in HCT116 colon cancer cell line

One of the most abundant cancers diagnosed across the world each year is colorectal cancer. Colon cancer is in the top three main causes of cancer-associated mortality (Arnold et al. 2016). To elucidate whether Pals1 is an important player in this disease, the histopathological examination of Pals1 in tissues from colon cancer patients was performed by Ludwig Lagleder. The obtained data appears to suggest that Pals1 decline correlates with colorectal tumor progression in patients. Thus, to deepen understanding of the role of Pals1 in colon cancer, two different cell lines with Pals1 knockdown in HCT116 colon cancer cell line were created using an shRNA approach. At the same time, HCT116 cells were transfected with a pSuperior vector containing Scrambled shRNA as a control. All HCT116 cells, transfected with pSuperior hPals1 sh1, pSuperior hPals1 sh2 or pSuperior Scrambled were selected for 2 weeks with 0.5 µg/ml puromycin until single cell colonies were formed. Each clone was then blotted against Pals1 and Actin to verify Pals1 decline under shRNA. The clones showing the most significant reduction of Pals1 expression were chosen for further studies (Figure 5.5.1 A).

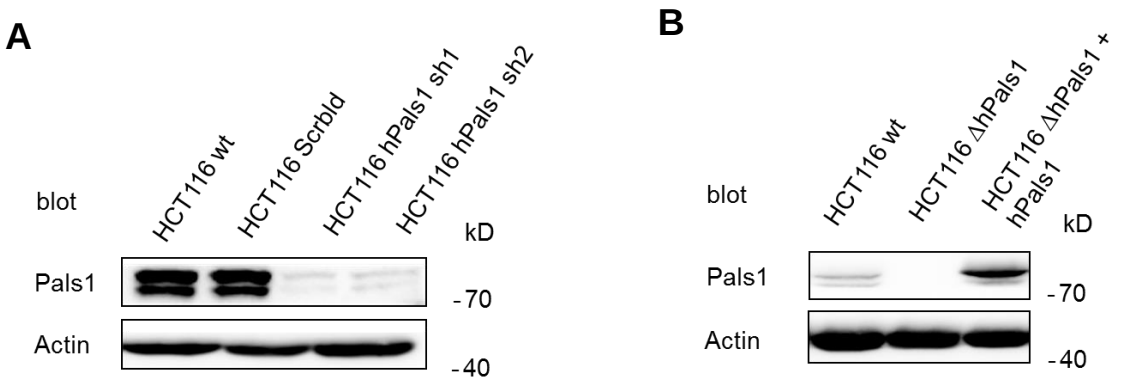

Figure 5.5.1: Stable Pals1 knockdown (A), knockout and rescue (B) cell lines, showing reduction, absence and recovery respectively of Pals1 protein levels in HCT116 cells

Cell lysates of determined cell lines were prepared and subjected to Western Blot using anti-Pals1 antibody. Representative Western Blot is shown together with actin blot to verify equal loading. Relative molecular mass is presented to the right in kilodaltons.

Moreover, as some of the human colon tissue samples showed as far as no Pals1 expression in cancer stage G3, it was of interest to explore the possible changes under complete Pals1 absence. Thus, using a CRISPR/Cas9 approach, an HCT116 cell line characterized by Pals1 knockout (KO) was created. To further verify that the changes upon Pals1 KO (ΔPals1) were directly due to the protein absence rather than off-target effects, the HCT116 ΔhPals1 cell line was rescued by the hPals1 expression construct (Figure 5.5.1 B). Whereas the introduction of the short hairpin RNAs sh1 and sh2 caused up to a 60%-80% reduction of endogenous Pals1 expression, Pals1 specific gRNA-guided CRISPR-Cas9 approach led to a complete Pals1 knockout, proved by immunoblot by the disappearance of the ~80 kDa bands representing Pals1. The introduction of nonsense shRNA had no influence on Pals1 expression (Figure 5.5.1 A). The rescue mutant of HCT116 ΔhPals1 is characterized by the reappearance of the Pals1 band in Western Blot. These results indicated successful Pals1 gene knockdown, knockout and further rescue.

To assess the impact of Pals1 on cell polarity, the Hippo pathway and EMT in the colon cancer HCT116 cell line, immunoblot and RT-PCR were performed as previously done for MDCK cells. Pals1 knockdown, as well as Pals1 knockout, drastically influence the expression of several polarity proteins, causing a strong reduction of E-cadherin, Par6γ and Cdc42 levels. Intriguingly, aPKC expression pattern, together with Par6α and Par6β remain almost unaffected. HCT116 ΔhPals1 + Pals1 rescue mutant restores normal levels of Par6γ, Cdc42, E-cadherin and caused reverse MET, seen as an αSMA reduction compared to HCT116 ΔhPals1 (Figure 5.5.2 A and B). Contrary to our expectations, whereby HCT116 hPals1-KD cell lines similarly to MDCK dogPals1-KD indicate upregulation of Hippo signaling, there were no changes of pYAP/YAP levels observed, when comparing HCT116 wt and HCT116 ΔhPals1.

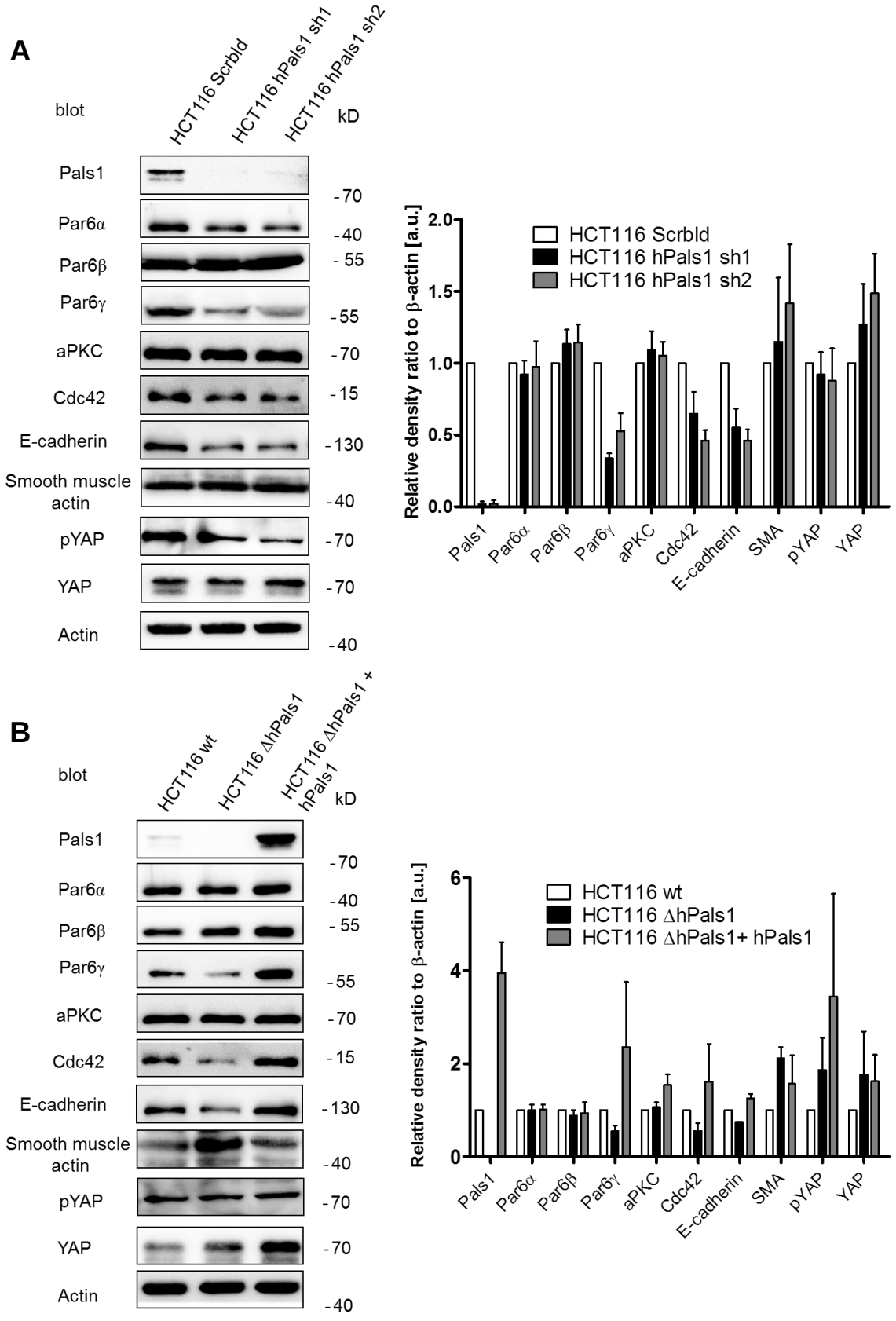

Figure 5.5.2: Western Blot analysis of stable HCT116 hPals1 knockdown (A) and knockout (B) cell lines

Differential protein expression levels were determined by immunoblotting. β – actin was used as a loading control. Representative Western Blots are shown **(left)** and quantifications **(right)** are then given as means + SEM from n = 3 independent experiments.

It is evident that Pals1 is highly important for EMT, as both Pals1-KD and KO result in E-cadherin expression decline and increased αSMA levels in HCT116 ΔhPals1. Further RT-PCR analysis of these cell lines supports our finding that the Hippo pathway is highly upregulated under Pals1-KD, showing a significant increase in the expression of Hippo signaling target genes CTGF, Birc2, and Cyr61, however unexpectedly less deregulated under Pals1 knockout (Figure 5.5.3 A and B).

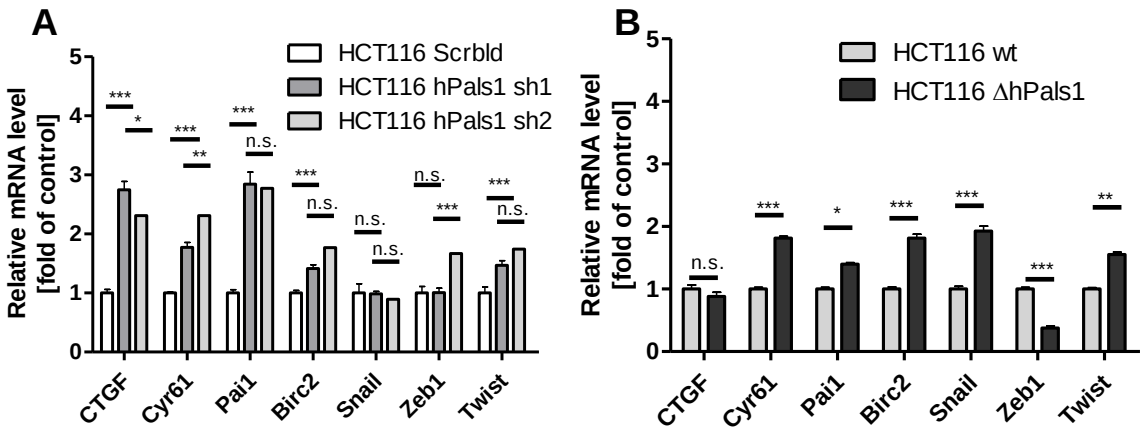

Figure 5.5.3: Relative mRNA expression of CTGF, Cyr61, Pai1, Birc2, ZEB1 and Snail in HCT116 hPals1-KD cell lines (A) and HCT116 ΔhPals1 cell line in contrast to the control

HCT 116 wt, HCT116 Scrbld, HCT 116 hPals1 sh1, sh2 and HCT116 ΔhPals1 cells were seeded in 12-well plates. The whole mRNA of each sample was extracted and after cDNA synthesis, real-time PCR was performed to quantify expression of defined genes. The fold of gene expression is defined as the fold of control of relative signal as compared to HCT116 Scrbld (A) or HCT116 wt cell line (B). Lamin A/C was used as a housekeeping gene control. The bars represent the means + SEM from n = 3 independent experiments. Asterisks indicate statistically significant differences between groups (ANOVA/ Dunnett post hoc test, *p < 0.5, **p < 0.01, ***p < 0.001).

Whereas Snail levels under Pals1 decline did not change, a complete absence of Pals1 stimulates Snail overexpression and might promote subsequent EMT and enhanced motility. Induction of Twist indicates EMT progression as well. Interestingly, ZEB1 - another central EMT mediator seems to be enhanced only in HCT116 hPals1 sh2 cell line and even seems to be downregulated in HCT116 ΔhPals1.

To assess whether the total absence of Pals1 expression also causes a similar phenotype in other epithelial cells, MDCK ΔdogPals1 and DLD1 ΔhPals1 mutant cell lines were created using the CRISPR/Cas9 method and immunoblotted. Both knockout cell lines showed a slight downregulation of Par6γ and E-cadherin, and strong overexpression of αSMA (Figure 5.5.4). Similar to HCT116 ΔhPals1, total Pals1 absence does not appear to influence the Hippo pathway in MDCK and DLD1 cell lines. To find out the probable reason for the subtly different phenotypes under Pals1 knockout, the initial levels of Pals1 protein were identified and compared among all investigated cell lines. For this purpose, MDCK wt, DLD1 wt and HCT116 wt together with their appropriate Pals1 knockout cell lines were lysed in TNT buffer, adjusted to 30 µg and subjected to Western Blot.

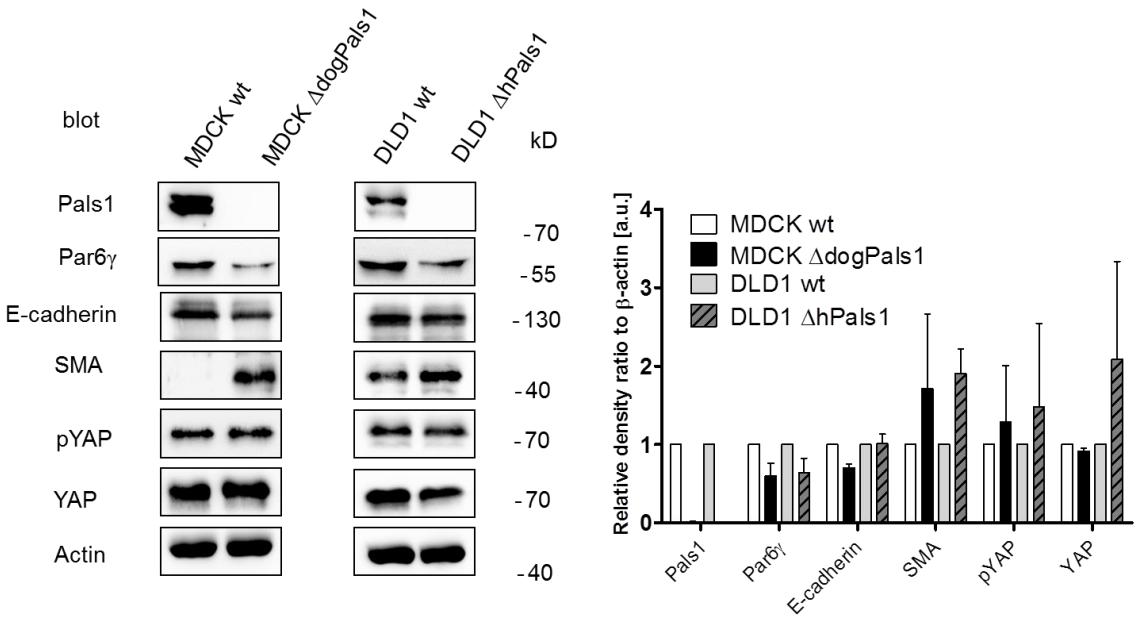

Figure 5.5.4: Western Blot analysis of stable MDCK dogPals1 and DLD1 hPals1 knockout cell lines

Cells were grown in 10 cm plates to confluence, starved overnight in medium w/o FCS. Afterwards, 20% FCS was added for 1 h, cells were scraped and lysed in Laemli lysis buffer with subsequent sonication. Differential protein expression levels were determined by immunoblotting. β – actin was used as a loading control. Representative Western Blots are shown **(left)** and quantifications **(right)** are then given as means + SEM from n = 3 independent experiments.

It was possible to compare the samples as they were adjusted to the same protein content in the cell lysate, and blotted and developed simultaneously on one membrane. It is evident that among three cell lines compared, the MDCK cell line is characterized by the highest Pals1 expression level. Analyzing the remaining two cell lines, HCT116 appears to show the lowest initial Pals1 protein amount (Figure 5.5.5).

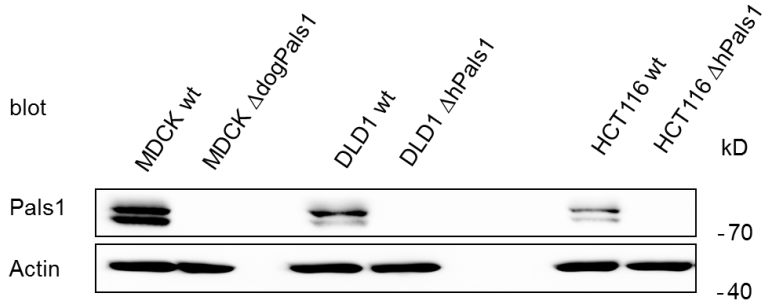

Figure 5.5.5: Comparative Western Blot analysis of MDCK, DLD1 and HCT116 wild type and their derivative Pals1 knockout cell lines

Cell lysates of determined cell lines were prepared and subjected to Western Blot using anti-Pals1 antibody. Representative Western Blot of n=3 is shown together with actin blot to verify equal loading. Relative molecular mass is presented to the right in kilodaltons.

5.6 Pals1-deficient cells show augmented cell proliferation

As described above, Pals1 may be an important regulator of the Hippo pathway. To check whether a reduction in Pals1 causes any impact on cell proliferation, MTT cell proliferation assays were carried out over one week for MDCK wt and MDCK ΔdogPals1 (Figure 5.6.1 A), HCT116 wt, HCT116 ΔhPals1 and HCT116 ΔhPals1+ hPals1 (Figure 5.6.1 B), DLD1 wt and DLD1 ΔhPals1 (Figure 5.6.1 C). Figure 5.6.1 shows elevated proliferation with MDCK and DLD1 ΔPals1 compared to their corresponding wildtype cells. Moreover, contact inhibition by confluence slows down parental cell lines, while both knockout cell lines continue propagating. This might again indicate Hippo deregulation, as it is known that the Hippo pathway controls cell proliferation by contact inhibition (Gumbiner, Kim 2014). Indeed, there were no noticeable differences in cell proliferation observed *in vitro,* comparing HCT116 wt with both HCT116 ΔhPals1 and HCT116 ΔhPals1+ hPals1 rescue mutant.

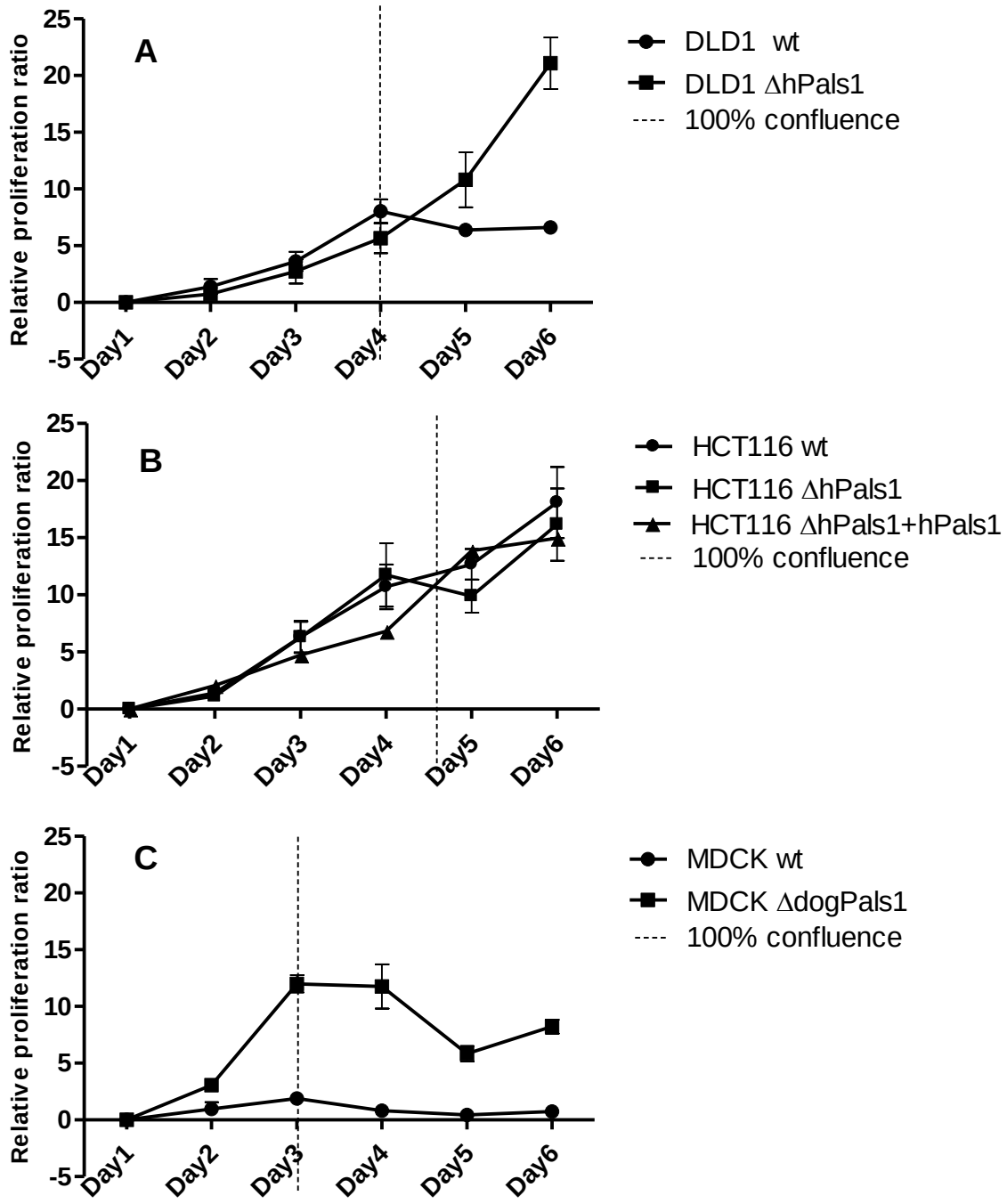

Figure 5.6.1: The effect of Pals1 knockout on the cell proliferation measured by the MTT test for MDCK (A), HCT116 (B) and DLD1 (C) cells.

For each cell line, six 12-well plates with 50 000 cells a well were prepared. Cell metabolic activity was measured every 24 h over 6 days by the MTT reduction test. Dotted lines indicate time point of cell confluence. Data shown are means + SD from n=3 independent experiments.

5.7 Lack of Pals1 expression leads to enhanced cell motility in epithelial and colon cancer cell lines

To confirm epithelial to mesenchymal transition and the probable impact of Pals1 decline on cell motility, scratch/wound healing assays were carried out for HCT116 hPals1-KDs and KO compared to HCT116 Scrbld and wt, respectively. HCT116 Scrbld, HCT116 hPals1 sh1 and HCT116 hPals1 sh2 cells were cultured until confluency in 6-well plates. Using a pipette tip, a “wound” was created and healing was observed after 16 h. To determine the role of Pals1 knockout in these cell lines, HCT116 wt, HCT 116 ΔhPals1 and HCT116 ΔhPals1+hPals1 cells were seeded and grown until a monolayer was formed around the insert. Thereafter the inserts were taken out, leaving a precise 0.5 mm open “wound”. Cell motility was characterized by observing cell migration capacity at 0 h and 16 h (Figure 5.7.1).

Intriguingly, there were no differences in cell motility observed between the HCT116 Scrbld cell line and both HCT116 cell lines with reduced Pals1. After 16 h, the wound closure under Pals1 knockdown was comparable to that of Scrbld. On the other hand, we can observe highly enhanced motility of cells completely lacking Pals1 in contrast to HCT116 wt. While HCT116 wt still did not manage to close the wound after 16 hours, HCT116 ΔhPals1 were markedly faster to close the gap and recover the monolayer. The restoration of Pals1 expression in the HCT116 ΔhPals1 cell line slowed cell motility almost to the level of HCT116 wt, indicating that Pals1 plays an important role in EMT and cell motility.

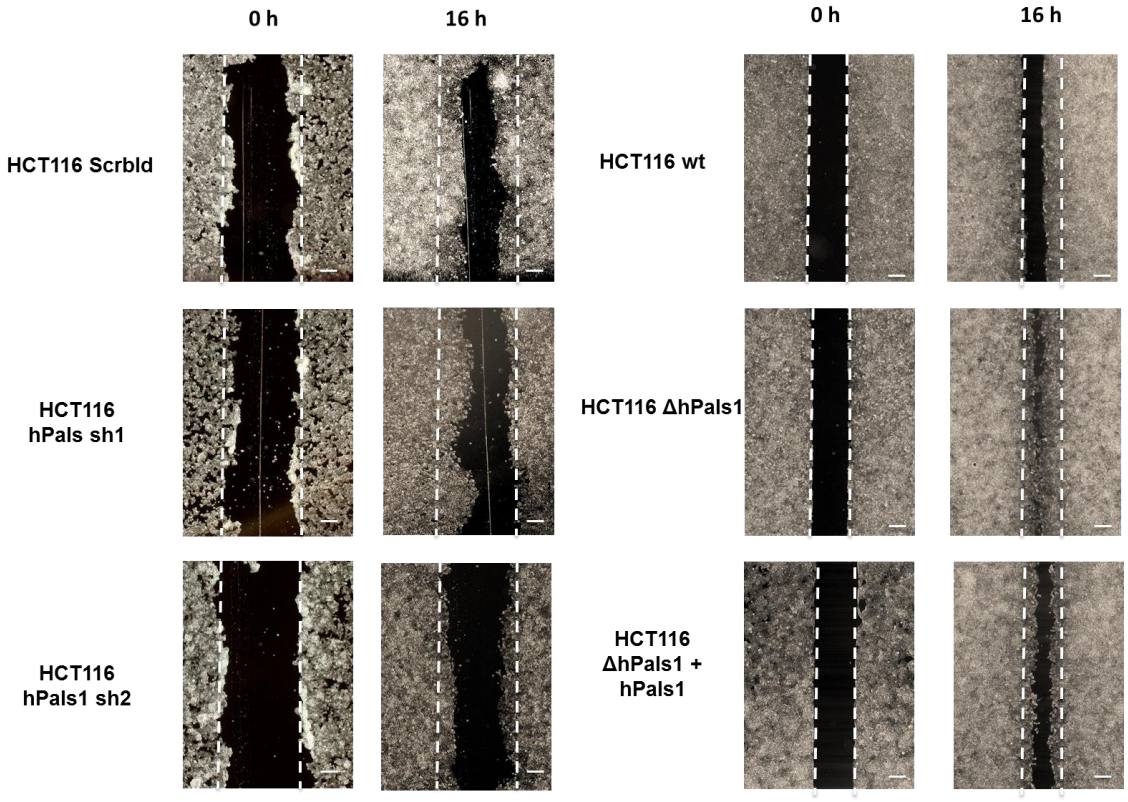

Figure 5.7.1: Scratch/wound healing assays of stable HCT116 Pals1-KDs, KO and rescue mutant cell lines

A confluent monolayer of cells was scratched with a tip to mimic the wound (for HCT116 Scrbld, HCT116 hPals sh1 and sh2), or the wound was created with Ibidi inserts (for HCT116 wt, HCT116 ΔhPals1+hPals1). Pictures, illustrating the healing, were taken at 0 h (immediately after scratch) and 16 h. One representative assay of n=3 independent experiments is shown. The scale bars = 200 µm.

Next, monolayer scratch assays were performed for MDCK and DLD1 cell lines, together with their derivative Pals1-KO cells respectively. To ensure that the observed wound closure was due to cell migration rather than cell proliferation, gap healing in MDCK was examined after 10 h. Comparing the migration capacity of MDCK and DLD1 cell lines with MDCK ΔdogPals1 and DLD1 ΔhPals1 cells, respectively, it is worth noting that Pals1 knockout drastically accelerates MDCK motility, but seems to have no significant impact on the DLD1 colon cancer cell line (Figure 5.7.2). Furthermore, both DLD1 wt and DLD1 ΔhPals1 did not manage to heal the wound even after 48h, suggesting a general migration inadequacy of DLD1 cells at least in such a scratch assay.

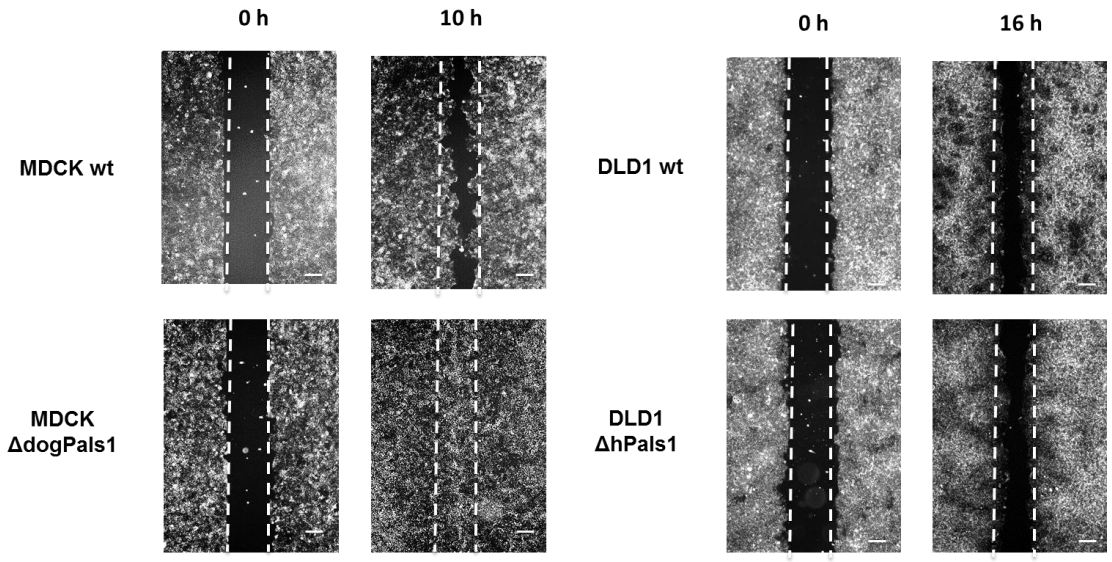

Figure 5.7.2: Scratch/wound healing assays of MDCK and DLD1 wild type and Pals1 knockout cell lines

Cells were grown in inserts to the confluence. Afterwards, the inserts were removed, leaving a gap. Pictures, illustrating the healing, were taken at 0 h (immediately after scratch) and 10 h for MDCK or 16 h for DLD1. One representative assay of n=3 independent experiments is shown. The scale bars = 200 µm.

5.8 Deregulation of Pals1 expression leads to cellular transformation and augmented tumorigenicity

One of the main hallmarks of malignant cells is their ability to grow in an anchorage-independent manner. The capacity of cells to grow in soft agar characterizes the cell transformation and tumorigenicity. Thus, to reveal the possible role of Pals1 in cellular tumor conversion, soft agar colony formation assays were performed for all previously described mutant cell lines. All investigated cells were adjusted to the same number, seeded in soft agar, covered with feeder medium and grown for 4 weeks. Afterwards, the colonies were stained and counted in ImageJ software. MDCK wt cells and the derived MDCK dogPals1 sh1, sh2 and KO cell lines are normal, thus they underwent anoikis and did not form any colonies in soft agar. There were also no differences observed comparing HCT 116 Scrbld with HCT116 hPals1 sh1 and HCT116 hPals1 sh2 cell lines. However, observing the anchorage-independent growth of HCT116 ΔhPals1 in contrast to HCT116 wt, and DLD1 ΔhPals1 compared to DLD1 wt, it was found that lack of Pals1 promotes further cellular

transformation, as both Pals1-KO cell lines formed more colonies compared to the controls (Figure 5.8.1 A and B). Rescue of the knockout mutant HCT116 ΔhPals1 caused a significant decline in colony number.

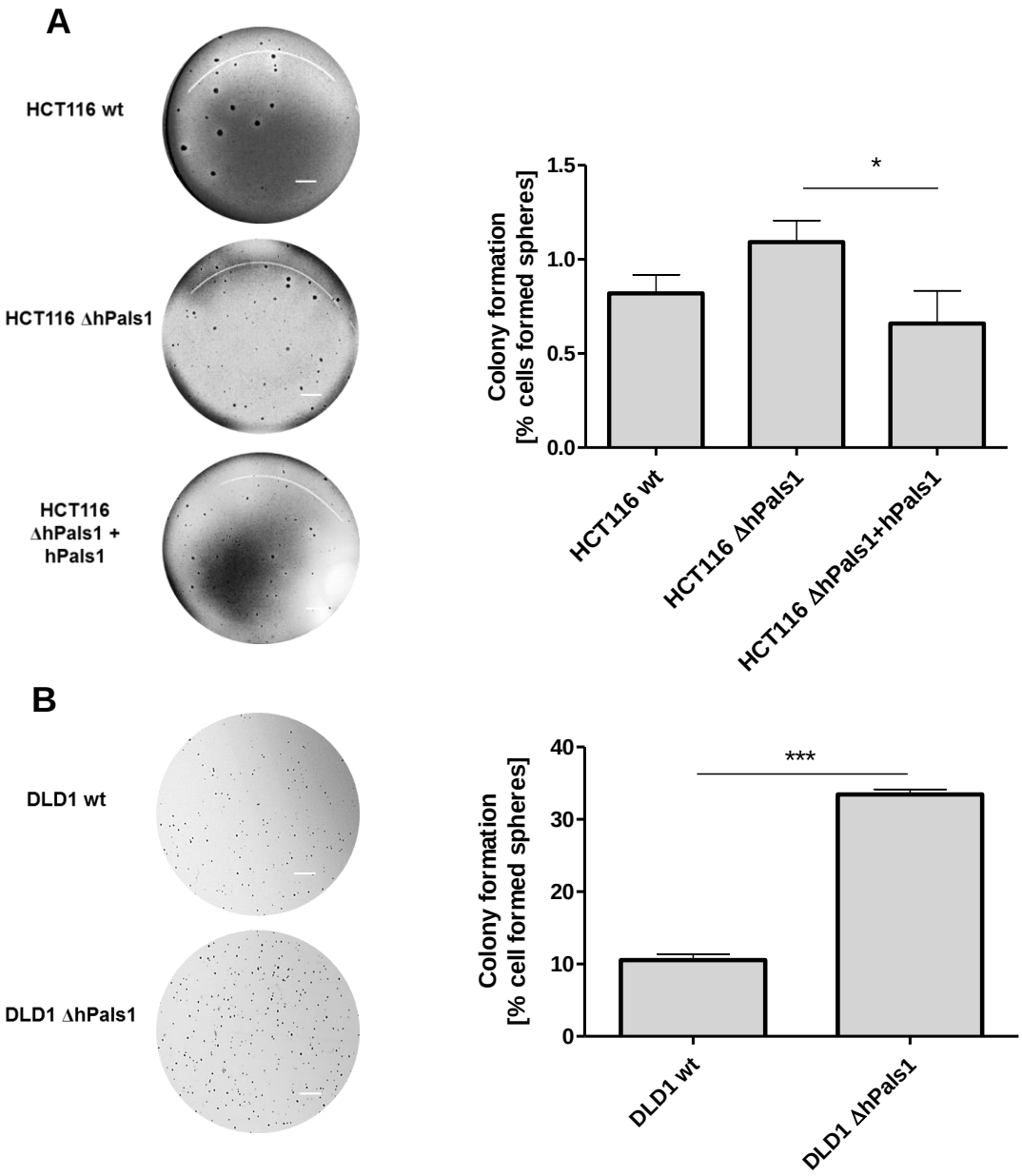

Figure 5.8.1: Soft agar colony formation assay of HCT116 wt, HCT116 ΔhPals1 and rescue mutant (A) together with DLD1 wt and DLD1 ΔhPals1 (B) cell lines.

Colony formation assay was performed in soft agar with 5000 cells per well. Colonies were stained with crystal violet 28 days after seeding. One representative assay is shown (left panel) and quantification (right panel) is given as means + SEM of n=4 (A) or n=3 (B) independent experiments. Numbers of colonies were quantified using ImageJ software and percentage of cells, capable of forming colonies in relation to a number of cells seeded, was identified. The scale bars = 200 µm. Asterisks indicate statistically significant differences between groups (ANOVA/ Dunnett post hoc test, *$p < 0.5$, ***$p < 0.001$).

5.9 Pals1 knockout in HCT116 cell line enhances cell motility and metastases formation in mice

To expand our knowledge and to confirm the role of Pals1 protein in cancer progression, in the next part of this study HCT116 wt, HCT116 Scrbld, HCT116 hPals1 sh1, sh2 and HCT116 ΔhPals1 cells were injected into NSG immunodeficient mice. For each cell line, 4-6 mice pups aged 3 days were injected subcutaneously with 20 000 cells per mouse in 20 µl of cell culture medium (Figure 5.9.1).

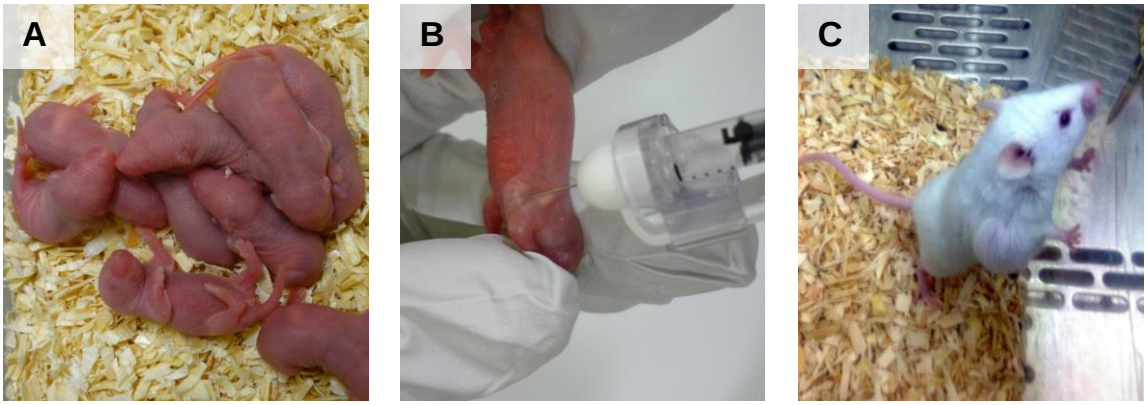

Figure 5.9.1: Subcutaneous injection of cultured cells (A, B) and xenograft growth (C) in mice

Each cell line was adjusted to 1 Mio cells/ml in cell culture medium w/o additives. Four to six aged 3 days mice (A) were taken per each cell line (group) and injected subcutaneously (B) with 20 000 cells per animal. Tumor growth was observed over the next 5 weeks (C).

Xenograft growth was monitored twice a week and tumor size was measured. After 5 weeks the mice were sacrificed; lungs, liver and brain were taken for further immunohistochemistry analysis.

In contrast to previous data obtained *in vitro*, where both HCT116 hPals1 knockdown sh1 and sh2 cell lines showed a similar phenotype, the tumors of HCT116 hPals1 sh2 grew much slower than those of the first HCT116 hPals1 knockdown cell line. Nevertheless, no differences in tumor size were observed when comparing the HCT116 Scrbld and HCT116 hPals1 sh1 cell lines. One should note that HCT116 ΔhPals1 cells formed dramatically larger tumors, compared to those developed from HCT116 wt (Figure 5.9.2).

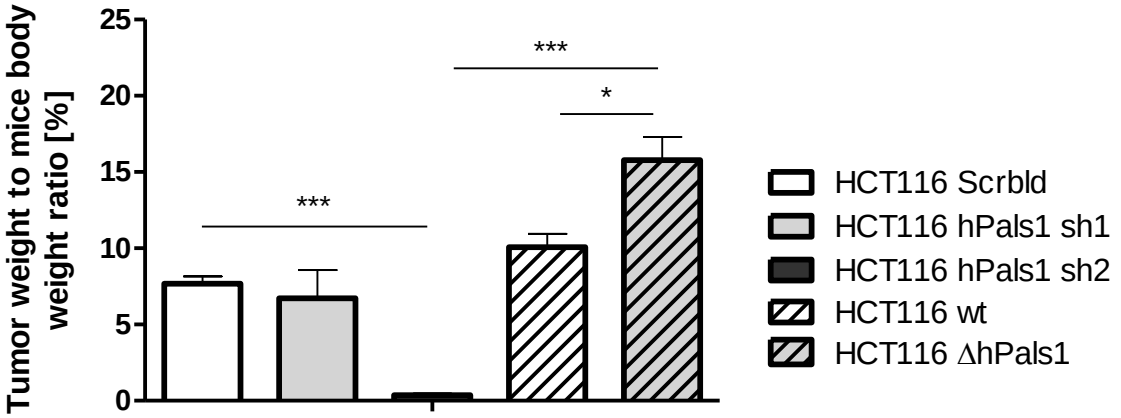

Figure 5.9.2: Average tumor weight to body weight index in each mice tumor xenograft group

Five weeks after injection all mice were sacrificed. Mice and tumors were weighed and tumor to body weight ratio was identified. Asterisks indicate statistically significant differences between groups (ANOVA/ Tukey's post hoc test, *$p < 0.5$, ***$p < 0.001$).

To validate whether Pals1 protein levels are crucial for tumor dissemination and metastasis formation, the liver and lungs of each mouse were used for immunohistochemical studies. For precise analysis, formalin fixed paraffin embedded tissue was serial sectioned at a thickness of 20 µm, and sections 200 µm apart were stained against specific anti-human pan Cytokeratin (panCK). Cytokeratins are cytoskeletal structural proteins found in the epithelium. This approach allows detection of only the human epithelia, separating it from the mouse tissue. The number of metastases found on 1 mm of each organ was counted and used to determine the overall number of metastases formed for each group investigated. Whereas no differences in metastatic formation were observed in HCT116 Scrbld xenografts compared to both HCT116 hPals1-KDs, there were significantly more metastases under Pals1 knockout compared to HCT116 wt xenografts (Figure 5.9.3).

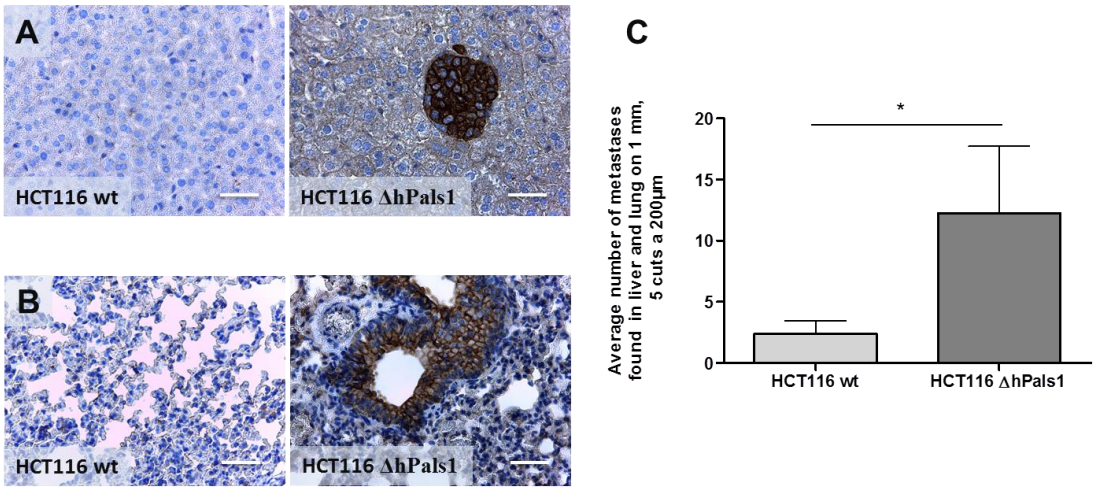

Figure 5.9.3: IHC analysis of human panCK in mouse liver (A), lung (B) and further quantification (C)

Representative pan Cytokeratin immunohistochemical staining of HCT116 wt and HCT116 ΔhPals1 xenografts, representing liver (A) and lung (B) metastatic formations. Scale bars = 50µm. Average numbers of metastases per mice, found in liver and lung on 1 mm were counted (C). Statistically significant differences between HCT116 wt and HCT ΔhPals1 derived metastases respectively are indicated: *p<0.05, Student's t-test.

It is also worth noting that there was a vast dissemination of HCT116 ΔhPals1 cells into the liver, while not a single liver metastasis was found in the HCT116 wt group. Altogether, this indicates that the absence of Pals1 plays a pivotal role in enhanced cell dissemination and increased metastatic potential.

5.10 TGF-β pathway is implicated in Pals1-dependend cell motility

To elucidate the mechanism underlying enhanced cell migration upon Pals1 deficiency, it was of interest to look closer on several pathways that are known to play a role in cell migration and metastatic process. In the next part of this study, several pathways were inhibited by specific inhibitors and the changes in cell migration were observed. Seeing as Pals1 is shown here to regulate the Hippo pathway, and recent findings in *Drosophila* showed this pathway also might mediate cell migration (Lucas et al. 2013), Verteporfin was used to inhibit YAP activity. Furthermore, SB431542 was applied to cells to block TGF-β receptors and to find out the possible influence of the TGF-β pathway in enhanced migration upon Pals1-deficiency. Figure 5.10.1 shows the scratch cell

migration assay of HCT116 wt and HCT116 ΔhPals1, with and without YAP- and TGF-β inhibitors.

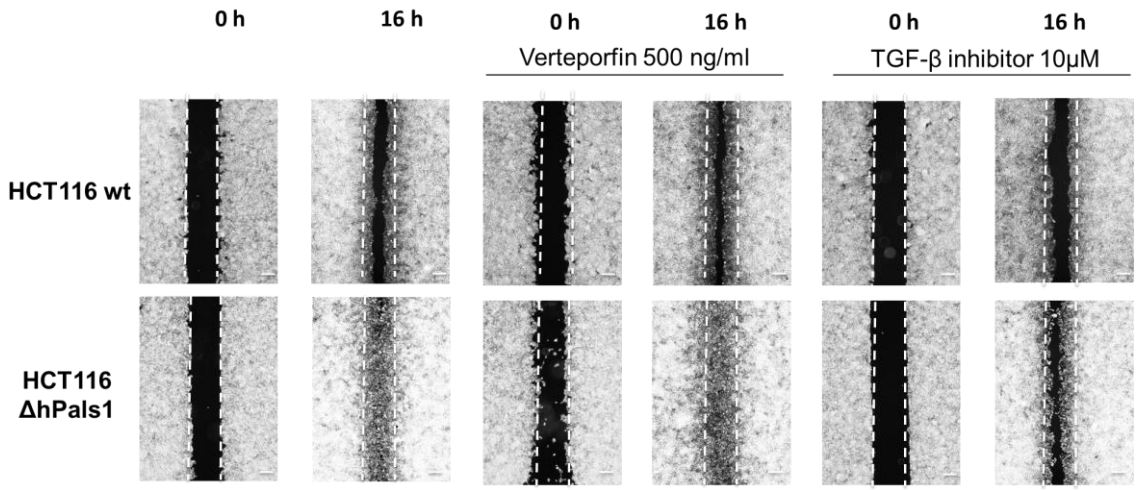

Figure 5.10.1: Scratch/wound healing assays of HCT116 wild type and Pals1 knockout cell lines under normal conditions or with inhibitors

Cells were grown in inserts to the confluence. Afterward, the inserts were removed, leaving a gap. Pictures, illustrating the healing, were taken at 0 h (immediately after scratch) and 16 h. The inhibitors were applied throughout the 16h. Representative assay of n=3 independent experiments is shown. The scale bars = 200 μm.

Comparing HCT116 wt with HCT116 ΔPals1, a lack of Pals1 again lead to accelerated cell migration. Interestingly, YAP-inhibition had no impact on the enhanced migration of HCT116 ΔhPals1 cells compared to the control HCT116 wt cell line, whereas abrogation of TGF-β signaling resulted in slower gap closure. This data provides the first hint to the mechanism of Pals1-dependened cell motility. However, to better understand the underlying mechanism, further *in vitro* and *in vivo* studies need to be performed.

VI. Discussion

Pals1 protein, a core component of Crb polarity complex, has been already shown to play a pivotal role in epithelial cell polarization. Prior studies in flies showed Stardust (Pals1 ortholog in *Drosophila*), together with other polarity regulators, to be essential for epithelial apicobasal polarization and proper subapical region (tight junction analog in flies) formation. Further works on Pals1 protein in mammals expanded previous findings and affirmed Pals1 to be a key player in epithelial cell polarity determination (Straight et al. 2004). Similar to flies, in mammals Pals1 directly interacts with Crb protein through its C-terminal domain, while the PDZ-domain governs its ability to bind to Patj and Par6 (Roh et al. 2002b; Penkert et al. 2004). Pals1 deficiency results in defects in TJ formation and apicobasal polarization (Straight et al. 2004). Remarkably, Pals1 is also shown to regulate myelination and radial sorting of axons (Zollinger et al. 2015). Recent findings revealed Pals1-deficiency to affect Hippo and TGF-β pathways and resulted in proteinuria and renal cyst development (Weide et al. 2017). This study aimed to deepen and expand the understanding of the biological functions of Pals1 in epithelial cells.

It is widely accepted that an excellent method for uncovering gene function in cells is to disrupt normal gene expression and explore the resulting phenotypes. The RNAi approach has been widely used for such loss-of-function studies, however it only reduces the expression of the gene of interest and might often result in off-target phenotypes (Sigoillot, King 2011). In contrast, off-target activity of CRISPR/Cas9-mediated knockout is fairly low (Gilbert et al. 2014) and enables complete gene silencing (Boettcher, McManus 2015).

So, in this study we combined and applied these two approaches to probe Pals1 function in epithelial cells. The data obtained not only confirms and extends previous findings of the Pals1 function in maintaining cell polarity, but also points to a novel link between cell polarity and tumor progression.

Pals1 knockdown reduced the expression of Par6γ and E-cadherin in both MDCK and HCT116 cells. On the one hand, Par6γ has been shown to be inactivated in a large number of epithelial cancers (Marques et al. 2016). On the other hand, loss of E-cadherin is one of the fundamental triggers in EMT and cell

dissemination in human carcinomas (Yilmaz, Christofori 2009). In addition, the E-cadherin immunostaining and Ca^{2+}-switch assays of MDCK Pals1-KD cells in this thesis are in line with Straight, Shin *et al.* 2004 and Wang, Chen *et al.* 2007, who show that Pals1 regulates E-cadherin trafficking and tight junction establishment. Taken together, simultaneous Par6γ and E-cadherin deregulation might be the first sign of cellular transformation under Pals1 knockdown.

Interestingly, a reduction in Pals1 causes a rise in Par6α expression and has no obvious impact on Par6β in MDCK cells. This suggests a further possible pathway for enhanced tumorigenicity in Pals1 deficient cells, as Par6α overexpression is shown to be responsible for hyperproliferation and enhanced invasiveness (Marques et al. 2016).

Elevated levels of Cdc42 were also observed under Pals1 knockdown in MDCK cells. Together with other Rho GTPases RhoA and Rac1, Cdc42 is known to regulate a variety of cellular processes, including microfilament and actin cytoskeleton network organization. Abnormal Cdc42 expression has been previously shown to promote testicular (Kamai et al. 2004) and breast cancer (Bray et al. 2013) progression. In contrast to normal tissue, an immunohistochemical study of squamous carcinoma in patients pointed again to an increased Cdc42 levels. Moreover, Cdc42 might be used as a new tumor marker, as it has been shown to contribute to colorectal cancer progression (Gomez Del Pulgar et al. 2008). Overexpression studies of Cdc42 in SW480 colon cancer cell line revealed a significant increase in cell motility in scratch/wound healing and Matrigel invasion assays (Gao et al. 2013).

Another important finding in this study is that both knockdown and knockout of Pals1 in all cell lines investigated, caused an extreme rise in alpha smooth muscle actin expression. This might suggest that Pals1 is an important regulator of EMT, as αSMA is known to be highly upregulated during epithelial to mesenchymal transition. EMT itself is characterized by weakening of cell-cell contacts, dissolutions of epithelial junctions, loss of apicobasal polarity, enhanced motility and invasive behavior (Derynck et al. 2014). Additionally, RT-PCR analysis of HCT116 ΔhPals1 and MDCK Pals-KD displayed Snail, ZEB1 and Twist upregulation compared to the control cell lines. These three proteins are well-known transcription factors activating EMT mechanisms during development and cancer progression. Snail is already shown to directly repress

E-cadherin and Crb3a (Harder et al. 2012), whereas ZEB1 interacts with YAP (Lehmann et al. 2016). On the other hand, MDCK and HCT116 Pals1-KD cells represent the downregulation and mislocalization of E-cadherin. Interestingly, E-cadherin destabilization is also one of the first hallmarks of EMT. Enhanced levels of αSMA and EMT transcription factors, together with reduced adherens junctions stability might specify epithelial to mesenchymal transition and enhanced tumorigenicity when Pals1 expression is reduced. This hypothesis is supported by the considerable increase in motility of MDCK Pals1-KD, MDCK ΔdogPals1 and HCT116 ΔhPals1 cells compared to the control, examined in this study by scratch/wound healing and transwell migration assays. The Cdc42 overexpression in MDCK cells lacking Pals1 described above might also contribute to augmented cell motility.

Intriguingly, there were no differences in cell motility identified between HCT116 Scrbld and both HCT116 hPals1-KD, as well as between DLD1 wt and DLD1 ΔhPals1.

It is important to understand why fairly efficient Pals1 decline in similar colon cancer cell lines results in differing migration capacities. In the first line, this may be due to different origin and tumor stage of these cells. According to the Dukes classification of colon cancer staging, the DLD1 cell line is classified as C stage, describing cancer spread to at least one lymph node. In turn, HCT116 represents a later stage D and is characterized by extensive metastases and advanced cancer progression (Ahmed et al. 2013b).

Secondly, regarding DLD1 cells, not only Pals1 knockout cells but also wildtype DLD1 cell line showed poor migration in the scratch assay. So, to confirm the data obtained it might be necessary to perform further experiments such as transwell or Matrigel migration assays. Nevertheless, in the literature one can find studies on DLD1 cell motility in scratch/wound healing assays during 24 h or even 48 h. Thus, another option is to extend the assay duration and add further time points of investigation. However, in this way cell migration might be confounded by cell proliferation, as DLD1 have a doubling time of approximately 20-24 h (Ahmed et al. 2013a), making it necessary to use blockers of proliferation.

Considering the HCT116 cell line, the cells migrate faster under total Pals1 absence compared to HCT116 wt, whereas a reduction in protein level

seems not to have an impact on cell motility. In contrast, Pals1 knockdown, as well as Pals1 knockout in MDCK cells both support increased cell migration. One of the reasons for this might be the different tissue and species origin of the cells. MDCK is a cell line isolated from the dog kidney while HCT116 is a human colon cancer cell line. The intial Pals1 level is of course also an important determinant. Referring to the Figure 5.5.5, it is clear that among all wildtype cell lines investigated, MDCK represents the highest Pals1 level and HCT116 the lowest. The greater difference between all explored cells is that MDCK a model for normal epithelial tissue, whereas HCT116 and DLD1 are originally isolated from high-grade primary tumors and are cancer cell lines. The biggest advantage here is limitless growth potential, however, one should remember that cancer cell lines are often genetically unstable and bear unknown mutations.

With regards to another finding, that Pals1 expression is downregulated in most colon cancer patient samples, especially in high graded tumors (according to data obtained by Ludwig Lagleder), it could be assumed that HCT116 already has reduced Pals1 levels from the very beginning and a further reduction has no further influence on cell motility, while complete Pals1 lack accelerates this cells even more. With this in mind, Pals1 might be an important regulator and might act as a tumor suppressor in advanced cancer stages.

In addition, DLD1 cells are characterized by a constitutively active Wnt-signalling pathway due to a mutation in the adenomatous polyposis coli gene (APC) (Boon et al. 2004). APC is a key tumor suppressor, found to be mutated in most colon cancers (Kinzler, Vogelstein 1996). Intriguingly, the HCT116 cell line has a wild type APC (Yang et al. 2006). Furthermore, karyotyping of diploid HCT116 and triploid DLD1 cell lines showed abnormal divergence between them (Knutsen et al. 2010). Hence, these might be the other explanations for the differences observed in these cell lines upon Pals1 knockout.

According to our data obtained in this study, Pals1 is not only crucial for cell motility but also plays a significant role in Hippo pathway regulation and cell proliferation. Although Western Blots show a decrease in the pYAP/YAP ratio in MDCK Pals1-KDs and HCT116 hPals1-KDs but not in MDCK, DLD1 and HCT116 ΔPals1, we observed an increase in the expression of YAP target genes in all Pals1-modified cell lines investigated. Moreover, YAP nuclear localization in MDCK Pals1-KD cells compared to MDCK wt supports Pals1 role

in Hippo signaling. Surprisingly, Pals1 knockout in HCT116 cells causes a less noticeable impact on the Hippo target genes CTGF, Cyr61 and Birc2 compared to those in the MDCK and HCT116 Pals1 knockdown cell lines. With the development of the new gene editing tool CRISPR/Cas9, it became much easier to modify the genome in an accurate and relative fast manner. However, it has already been shown that knockdown and knockout might have distinct effects. Knockout of the gene of interest might attenuate consequences or even completely compensate deficits, observed under protein knockdown (Khatodia et al. 2016). Hence, considering the Hippo pathway, it might be that Pals1 knockout triggers some compensatory mechanisms which slightly reduce the impact of Pals1 loss, compared to Pals1 decline.

The Hippo pathway itself is known to regulate organ size and cell proliferation. First, in this study, we show that Pals1 knockout drastically accelerates cell proliferation in MDCK and DLD1 cells. Contrary to our expectations in the MTT cell proliferation assay, neither HCT116 ΔhPals1 nor HCT116 ΔhPals1+hPals1 cell lines displayed any changes in cell growth compared to HCT116 wt. Nevertheless, *in vitro* data underlines Hippo pathway deregulation in HCT116 ΔhPals1 cells, and thus enhanced cell proliferation similar to MDCK and DLD1 Pals1 knockout cells might be evident. However, it should be recalled, HCT116 cells derived from high-grade cancer and probably because of their phenotype are characterized by weakened TJ. This is then probably the cause of the impaired contact inhibition and already in wildtype HCT116 deregulated Hippo signaling.

Nevertheless, investigating the impact of Pals1 knockout on cell transformation and colony growth in soft agar assay, it was found out DLD1 and HCT116 cells lacking Pals1 had an enhanced proliferation ability in a semisolid culture media in contrast to their controls. Pals1 rescue by stable overexpression of Pals1 in HCT116 ΔhPals1 also reduced the number of colonies. Thus, Pals1 has an effect not only on cell proliferation and cell migration, but a more dramatic influence on cell transformation as assessed by growth in soft agar.

It is widely known that loss of cell-cell contacts and deregulation in cell polarity within the epithelium is commonly related to advanced cancer progression (Khursheed, Bashyam 2014; Lee, Vasioukhin 2008; Martin-Belmonte, Perez-Moreno 2012). However, it is still not known exactly how

disruption of cell polarity leads to tumorigenesis. In fact, *Drosophila* studies on the Scribble polarity complex revealed neoplastic tumor formation in Lgl, Scribble or Dlg mutants. Nevertheless, enhanced tissue overgrowth and increased invasiveness in these mutants were observed only when combined with disruption of Notch or Ras signaling (Wodarz, Nathke 2007). In line with this, reduced Scribble complex members correlate with invasiveness in human cancers. Furthermore, a number of studies describe frequent alterations in both human aPKC isoforms, together with tumor suppressor Par3 and pro-oncogenic Par6 proteins. Crb3 and Patj, direct Pals1 interaction partners, have both already been shown to act as tumor suppressors (Lo et al. 2012; Whiteman et al. 2014). Although most of the polarity proteins have been shown to be involved in oncogenic transformations (Lin et al. 2015), there is still little known about Pals1. This study for the first time highlights Pals1 as a possible tumor suppressor.

To strengthen our supposition that Pals1, apart from its role in maintaining cell polarity, has a tumor suppressor function, we used the mouse xenograft model in which HCT116 cells harboring deletion of Pals1 were implanted into NSG mice. In agreement with results obtained from the *in vitro* soft agar colony formation assay, HCT116 ΔhPals1 xenografts grew significantly faster, compared to tumors derived from HCT116 wt. This finding implicates Pals1 in cell proliferation not only *in vitro* but also *in vivo*. Additionally, in immunohistochemical studies we observed the extensive propagation of injected tumor cells into mouse organs.

It is important to realize that among all the immunodeficient mouse strains used for human cell engraftment, the NSG mouse provides the best *in vivo* study model. This Nod-Scid mouse with IL2γ receptor knockout is characterized by T and B cell depletion, together with extremely low NK cell function and an impaired complement system. Notably, the main advantage of the NSG mouse model is that tumor metastases in these mice are highly similar to those observed in humans (Puchalapalli et al. 2016). As found by Riihimaki *et al.,* the most common sites of colorectal cancer metastasis in humans are the liver (around 70 %) and the thorax (around 30 %). Metastatic spread to the nervous system is found to be very rare, occurring only in 5 % of cases investigated (Riihimaki et al. 2016).

Similarly to humans, NSG mice bearing HCT116 Pals1 mutant xenografts disseminated into liver and lungs, however, no metastatic formations were found in the brains. Interestingly, it was only HCT116 ΔhPals1 cells that managed to spread into the liver, whereas no dissemination of HCT116 wt in this organ was found. This could be the most compelling evidence of the role of Pals1 as a tumor suppressor regulating metastatic progression.

Pals1 deficiency leads to attenuated Hippo pathway activation, so cells lacking Pals1 proliferate faster and thus this protein might play a role in the first step of cancer development, namely tumor initiation. While this does not explain the markedly accelerated tumor progression and invasiveness of Pals1 impaired cell, the role of the Hippo pathway in promoting cell motility is still an open question. Until now, there are few studies in *Drosophila* underlining Hippo implication in cell migration (Lin et al. 2014; Ma et al. 2017). Nevertheless, the possible role of this pathway in EMT and cell invasiveness in humans should be still closely investigated.

The role of Pals1 in other pathways related to cell invasion should also not be excluded. It is metastatic spread rather than the primary tumor that is largely responsible for high cancer mortality (Guan 2015). Aberrant expression of E-cadherin and some tight junction proteins as a consequence of Pals1 deregulation, might be the first key point in the epithelial to mesenchymal transition. Further EMT progression is shown to rely on Receptor Tyrosine Kinases, the transforming growth factor β superfamily, Wnt and Notch signaling together with NFκB driven mechanisms (Geiger, Peeper 2009). Pals1 has already shown to mediate NFκB activation in T lymphocytes (Carvalho et al. 2011b). Because of its implication in YAP-regulation, it seems plausible that Pals1 might also be closely linked to Wnt signaling. Interestingly, recent insights determined the most common mechanism leading to colon cancer metastasis is loss-of-function mutations of the antagonist of the PI3K/Akt pathway – PTEN, which in its turn stimulates Akt-regulated cell dissemination (Tariq, Ghias 2016). Another thing to remember is that the repression of E-cadherin and the induction of Snail and other pro-EMT regulators can be initiated by TGF-β signaling. Disruption of TGF-β functionality in the HCT116 ΔhPals1 cell line by TGF-β receptor inhibitor resulted in slowing down of migration, indicating a direct involvement of this pathway. Thus, it would be of interest to explore in more

detail the potential function of Pals1 in relation to the pathways described above, in particular TGF-β and PI3K/Akt signaling.

To summarize, in agreement with recent findings, this study strengthens the importance of Pals1 in epithelial cell polarity maintenance and Hippo pathway regulation. Moreover, for the first time Pals1 is shown to be crucial for EMT and cancer progression. However, the reason for enhanced migration and invasiveness in Pals1-deficient cells remains unclear and needs to be investigated further.

VII. Conclusion and Outlook

Epithelial cell polarity is of crucial importance for many tissues. Disruption of epithelial cell polarity leads to disassembly of cell-cell and cell-matrix contacts, tissue disorganization and finally results in epithelial-to-mesenchymal transition, which is implicated in carcinogenesis and metastasis.

The present study was designed to investigate the role of Pals1 in epithelial cell polarization and explore the molecular link between cell polarity and cancer progression. To assess the function of the protein, knockdown and knockout studies of the Pals1 function were performed. According to the data obtained *in vitro*, Pals1 deficiency causes abnormal cell morphology and Hippo pathway deregulation. Furthermore, lack of Pals1 leads to reduction of E-cadherin and increased EMT-markers, resulting in enhanced cell motility and metastatic formation *in vivo*. These data, for the first time, point towards Pals1 being a regulator of a wide range of cellular processes aside from cell polarity and suggest the existence of a novel Pals1-mediated mechanism of tumor suppression.

In the future, it will be important to gain a more accurate and complete understanding of the interplay of Pals1 with other mediators of epithelial cell polarity. Another crucial point to consider is the mechanism behind the increased cell motility occurring with Pals1 deficiency and its convergence with other pathways.

In conclusion, it is essential to deepen the knowledge of Pals1 function as a novel tumor suppressor, with the aim of designing new drugs against the deregulation it provokes in a range of pathophysiological conditions.

VIII. Supplements

8.1. List of figures

8.2. List of tables

IX. References

Adachi, Makoto; Hamazaki, Yoko; Kobayashi, Yuka; Itoh, Masahiko; Tsukita, Sachiko; Furuse, Mikio; Tsukita, Shoichiro (2009): Similar and distinct properties of MUPP1 and Patj, two homologous PDZ domain-containing tight-junction proteins. In *Molecular and cellular biology* 29 (9), pp. 2372–2389. DOI: 10.1128/MCB.01505-08.

Ahmed, D.; Eide, P. W.; Eilertsen, I. A.; Danielsen, S. A.; Eknaes, M.; Hektoen, M. et al. (2013a): Epigenetic and genetic features of 24 colon cancer cell lines. In *Oncogenesis* 2, pp. e71. DOI: 10.1038/oncsis.2013.35.

Ahmed, D.; Eide, P. W.; Eilertsen, I. A.; Danielsen, S. A.; Eknaes, M.; Hektoen, M. et al. (2013b): Epigenetic and genetic features of 24 colon cancer cell lines. In *Oncogenesis* 2, pp. e71. DOI: 10.1038/oncsis.2013.35.

Aranda, V.; Nolan, M. E.; Muthuswamy, S. K. (2008): Par complex in cancer: a regulator of normal cell polarity joins the dark side. In *Oncogene* 27 (55), pp. 6878–6887. DOI: 10.1038/onc.2008.340.

Arnold, Melina; Sierra, Monica S.; Laversanne, Mathieu; Soerjomataram, Isabelle; Jemal, Ahmedin; Bray, Freddie (2016): Global patterns and trends in colorectal cancer incidence and mortality. In *Gut. DOI:* 10.1136/gutjnl-2015-310912.

Assemat, Emeline; Bazellieres, Elsa; Pallesi-Pocachard, Emilie; Le Bivic, Andre; Massey-Harroche, Dominique (2008): Polarity complex proteins. In *Biochimica et biophysica acta* 1778 (3), pp. 614–630. DOI: 10.1016/j.bbamem.2007.08.029.

Bachelder, Robin E.; Yoon, Sang-Oh; Franci, Clara; Herreros, Antonio Garcia de; Mercurio, Arthur M. (2005): Glycogen synthase kinase-3 is an endogenous inhibitor of Snail transcription: implications for the epithelial-mesenchymal transition. In *The Journal of Cell Biology* 168 (1), pp. 29–33. DOI: 10.1083/jcb.200409067.

Betschinger, Jorg; Mechtler, Karl; Knoblich, Juergen A. (2003): The Par complex directs asymmetric cell division by phosphorylating the cytoskeletal protein Lgl. In *Nature* 422 (6929), pp. 326–330. DOI: 10.1038/nature01486.

Betts, J. Gordon (2013): Anatomy & physiology. Houston, Texas: OpenStax College.

Boettcher, Michael; McManus, Michael T. (2015): Choosing the Right Tool for the Job: RNAi, TALEN, or CRISPR. In *Molecular Cell* 58 (4), pp. 575–585. DOI: 10.1016/j.molcel.2015.04.028.

Boon, E. M. J.; Keller, J. J.; Wormhoudt, T. A. M.; Giardiello, F. M.; Offerhaus, G. J. A.; van der Neut, R.; Pals, S. T. (2004): Sulindac targets nuclear beta-catenin accumulation and Wnt signalling in adenomas of patients with familial adenomatous polyposis and in human colorectal cancer cell lines. In *British journal of cancer* 90 (1), pp. 224–229. DOI: 10.1038/sj.bjc.6601505.

Bray, Freddie; Moller, Bjorn (2006): Predicting the future burden of cancer. In *Nature reviews. Cancer* 6 (1), pp. 63–74. DOI: 10.1038/nrc1781.

Bray, Kristi; Gillette, Melissa; Young, Jeanette; Loughran, Elizabeth; Hwang, Melissa; Sears, James Cooper; Vargo-Gogola, Tracy (2013): Cdc42 overexpression induces hyperbranching in the developing mammary gland by enhancing cell migration. In *Breast cancer research : BCR* 15 (5), pp. R91. DOI: 10.1186/bcr3487.

Bulgakova, Natalia A.; Knust, Elisabeth (2009): The Crumbs complex: from epithelial-cell polarity to retinal degeneration. In *Journal of cell science* 122 (Pt 15), pp. 2587–2596. DOI: 10.1242/jcs.023648.

Carvalho, Gabrielle; Poalas, Konstantinos; Demian, Catherine; Hatchi, Emeline; Vazquez, Aime; Bidere, Nicolas (2011a): Participation of the cell polarity protein PALS1 to T-cell receptor-mediated NF-kappaB activation. In *PloS one* 6 (3), pp. e18159. DOI: 10.1371/journal.pone.0018159.

Carvalho, Gabrielle; Poalas, Konstantinos; Demian, Catherine; Hatchi, Emeline; Vazquez, Aime; Bidere, Nicolas (2011b): Participation of the cell polarity protein PALS1 to T-cell receptor-mediated NF-kappaB activation. In *PloS one* 6 (3), pp. e18159. DOI: 10.1371/journal.pone.0018159.

Chen, Jia; Zhang, Mingjie (2013): The Par3/Par6/aPKC complex and epithelial cell polarity. In *Experimental cell research* 319 (10), pp. 1357–1364. DOI: 10.1016/j.yexcr.2013.03.021.

Cho, M. J.; Thompson, D. P.; Cramer, C. T.; Vidmar, T. J.; Scieszka, J. F. (1989): The Madin Darby canine kidney (MDCK) epithelial cell monolayer as a model cellular transport barrier. In *Pharmaceutical research* 6 (1), pp. 71–77.

Crespo, Carolina Lage; Vernieri, Claudio; Keller, Philipp J.; Garre, Massimiliano; Bender, Jeffrey R.; Wittbrodt, Joachim; Pardi, Ruggero (2014): The PAR complex controls the spatiotemporal dynamics of F-actin and the MTOC in directionally migrating leukocytes. In *Journal of cell science* 127 (Pt 20), pp. 4381–4395. DOI: 10.1242/jcs.146217.

Derynck, Rik; Muthusamy, Baby Periyanayaki; Saeteurn, Koy Y. (2014): Signaling pathway cooperation in TGF-beta-induced epithelial-mesenchymal transition. In *Current opinion in cell biology* 31, pp. 56–66. DOI: 10.1016/j.ceb.2014.09.001.

Devenport, Danelle (2014): The cell biology of planar cell polarity. In *The Journal of Cell Biology* 207 (2), pp. 171–179. DOI: 10.1083/jcb.201408039.

Diamantopoulou, Zoi; White, Gavin; Fadlullah, Muhammad Z. H.; Dreger, Marcel; Pickering, Karen; Maltas, Joe et al. (2017): TIAM1 Antagonizes TAZ/YAP Both in the Destruction Complex in the Cytoplasm and in the Nucleus to Inhibit Invasion of Intestinal Epithelial Cells. In *Cancer cell* 31 (5), p. 621-634.e6. DOI: 10.1016/j.ccell.2017.03.007.

Diaz, V. M.; Vinas-Castells, R.; Garcia de Herreros, A. (2014): Regulation of the protein stability of EMT transcription factors. In *Cell adhesion & migration* 8 (4), pp. 418–428. DOI: 10.4161/19336918.2014.969998.

Dukes, Joseph D.; Whitley, Paul; Chalmers, Andrew D. (2011): The MDCK variety pack: choosing the right strain. In *BMC cell biology* 12, p. 43. DOI: 10.1186/1471-2121-12-43.

Ehmer, Ursula; Sage, Julien (2016): Control of Proliferation and Cancer Growth by the Hippo Signaling Pathway. In *Molecular cancer research : MCR* 14 (2), pp. 127–140. DOI: 10.1158/1541-7786.MCR-15-0305.

Elsum, Imogen A.; Martin, Claire; Humbert, Patrick O. (2013): Scribble regulates an EMT polarity pathway through modulation of MAPK-ERK signaling to mediate

junction formation. In *Journal of cell science* 126 (Pt 17), pp. 3990–3999. DOI: 10.1242/jcs.129387.

Ernkvist, Mira; Luna Persson, Nathalie; Audebert, Stephane; Lecine, Patrick; Sinha, Indranil; Liu, Miaoliang et al. (2009): The Amot/Patj/Syx signaling complex spatially controls RhoA GTPase activity in migrating endothelial cells. In *Blood* 113 (1), pp. 244–253. DOI: 10.1182/blood-2008-04-153874.

Etienne-Manneville, Sandrine; Manneville, Jean-Baptiste; Nicholls, Sarah; Ferenczi, Michael A.; Hall, Alan (2005): Cdc42 and Par6-PKCzeta regulate the spatially localized association of Dlg1 and APC to control cell polarization. In *The Journal of Cell Biology* 170 (6), pp. 895–901. DOI: 10.1083/jcb.200412172.

Frantz, Christian; Stewart, Kathleen M.; Weaver, Valerie M. (2010): The extracellular matrix at a glance. In *Journal of cell science* 123 (Pt 24), pp. 4195–4200. DOI: 10.1242/jcs.023820.

Gao, Lin; Macara, Ian G. (2004): Isoforms of the polarity protein par6 have distinct functions. In *The Journal of biological chemistry* 279 (40), pp. 41557–41562. DOI: 10.1074/jbc.M403723200.

Gaush, C. R.; Hard, W. L.; Smith, T. F. (1966): Characterization of an Established Line of Canine Kidney Cells (MDCK). In *Experimental Biology and Medicine* 122 (3), pp. 931–935. DOI: 10.3181/00379727-122-31293.

Geiger, Thomas R.; Peeper, Daniel S. (2009): Metastasis mechanisms. In *Biochimica et biophysica acta* 1796 (2), pp. 293–308. DOI: 10.1016/j.bbcan.2009.07.006.

Gibson, Matthew C.; Perrimon, Norbert (2003): Apicobasal polarization: epithelial form and function. In *Current opinion in cell biology* 15 (6), pp. 747–752.

Gilbert, Luke A.; Horlbeck, Max A.; Adamson, Britt; Villalta, Jacqueline E.; Chen, Yuwen; Whitehead, Evan H. et al. (2014): Genome-Scale CRISPR-Mediated Control of Gene Repression and Activation. In *Cell* 159 (3), pp. 647–661. DOI: 10.1016/j.cell.2014.09.029.

Gomez Del Pulgar, Teresa; Valdes-Mora, Fatima; Bandres, Eva; Perez-Palacios, Rosa; Espina, Carolina; Cejas, Paloma et al. (2008): Cdc42 is highly expressed

in colorectal adenocarcinoma and downregulates ID4 through an epigenetic mechanism. In *International journal of oncology* 33 (1), pp. 185–193.

Grabowska, Magdalena M.; Day, Mark L. (2012): Soluble E-cadherin: More Than a Symptom of Disease. In *Frontiers in bioscience (Landmark edition)* 17, pp. 1948–1964.

Guan, Xiangming (2015): Cancer metastases: challenges and opportunities. In *Acta pharmaceutica Sinica. B* 5 (5), pp. 402–418. DOI: 10.1016/j.apsb.2015.07.005.

Gumbiner, Barry M.; Kim, Nam-Gyun (2014): The Hippo-YAP signaling pathway and contact inhibition of growth. In *Journal of cell science* 127 (Pt 4), pp. 709–717. DOI: 10.1242/jcs.140103.

Hao, Jin; Zhang, Yueling; Wang, Yating; Ye, Rui; Qiu, Jingyi; Zhao, Zhihe; Li, Juan (2014): Role of extracellular matrix and YAP/TAZ in cell fate determination. In *Cellular signalling* 26 (2), pp. 186–191. DOI: 10.1016/j.cellsig.2013.11.006.

Harder, Jennifer L.; Whiteman, Eileen L.; Pieczynski, Jay N.; Liu, Chia-Jen; Margolis, Ben (2012): Snail destabilizes cell surface Crumbs3a. In *Traffic (Copenhagen, Denmark)* 13 (8), pp. 1170–1185. DOI: 10.1111/j.1600-0854.2012.01376.x.

Humbert, P. O.; Grzeschik, N. A.; Brumby, A. M.; Galea, R.; Elsum, I.; Richardson, H. E. (2008): Control of tumourigenesis by the Scribble/Dlg/Lgl polarity module. In *Oncogene* 27 (55), pp. 6888–6907. DOI: 10.1038/onc.2008.341.

Hurd, Toby W.; Gao, Lin; Roh, Michael H.; Macara, Ian G.; Margolis, Ben (2003): Direct interaction of two polarity complexes implicated in epithelial tight junction assembly. In *Nat. Cell Biol.* 5 (2), pp. 137–142. DOI: 10.1038/ncb923.

Justice, R. W.; Zilian, O.; Woods, D. F.; Noll, M.; Bryant, P. J. (1995): The Drosophila tumor suppressor gene warts encodes a homolog of human myotonic dystrophy kinase and is required for the control of cell shape and proliferation. In *Genes & development* 9 (5), pp. 534–546.

Kalluri, Raghu (2009): EMT: when epithelial cells decide to become mesenchymal-like cells. In *The Journal of clinical investigation* 119 (6), pp. 1417–1419. DOI: 10.1172/JCI39675.

Kamai, Takao; Yamanishi, Tomonori; Shirataki, Hiromichi; Takagi, Kentaro; Asami, Hidekazu; Ito, Yuji; Yoshida, Ken-Ichiro (2004): Overexpression of RhoA, Rac1, and Cdc42 GTPases is associated with progression in testicular cancer. In *Clinical cancer research : an official journal of the American Association for Cancer Research* 10 (14), pp. 4799–4805. DOI: 10.1158/1078-0432.CCR-0436-03.

Karp, Cristina M.; Tan, Ting Ting; Mathew, Robin; Nelson, Deidre; Mukherjee, Chandreyee; Degenhardt, Kurt et al. (2008): Role of the polarity determinant crumbs in suppressing mammalian epithelial tumor progression. In *Cancer research* 68 (11), pp. 4105–4115. DOI: 10.1158/0008-5472.CAN-07-6814.

Katsuno, Yoko; Lamouille, Samy; Derynck, Rik (2013): TGF-beta signaling and epithelial-mesenchymal transition in cancer progression. In *Current opinion in oncology* 25 (1), pp. 76–84. DOI: 10.1097/CCO.0b013e32835b6371.

Khatodia, Surender; Bhatotia, Kirti; Passricha, Nishat; Khurana, S. M. P.; Tuteja, Narendra (2016): The CRISPR/Cas Genome-Editing Tool: Application in Improvement of Crops. In *Frontiers in plant science* 7, p. 506. DOI: 10.3389/fpls.2016.00506.

Khursheed, Mohammed; Bashyam, Murali Dharan (2014): Apico-basal polarity complex and cancer. In *Journal of biosciences* 39 (1), pp. 145–155.

Kinzler, K. W.; Vogelstein, B. (1996): Lessons from hereditary colorectal cancer. In *Cell* 87 (2), pp. 159–170.

Knights, Alexander J.; Funnell, Alister P. W.; Crossley, Merlin; Pearson, Richard C. M. (2012): Holding Tight: Cell Junctions and Cancer Spread. In *Trends in cancer research* 8, pp. 61–69.

Knust, Elisabeth; Bossinger, Olaf (2002): Composition and Formation of Intercellular Junctions in Epithelial Cells. In *Science (New York, N.Y.)* 298, pp. 1955–1959. Available online at

http://www.sciencemag.org/content/298/5600/1955.full.pdf, checked on 7/20/2015.

Knutsen, Turid; Padilla-Nash, Hesed M.; Wangsa, Danny; Barenboim-Stapleton, Linda; Camps, Jordi; McNeil, Nicole et al. (2010): Definitive molecular cytogenetic characterization of 15 colorectal cancer cell lines. In *Genes, chromosomes & cancer* 49 (3), pp. 204–223. DOI: 10.1002/gcc.20730.

Lamouille, Samy; Xu, Jian; Derynck, Rik (2014): Molecular mechanisms of epithelial-mesenchymal transition. In *Nature reviews. Molecular cell biology* 15 (3), pp. 178–196. DOI: 10.1038/nrm3758.

Lee, Minhui; Vasioukhin, Valeri (2008): Cell polarity and cancer--cell and tissue polarity as a non-canonical tumor suppressor. In *J. Cell. Sci.* 121 (Pt 8), pp. 1141–1150. DOI: 10.1242/jcs.016634.

Lehmann, Waltraut; Mossmann, Dirk; Kleemann, Julia; Mock, Kerstin; Meisinger, Chris; Brummer, Tilman et al. (2016): ZEB1 turns into a transcriptional activator by interacting with YAP1 in aggressive cancer types. In *Nat Comms* 7, p. 10498. DOI: 10.1038/ncomms10498.

Lin, Tzu-Huai; Yeh, Tsung-Han; Wang, Tsu-Wei; Yu, Jenn-Yah (2014): The Hippo pathway controls border cell migration through distinct mechanisms in outer border cells and polar cells of the Drosophila ovary. In *Genetics* 198 (3), pp. 1087–1099. DOI: 10.1534/genetics.114.167346.

Lin, Wan-Hsin; Asmann, Yan W.; Anastasiadis, Panos Z. (2015): Expression of polarity genes in human cancer. In *Cancer informatics* 14 (Suppl 3), pp. 15–28. DOI: 10.4137/CIN.S18964.

Liu, Fei; Lagares, David; Choi, Kyoung Moo; Stopfer, Lauren; Marinkovic, Aleksandar; Vrbanac, Vladimir et al. (2015): Mechanosignaling through YAP and TAZ drives fibroblast activation and fibrosis. In *American journal of physiology. Lung cellular and molecular physiology* 308 (4), p. L344-57. DOI: 10.1152/ajplung.00300.2014.

Lo, Priscilla; Hawrot, Hannah; Georgiou, Marios (2012): Apicobasal polarity and its role in cancer progression. In *Biomolecular concepts* 3 (6), pp. 505–521. DOI: 10.1515/bmc-2012-0020.

Lucas, Eliana P.; Khanal, Ichha; Gaspar, Pedro; Fletcher, Georgina C.; Polesello, Cedric; Tapon, Nicolas; Thompson, Barry J. (2013): The Hippo pathway polarizes the actin cytoskeleton during collective migration of Drosophila border cells. In *The Journal of Cell Biology* 201 (6), pp. 875–885. DOI: 10.1083/jcb.201210073.

Ma, Xianjue; Wang, Hongxiang; Ji, Jiansong; Xu, Wenyan; Sun, Yihao; Li, Wenzhe et al. (2017): Hippo signaling promotes JNK-dependent cell migration. In *Proceedings of the National Academy of Sciences of the United States of America* 114 (8), pp. 1934–1939. DOI: 10.1073/pnas.1621359114.

Makarova, Olga; Roh, Michael H.; Liu, Chia-Jen; Laurinec, Stephanie; Margolis, Ben (2003): Mammalian Crumbs3 is a small transmembrane protein linked to protein associated with Lin-7 (Pals1). In *Gene* 302 (1-2), pp. 21–29. DOI: 10.1016/S0378111902010843.

Marques, E.; Englund, J. I.; Tervonen, T. A.; Virkunen, E.; Laakso, M.; Myllynen, M. et al. (2016): Par6G suppresses cell proliferation and is targeted by loss-of-function mutations in multiple cancers. In *Oncogene* 35 (11), pp. 1386–1398. DOI: 10.1038/onc.2015.196;

Martin-Belmonte, Fernando; Perez-Moreno, Mirna (2012): Epithelial cell polarity, stem cells and cancer. In *Nature reviews. Cancer* 12 (1), pp. 23–38. DOI: 10.1038/nrc3169.

McCaffrey, Luke Martin; Montalbano, JoAnne; Mihai, Constantina; Macara, Ian G. (2012): Loss of the Par3 polarity protein promotes breast tumorigenesis and metastasis. In *Cancer cell* 22 (5), pp. 601–614. DOI: 10.1016/j.ccr.2012.10.003.

Mehta, Shameer; Nijhuis, Anke; Kumagai, Tomoko; Lindsay, James; Silver, Andrew (2015): Defects in the adherens junction complex (E-cadherin/ beta-catenin) in inflammatory bowel disease. In *Cell and tissue research* 360 (3), pp. 749–760. DOI: 10.1007/s00441-014-1994-6.

Meng, Zhipeng; Moroishi, Toshiro; Guan, Kun-Liang (2016): Mechanisms of Hippo pathway regulation. In *Genes & development* 30 (1), pp. 1–17. DOI: 10.1101/gad.274027.115.

Mescher, Anthony L.; Junqueira, Luiz Carlos Uchôa (2010): Junqueira's basic histology. Text and atlas / Anthony L. Mescher. Thirteenth edition.

Michel, Didier; Arsanto, Jean-Pierre; Massey-Harroche, Dominique; Beclin, Christophe; Wijnholds, Jan; Le Bivic, Andre (2005): PATJ connects and stabilizes apical and lateral components of tight junctions in human intestinal cells. In *Journal of cell science* 118 (Pt 17), pp. 4049–4057. DOI: 10.1242/jcs.02528.

Mo, Jung-Soon; Park, Hyun Woo; Guan, Kun-Liang (2014): The Hippo signaling pathway in stem cell biology and cancer. In *EMBO reports* 15 (6), pp. 642–656. DOI: 10.15252/embr.201438638.

Moleirinho, Susana; Hoxha, Sany; Mandati, Vinay; Curtale, Graziella; Troutman, Scott; Ehmer, Ursula; Kissil, Joseph L. (2017): Regulation of localization and function of the transcriptional co-activator YAP by angiomotin. In *eLife* 6. DOI: 10.7554/eLife.23966.

Moustakas, Aristidis; Heldin, Carl-Henrik (2007): Signaling networks guiding epithelial-mesenchymal transitions during embryogenesis and cancer progression. In *Cancer science* 98 (10), pp. 1512–1520. DOI: 10.1111/j.1349-7006.2007.00550.x.

Mu, Yabing; Gudey, Shyam Kumar; Landstrom, Marene (2012): Non-Smad signaling pathways. In *Cell and tissue research* 347 (1), pp. 11–20. DOI: 10.1007/s00441-011-1201-y.

Nistico, Paola; Bissell, Mina J.; Radisky, Derek C. (2012): Epithelial-mesenchymal transition: general principles and pathological relevance with special emphasis on the role of matrix metalloproteinases. In *Cold Spring Harbor Perspectives in Biology* 4 (2). DOI: 10.1101/cshperspect.a011908.

Onder, Tamer T.; Gupta, Piyush B.; Mani, Sendurai A.; Yang, Jing; Lander, Eric S.; Weinberg, Robert A. (2008): Loss of E-cadherin promotes metastasis via multiple downstream transcriptional pathways. In *Cancer research* 68 (10), pp. 3645–3654. DOI: 10.1158/0008-5472.CAN-07-2938.

Ortiz, Angelica; Lee, Yu-Chen; Yu, Guoyu; Liu, Hsuan-Chen; Lin, Song-Chang; Bilen, Melmet Asim et al. (2014): Angiomotin is a novel component of cadherin-

11/β-catenin/p120 complex and is critical for cadherin-11-mediated cell migration. In *The FASEB Journal* 29 (3), pp. 1080–1091. DOI: 10.1096/fj.14-261594.

Ozdamar, Barish; Bose, Rohit; Barrios-Rodiles, Miriam; Wang, Hong-Rui; Zhang, Yue; Wrana, Jeffrey L. (2005): Regulation of the polarity protein Par6 by TGFbeta receptors controls epithelial cell plasticity. In *Science (New York, N.Y.)* 307 (5715), pp. 1603–1609. DOI: 10.1126/science.1105718.

Papageorgis, Panagiotis; Stylianopoulos, Triantafyllos (2015): Role of TGFbeta in regulation of the tumor microenvironment and drug delivery (review). In *International journal of oncology* 46 (3), pp. 933–943. DOI: 10.3892/ijo.2015.2816.

Pegtel, D. Michiel; Ellenbroek, Saskia I. J.; Mertens, Alexander E. E.; van der Kammen, Rob A; Rooij, Johan de; Collard, John G. (2007): The Par-Tiam1 complex controls persistent migration by stabilizing microtubule-dependent front-rear polarity. In *Current biology : CB* 17 (19), pp. 1623–1634. DOI: 10.1016/j.cub.2007.08.035.

Peinado, Hector; Olmeda, David; Cano, Amparo (2007): Snail, Zeb and bHLH factors in tumour progression: an alliance against the epithelial phenotype? In *Nature reviews. Cancer* 7 (6), pp. 415–428. DOI: 10.1038/nrc2131.

Penkert, Rhiannon R.; DiVittorio, Heather M.; Prehoda, Kenneth E. (2004): Internal recognition through PDZ domain plasticity in the Par-6-Pals1 complex. In *Nature structural & molecular biology* 11 (11), pp. 1122–1127. DOI: 10.1038/nsmb839.

Peterson, Francis C.; Penkert, Rhiannon R.; Volkman, Brian F.; Prehoda, Kenneth E. (2004): Cdc42 Regulates the Par-6 PDZ Domain through an Allosteric CRIB-PDZ Transition. In *Molecular Cell* 13 (5), pp. 665–676. DOI: 10.1016/S1097-2765(04)00086-3.

Pieczynski, Jay; Margolis, Ben (2011a): Protein complexes that control renal epithelial polarity. In *American journal of physiology. Renal physiology* 300 (3), p. F589-601. DOI: 10.1152/ajprenal.00615.2010.

Pieczynski, Jay; Margolis, Ben (2011b): Protein complexes that control renal epithelial polarity. In *American journal of physiology. Renal physiology* 300 (3), p. F589-601. DOI: 10.1152/ajprenal.00615.2010.

Plant, Pamela J.; Fawcett, James P.; Lin, Dan C. C.; Holdorf, Amy D.; Binns, Kathleen; Kulkarni, Sarang; Pawson, Tony (2003): A polarity complex of mPar-6 and atypical PKC binds, phosphorylates and regulates mammalian Lgl. In *Nature cell biology* 5 (4), pp. 301–308. DOI: 10.1038/ncb948.

Pocha, Shirin Meher; Knust, Elisabeth (2013): Complexities of Crumbs function and regulation in tissue morphogenesis. In *Current biology : CB* 23 (7), p. R289-93. DOI: 10.1016/j.cub.2013.03.001.

Puchalapalli, Madhavi; Zeng, Xianke; Mu, Liang; Anderson, Aubree; Hix Glickman, Laura; Zhang, Ming et al. (2016): NSG Mice Provide a Better Spontaneous Model of Breast Cancer Metastasis than Athymic (Nude) Mice. In *PloS one* 11 (9), pp. e0163521. DOI: 10.1371/journal.pone.0163521.

Reynolds, Albert B.; Roczniak-Ferguson, Agnes (2004): Emerging roles for p120-catenin in cell adhesion and cancer. In *Oncogene* 23 (48), pp. 7947–7956. DOI: 10.1038/sj.onc.1208161.

Riihimaki, Matias; Hemminki, Akseli; Sundquist, Jan; Hemminki, Kari (2016): Patterns of metastasis in colon and rectal cancer. In *Scientific reports* 6, p. 29765. DOI: 10.1038/srep29765.

Rodriguez, Fausto J.; Lewis-Tuffin, Laura J.; Anastasiadis, Panos Z. (2012): E-cadherin's dark side: possible role in tumor progression. In *Biochimica et biophysica acta* 1826 (1), pp. 23–31. DOI: 10.1016/j.bbcan.2012.03.002.

Roh, Michael H.; Liu, Chia-Jen; Laurinec, Stephanie; Margolis, Ben (2002a): The carboxyl terminus of zona occludens-3 binds and recruits a mammalian homologue of discs lost to tight junctions. In *The Journal of biological chemistry* 277 (30), pp. 27501–27509. DOI: 10.1074/jbc.M201177200.

Roh, Michael H.; Makarova, Olga; Liu, Chia-Jen; Shin, Kunyoo; Lee, Seonok; Laurinec, Stephanie et al. (2002b): The Maguk protein, Pals1, functions as an adapter, linking mammalian homologues of Crumbs and Discs Lost. In *The Journal of Cell Biology* 157 (1), pp. 161–172. DOI: 10.1083/jcb.200109010.

Royer, C.; Lu, X. (2011): Epithelial cell polarity: a major gatekeeper against cancer? In *Cell death and differentiation* 18 (9), pp. 1470–1477. DOI: 10.1038/cdd.2011.60.

Saitoh, Masao (2015): Epithelial-mesenchymal transition is regulated at post-transcriptional levels by transforming growth factor-beta signaling during tumor progression. In *Cancer science* 106 (5), pp. 481–488. DOI: 10.1111/cas.12630.

Schneider, Marlon R.; Hiltwein, Felix; Grill, Jessica; Blum, Helmut; Krebs, Stefan; Klanner, Andrea et al. (2014): Evidence for a role of E-cadherin in suppressing liver carcinogenesis in mice and men. In *Carcinogenesis* 35 (8), pp. 1855–1862. DOI: 10.1093/carcin/bgu109.

Sen, Arnab; Nagy-Zsver-Vadas, Zsanett; Krahn, Michael P. (2012): Drosophila PATJ supports adherens junction stability by modulating Myosin light chain activity. In *The Journal of Cell Biology* 199 (4), pp. 685–698. DOI: 10.1083/jcb.201206064.

Shin, Kunyoo; Straight, Sam; Margolis, Ben (2005): PATJ regulates tight junction formation and polarity in mammalian epithelial cells. In *J. Cell Biol.* 168 (5), pp. 705–711. DOI: 10.1083/jcb.200408064.

Shin, Kunyoo; Wang, Qian; Margolis, Ben (2007): PATJ regulates directional migration of mammalian epithelial cells. In *EMBO reports* 8 (2), pp. 158–164. DOI: 10.1038/sj.embor.7400890.

Sigoillot, Frederic D.; King, Randall W. (2011): Vigilance and validation: Keys to success in RNAi screening. In *ACS chemical biology* 6 (1), pp. 47–60. DOI: 10.1021/cb100358f.

Singhai, Rajeev; Patil, Vinayak W.; Jaiswal, Sanjog R.; Patil, Shital D.; Tayade, Mukund B.; Patil, Amit V. (2011): E-Cadherin as a diagnostic biomarker in breast cancer. In *North American journal of medical sciences* 3 (5), pp. 227–233. DOI: 10.4297/najms.2011.3227.

Slavotinek, Anne M. (2016): The Family of Crumbs Genes and Human Disease. In *Molecular syndromology* 7 (5), pp. 274–281. DOI: 10.1159/000448109.

Solecki, David J.; Model, Lynn; Gaetz, Jedidiah; Kapoor, Tarun M.; Hatten, Mary E. (2004): Par6alpha signaling controls glial-guided neuronal migration. In *Nature neuroscience* 7 (11), pp. 1195–1203. DOI: 10.1038/nn1332.

Straight, Samuel W.; Shin, Kunyoo; Fogg, Vanessa C.; Fan, Shuling; Liu, Chia-Jen; Roh, Michael; Margolis, Ben (2004): Loss of PALS1 expression leads to tight junction and polarity defects. In *Mol. Biol. Cell* 15 (4), pp. 1981–1990. DOI: 10.1091/mbc.E03-08-0620.

Su, Wen-Hui; Mruk, Dolores D.; Wong, Elissa W. P.; Lui, Wing-Yee; Cheng, C. Yan (2012): Polarity Protein Complex Scribble/Lgl/Dlg and Epithelial Cell Barriers. In *Advances in experimental medicine and biology* 763, pp. 149–170.

Tabaries, S.; Siegel, P. M. (2016): The role of claudins in cancer metastasis. In *Oncogene. DOI:* 10.1038/onc.2016.289.

Tapon, Nicolas; Harvey, Kieran F.; Bell, Daphne W.; Wahrer, Doke C. R.; Schiripo, Taryn A.; Haber, Daniel A.; Hariharan, Iswar K. (2002): salvador Promotes both cell cycle exit and apoptosis in Drosophila and is mutated in human cancer cell lines. In *Cell* 110 (4), pp. 467–478.

Tariq, Kanwal; Ghias, Kulsoom (2016): Colorectal cancer carcinogenesis: a review of mechanisms. In *Cancer biology & medicine* 13 (1), pp. 120–135. DOI: 10.28092/j.issn.2095-3941.2015.0103.

Tepass, U.; Knust, E. (1993): Crumbs and stardust act in a genetic pathway that controls the organization of epithelia in Drosophila melanogaster. In *Developmental biology* 159 (1), pp. 311–326. DOI: 10.1006/dbio.1993.1243.

Varelas, Xaralabos; Samavarchi-Tehrani, Payman; Narimatsu, Masahiro; Weiss, Alexander; Cockburn, Katie; Larsen, Brett G. et al. (2010): The Crumbs complex couples cell density sensing to Hippo-dependent control of the TGF-beta-SMAD pathway. In *Developmental cell* 19 (6), pp. 831–844. DOI: 10.1016/j.devcel.2010.11.012.

Wang, Hong-Rui; Zhang, Yue; Ozdamar, Barish; Ogunjimi, Abiodun A.; Alexandrova, Evguenia; Thomsen, Gerald H.; Wrana, Jeffrey L. (2003): Regulation of cell polarity and protrusion formation by targeting RhoA for

degradation. In *Science (New York, N.Y.)* 302 (5651), pp. 1775–1779. DOI: 10.1126/science.1090772.

Wang, Qian; Chen, Xiao-Wei; Margolis, Ben (2007): PALS1 regulates E-cadherin trafficking in mammalian epithelial cells. In *Molecular biology of the cell* 18 (3), pp. 874–885. DOI: 10.1091/mbc.E06-07-0651.

Weide, Thomas; Vollenbroker, Beate; Schulze, Ulf; Djuric, Ivona; Edeling, Maria; Bonse, Jakob et al. (2017): Pals1 Haploinsufficiency Results in Proteinuria and Cyst Formation. In *Journal of the American Society of Nephrology : JASN. DOI:* 10.1681/ASN.2016040474.

Wells, Clark D.; Fawcett, James P.; Traweger, Andreas; Yamanaka, Yojiro; Goudreault, Marilyn; Elder, Kelly et al. (2006): A Rich1/Amot complex regulates the Cdc42 GTPase and apical-polarity proteins in epithelial cells. In *Cell* 125 (3), pp. 535–548. DOI: 10.1016/j.cell.2006.02.045.

Whiteman, Eileen L.; Fan, Shuling; Harder, Jennifer L.; Walton, Katherine D.; Liu, Chia-Jen; Soofi, Abdul et al. (2014): Crumbs3 is essential for proper epithelial development and viability. In *Molecular and cellular biology* 34 (1), pp. 43–56. DOI: 10.1128/MCB.00999-13.

Wodarz, A. (2000): Tumor suppressors: linking cell polarity and growth control. In *Current biology : CB* 10 (17), p. R624-6.

Wodarz, A.; Hinz, U.; Engelbert, M.; Knust, E. (1995): Expression of crumbs confers apical character on plasma membrane domains of ectodermal epithelia of Drosophila. In *Cell* 82 (1), pp. 67–76.

Wodarz, Andreas; Nathke, Inke (2007): Cell polarity in development and cancer. In *Nature cell biology* 9 (9), pp. 1016–1024. DOI: 10.1038/ncb433.

Woods, D. F.; Hough, C.; Peel, D.; Callaini, G.; Bryant, P. J. (1996): Dlg protein is required for junction structure, cell polarity, and proliferation control in Drosophila epithelia. In *The Journal of Cell Biology* 134 (6), pp. 1469–1482.

Wu, Y.; Zhou, B. P. (2010): TNF-alpha/NF-kappaB/Snail pathway in cancer cell migration and invasion. In *British journal of cancer* 102 (4), pp. 639–644. DOI: 10.1038/sj.bjc.6605530.

Xu, T.; Wang, W.; Zhang, S.; Stewart, R. A.; Yu, W. (1995): Identifying tumor suppressors in genetic mosaics: the Drosophila lats gene encodes a putative protein kinase. In *Development (Cambridge, England)* 121 (4), pp. 1053–1063.

Yang, Jun; Zhang, Wen; Evans, Paul M.; Chen, Xi; He, Xi; Liu, Chunming (2006): Adenomatous polyposis coli (APC) differentially regulates beta-catenin phosphorylation and ubiquitination in colon cancer cells. In *The Journal of biological chemistry* 281 (26), pp. 17751–17757. DOI: 10.1074/jbc.M600831200.

Yi, Chunling; Shen, Zhewei; Stemmer-Rachamimov, Anat; Dawany, Noor; Troutman, Scott; Showe, Louise C. et al. (2013): The p130 isoform of angiomotin is required for Yap-mediated hepatic epithelial cell proliferation and tumorigenesis. In *Science signaling* 6 (291), pp. ra77. DOI: 10.1126/scisignal.2004060.

Yilmaz, Mahmut; Christofori, Gerhard (2009): EMT, the cytoskeleton, and cancer cell invasion. In *Cancer metastasis reviews* 28 (1-2), pp. 15–33. DOI: 10.1007/s10555-008-9169-0.

Yu, Fa-Xing; Zhao, Bin; Guan, Kun-Liang (2015): Hippo Pathway in Organ Size Control, Tissue Homeostasis, and Cancer. In *Cell* 163 (4), pp. 811–828. DOI: 10.1016/j.cell.2015.10.044.

Yu, Jason S. L.; Cui, Wei (2016): Proliferation, survival and metabolism: the role of PI3K/AKT/mTOR signalling in pluripotency and cell fate determination. In *Development (Cambridge, England)* 143 (17), pp. 3050–3060. DOI: 10.1242/dev.137075.

Zallen, Jennifer A. (2007): Planar polarity and tissue morphogenesis. In *Cell* 129 (6), pp. 1051–1063. DOI: 10.1016/j.cell.2007.05.050.

Zhang, Lin; Yang, Shuping; Wennmann, Dirk Oliver; Chen, Yuanhong; Kremerskothen, Joachim; Dong, Jixin (2014): KIBRA: In the brain and beyond. In *Cellular signalling* 26 (7), pp. 1392–1399. DOI: 10.1016/j.cellsig.2014.02.023.

Zhao, Bin; Li, Li; Guan, Kun-Liang (2010a): Hippo signaling at a glance. In *Journal of cell science* 123 (Pt 23), pp. 4001–4006. DOI: 10.1242/jcs.069070.

Zhao, Bin; Li, Li; Lei, Qunying; Guan, Kun-Liang (2010b): The Hippo-YAP pathway in organ size control and tumorigenesis: an updated version. In *Genes & development* 24 (9), pp. 862–874. DOI: 10.1101/gad.1909210.

Zhao, Bin; Li, Li; Lu, Qing; Wang, Lloyd H.; Liu, Chen-Ying; Lei, Qunying; Guan, Kun-Liang (2011): Angiomotin is a novel Hippo pathway component that inhibits YAP oncoprotein. In *Genes & development* 25 (1), pp. 51–63. DOI: 10.1101/gad.2000111.

Zihni, Ceniz; Balda, Maria S.; Matter, Karl (2014): Signalling at tight junctions during epithelial differentiation and microbial pathogenesis. In *Journal of cell science* 127 (Pt 16), pp. 3401–3413. DOI: 10.1242/jcs.145029.

Zollinger, Daniel R.; Chang, Kae-Jiun; Baalman, Kelli; Kim, Seonhee; Rasband, Matthew N. (2015): The Polarity Protein Pals1 Regulates Radial Sorting of Axons. In *The Journal of neuroscience : the official journal of the Society for Neuroscience* 35 (29), pp. 10474–10484. DOI: 10.1523/JNEUROSCI.1593-15.2015.